All Optical Wavelength Conversion and Parametric Amplification in Ti:PPLN Channel Waveguides for Telecommunication Applications

Dem Department Physik der
Universität Paderborn
zur Erlangung des akademischen Grades eines
Doktors der Naturwissenschaften (Dr. rer. nat.)
vorgelegte
Dissertation
von

Rahman Nouroozi

1. Gutachter: Prof. Dr. Wolfgang Sohler
2. Gutachter: Prof. Dr. Christine Silberhorn

Tag der Einreichung: 19.10.2010

dedicated to

Nasrin
&
Sana

Abstract

Efficient ultra-fast integrated all-optical wavelength converters and parametric amplifiers transparent to the polarization, phase, and modulation-level and -format are investigated. The devices take advantage of the optical nonlinearity of Ti:PPLN waveguides exploiting difference frequency generation (DFG). In a DFG, the signal (λ_s) is mixed with a pump (λ_p) to generate a wavelength shifted idler ($1/\lambda_i = 1/\lambda_p - 1/\lambda_s$). The mode-selective excitation of the pump (shorter wavelength) is difficult in a directly pumped DFG. However, by internal generation of the pump via cascaded second harmonic generation and DFG (cSHG/DFG) or sum frequency generation and DFG (cSFG/DFG), the phasematched pump (SH or SF) mode can be excited selectively. Therefore, efficient generation of the pump in Ti:PPLN channel guides is investigated using different approaches.

In the waveguide resonators, first a resonance of the fundamental wave alone is considered. It is shown that the maximum power enhancement of the fundamental wave, and therefore the maximum SHG efficiency, can be achieved with low loss matched resonators. By this way, SHG efficiency of ~ 10300%/W (10.3 %/mW) has been achieved in a 65 mm long waveguide resonator. Its operation for cSHG/DFG requires narrowband reflector for fundamental wave only. Thus, the SH (pump) wave resonator is investigated. The SH-wave resonator enhances the intracavity SH power only. Based on this scheme, an improvement of ~ 10 dB for cSHG/DFG-based wavelength conversion efficiency has been achieved with 50 mW of coupled fundamental power in a 30 mm long Ti:PPLN. However, operation was limited to relatively small fundamental power levels (< 50 mW) due to the onset of photo-refractive instabilities destroying the cavity stabilization.

The cSHG/DFG efficiency can be considerably improved by using a double-pass configuration in which all the interacting waves were reflected by a broadband dielectric mirror deposited on the one endface of the waveguide. However, due to the wavelength dependent phase change by the dielectric folding mirror phase compensation is required to maintain an optimum power transfer. Three different approaches are investigated and up to 9 dB improvement of the wavelength conversion efficiency in comparison with the single-pass configuration is achieved.

Polarization-insensitive wavelength conversion is based on a polarization maintaining fiber loop configuration. Since both polarization components can be converted in a contra-directional single-pass waveguide, differential group delay (DGD) equalization between them is automatically provided. With such polarization diversity scheme an error-free polarization insensitive conversion of 320 Gb/s differential quaternary phase shift keying (DQPSK) data with signal pulses of 1.4 ps width has been achieved using the packaged and pigtailed cSHG/DFG-based

wavelength converter. No significant broadening or distortion of the converted data pulses was observed. This indicates an almost unlimited bandwidth for cSHG/DFG.

Using a ring type diversity scheme, a tuneable polarization insensitive cSFG/DFG is investigated. This approach results in a tuneable output wavelength of the idler whereas the input signal wavelength can be kept fixed. In a 70 mm long Ti:PPLN channel guide a conversion efficiency of ~ -7.5 dB has been achieved by 80 mW (20 mW) of coupled pump (control) power level with less than ± 0.5 dB of residual polarization dependence. The tuning range of the idler covers the whole C-band. However, in contrast to cSHG/DFG, pulse broadening of the converted signal will limit the data rate for cSFG/DFG.

For sufficiently high pump power levels wavelength conversion by DFG is accompanied by significant optical parametric amplification (OPA) of the input signal. To increase the fundamental power handling flexibility and to avoid photo-refractive effect, a low duty cycle Q-switched diode-pumped-solid-state (DPSS) laser has been used as the fundamental source. With 2.5 W of fundamental peak power ~ 22 dB of signal gain has been measured.

Contents

1. Introduction

Low-loss single-mode optical fiber offers the possibility to build optical transmission systems with demonstrated bandwidths of several terahertz. Terabits-per-second communication systems are rapidly being developed and will be the backbone for the global interconnection in the foreseeable future. Such optical communication systems are based on the dense wavelength-division multiplexing (DWDM) [1], which involves simultaneous propagation of multiple data signals, each at a different wavelength in a single optical line. The cpacity of a DWDM data channel can be then increased using the optical time-division multiplexing (OTDM) [2], where multiple relatively low-bit-rate streams of data with the same carrier frequency are interleaved to create a single channel high-bit-rate stream. The goal of this research work was to develop an efficient wavelength conversion device to resolve the contention in such a high bit rate DWDM network.

1.1 Motivation

With the introduction of the high definition video transmission via internet, the data rates have exploded. Therefore, there is a need for basic research in solutions to the network congestion problems (where the probability of the data packet loss or the contention of new connections are high). To go far beyond 100 Gbit/s, which is the current electrical state-of-the-art in the research labs [3], the optical techniques are required. Increasing the data rate using the interplay between DWDM network topologies and ultrahigh-speed OTDM [4] could be one of the ways to increase the aggregate capacity. By combining OTDM and DWDM, point-to-point optical links with data capacities close to the theoretical limit can be designed. For instance, an impressive 32 Tbit/s data transmission over 580 km using return-to-zero (RZ) shape polarization division multiplexed (PDM) 8 quadrature-amplitude-modulation (QAM) format was demonstrated recently [5].

In a fiber optical network mentioned above, the number of interconnection nodes is often too small to support a large number of different wavelengths. Thus, the blocking probability rises due to a possible wavelength contention when two channels at the same wavelength are to be routed into the same output. One solution to this problem is to convert a signal from one wavelength to another [6], as

illustrated in Fig. 1.1. Wavelength conversion also allows distributing the network control and management into smaller sub-networks, thus wavelength can be flexibly assigned within each sub-network.

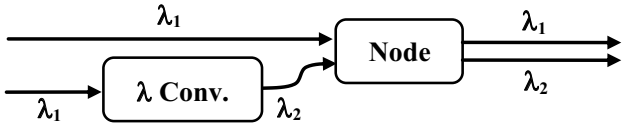

Fig. 1.1: Network blocking probabilities can be resolved by wavelength-conversion.

All-optical wavelength conversion of a data channel can effectively resolve contention and dramatically increase network throughput. Since advanced phase modulation formats such as differential binary phase-shift-keying (DPSK) and differential-quadrature-phase-shift-keying (DQPSK) are more and more used in optical communication systems phase transparency is required for wavelength conversion of such advanced modulation formats. Therefore, the goal of this research was the development of efficient ultra-fast integrated all-optical wavelength converters (AOWC) for contention resolution and parametric amplifiers for fibre optical DWDM communication systems. Such a device should feature transparency to polarization, phase, modulation-level and modulation-format of the data channel.

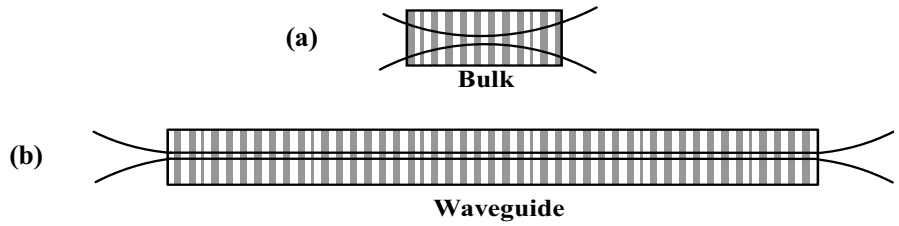

Fig. 2.1: Schematic drawings of beam propagation in a bulk (a) and in a waveguide (b). Diffraction associated with bulk media whereas, optical confinement provided by a waveguide.

Confined optical fields in waveguides that can interact over a long distance will considerably enhance the efficiency of nonlinear optical processes in comparison to processes in bulk media. Fig. 2.1 shows a schematic drawing of beam propagation in a bulk medium and in a waveguide. When a tightly focused wave propagates in a bulk device it will diffract, so high efficiency cannot be achieved. In waveguides the mode profile is spatially confined in a cross-section on the order of the wavelength. High optical intensities can be maintained over considerable distances to improve the efficiency of the nonlinear interaction by orders of magnitude in comparison with bulk devices. The efficiency of the nonlinear optical process η_{nl} is strongly proportional to the interaction length L, thus fabrication of long, homogeneous, and low-loss waveguides is essential for efficient AOWC.

Several nonlinear optical techniques have been demonstrated for all-optical wavelength conversion including self-phase modulation (SPM) or cross-phase modulation (XPM) [7], [8], and four-wave mixing (FWM) [9], [10] in (highly nonlinear) fibers. Also three-wave nonlinear optical frequency mixing in integrated optical waveguides utilizing $\chi^{(2)}$ nonlinearity of lithium niobate substrate represent such scheme, as proposed in [11], [12]. The AOWC provides large bandwidth, low (quantum-limited) noise, coherent and phase sensitive responce. Thus, corresponding devices are completely transparent [13], [14]. Besides the main motivation, the realized device is important also to operate as midspan dispersion compensation (chromatic compensation) [15].

Phasematching among the interacting waves must be preserved to ensure the efficient accumulation of the fields generated by the nonlinearities along the whole length of the device. Hence the weak nonlinearities impose technical challenges on the realization of efficient and broadband wavelength converters.

In a dispersive medium such as $LiNbO_3$, different wavelengths have different refractive indices. Therefore, the interacting waves in a parametric process go out of phase after propagating a distance L_c, so called coherence length. The generated wavelength over a coherence length converts back to the input wavelengths during the next coherence length. Quasi-phase-matching (QPM) compensates for phase mismatch by changing the sign of the nonlinear coefficient every coherence length [16]. This periodic reversal with the (micro-domain) periodicity of $\Lambda_{QPM} = L_c/2$ preserves the direction of energy flow from the input waves to the output waves, ensuring that the output increases monotonically with propagation distance.

The integrated AOWC in lithium niobate for telecommunication operation is based on the difference frequency generation (DFG) process. Wavelength conversion by DFG of a signal in the 1.55 μm band requires a pump of about 0.78 μm wavelength. This is problematic as waveguides, which are single mode at $\lambda \sim 1.55$ μm, typically are multimode at half the wavelength. However, the pump wave can be generated internally by second harmonic generation (SHG) of a "fundamental" wave in the 1.55 μm band with simultaneous QPM for SHG and DFG [11]. This attractive mode of operation is known as cascaded SHG/DFG or cSHG/DFG. It has number of advantages compared to the fiber-based AOWC:

1. Lithium niobate is an outstanding $\chi^{(2)}$ nonlinear optical material [17]; waveguides of excellent properties can be fabricated by Ti-indiffusion. Therefore, efficient AOWC devices can be realized with a few centimeter long waveguide.
2. The AOWC can be tailored within the whole transparency range of $LiNbO_3$ by proper periodicity of micro-domain grating of PPLN.

3. The cascaded processes allows the use of commercial telecom sources and amplifiers.
4. The internal generation of the pump wave by SHG (or SFG) automatically provides a selective mode excitation even though the waveguides are multimode at the pump wavelength.
5. At the required pump power levels, $\chi^{(3)}$ related nonlinear processes like self and cross phase modulation or stimulated Brillouin scattering (SBS), which might be detrimental for fiber-based AOWC, are negligible in PPLN-based AOWC.
6. The monolithic integration of such a device with other components opens up a variety of devices of higher functionality.

1.2 Overview of the Dissertation

This dissertation is organized as follows:

Chapter 2 is a brief review of the theory behind guided wave optical parametric processes in PPLN waveguides.

Chapter 3 presents the preparation method of straight and bent Ti indiffused periodically poled lithium niobate (Ti:PPLN) waveguides.

In chapter 4, SHG- and DFG-based wavelength converters are presented. An efficient SHG device using matched waveguide resonators to enhance the fundamental wave is developed. Directly pumped DFG-based wavelength conversion is studied in this chapter as well.

Chapter 5 describes the polarization sensitive and insensitive cSHG/DFG-based wavelength converters together with different methods for increasing the conversion efficiency such as: separated SHG and DFG in a counter propagation scheme, cSHG/DFG in long bent waveguides, double-pass cSHG/DFG and cSHG/DFG in a pump wave enhancement waveguide resonator are reported.

In chapter 6 cSFG/DFG-based tuneable wavelength conversion is introduced and experimentally demonstrated. Wavelength conversion of 1.4 ps pulses are studied theoretically and verified experimentally.

The optical parametric amplification (OPA) in CW and pulse mode of operation is presented in chapter 7.

Chapter 8 concludes the dissertation.

The research work which led to this thesis has been funded by the Deutsche Forschungsgemeinschaft within the project “Contention Resolution in Optical Burst Switching (OBS) using Wavelength Conversion”.

2. Theory of Guided-Wave Quasi-Phase-Matched Optical Wavelength Conversion

The all-optical wavelength converters (AOWCs) developed in this work are based on second order nonlinear ($\chi^{(2)}$) guided-wave QPM processes implemented by difference frequency generation (DFG) and cascaded $\chi^{(2)}$:$\chi^{(2)}$ nonlinear parametric process. $\chi^{(2)}$ interaction involves three waves which may either be input or generated within the nonlinear medium. Three kinds of interactions are investigated in this dissertation; second harmonic generation (SHG), sum frequency generation (SFG) and difference frequency generation (DFG). These different second order nonlinear processes are sketched in Fig. 2.1.

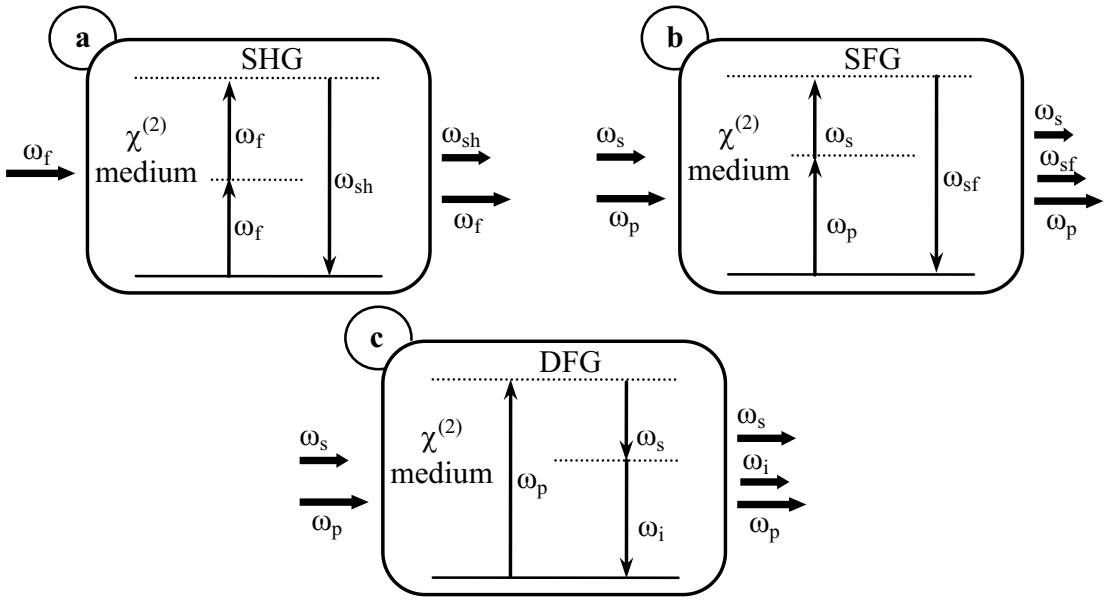

Fig. 2.1: Sketch of different $\chi^{(2)}$ nonlinear processes; (a) SHG- second harmonic generation, (b) SFG- sum frequency generation, and (c) DFG- difference frequency generation. Thick arrows indicate the power of the interacting waves.

In this chapter, the quasi-phase-matching is discussed in section 2.1. Then after short introduction of (guided wave) nonlinear optics, a brief theory of $\chi^{(2)}$-based parametric processes, which are used for AOWC in the communication window around 1550 nm, is presented. Basic concepts of nonlinear optics and waveguide theory used in the derivation can be found in several textbooks [21], [22], [23] and

will be briefly introduced in this chapter. The software code (see appendix C) which is used to perform all the calculations her was developed by Werner Grundkötter [19].

2.1 Quasi-Phase-Matching

Phasematching among the interacting waves must be preserved to ensure the efficient accumulation of the fields generated by the nonlinearities along the whole length of the device. In a three-wave mixing process, as an example, in the case of second harmonic generation, the fundamental wave at frequency ω generates linear and nonlinear polarizations at frequencies ω and 2ω, respectively. The accumulated phase of fundamental and generated second harmonic fields while travelling Δz in the medium are $\Delta\varphi_\omega = \beta_\omega \Delta z \equiv (\omega n_\omega/c)\Delta z$ and $\Delta\varphi_{2\omega} = \beta_{2\omega}\Delta z \equiv (2\omega n_{2\omega}/c)\Delta z$. β_j is the propagation constant of the wave in frequency j. If a medium without dispersion ($n_{2\omega} = n_\omega$) is used such that the phase velocities of light for all interacting waves are identical, then accumulated phase of fundamental wave exactly compensates the phase difference of the fields at 2ω. Therefore, the energy can be efficiently transferred to the generated optical wave leading to a quadratic growth of the second harmonic power with propagation distance (curve (a) in Fig. 2.2). Otherwise, there is a phase mismatch of $\Delta\varphi_{SHG} = (\beta_{2\omega} - 2\beta_\omega)\Delta z$ which leads to oscillations of the power in the second harmonic (curve (b) in Fig. 2.2).

The maximum second harmonic power in this case is limited to the power generated over an interaction distance equal to the so called coherence length:

$$L_c = \frac{\pi}{\Delta\beta} \equiv \frac{\pi}{\beta_{2\omega} - 2\beta_\omega} \equiv \frac{\lambda_{2\omega}}{2(n_{2\omega} - n_\omega)} \qquad (2.1)$$

Where Δβ is the mismatch of the propagation constants and $\lambda_{2\omega}$ is the second harmonic wavelength. It is clear from 2.1 that the coherence length is the distance over which the phase mismatch becomes equal to π.

The coherence length in most nonlinear media is very small. For instance, in lithium niobate the coherence length for second harmonic generation of infrared light (775 nm range) is about 8 μm for type 0 phase matching (where both fundamental and SH waves are TM polarized). Such a small interaction length is usually not adequate for efficient energy transfer to the new frequency component. Therefore, for efficient nonlinear wavelength conversion, phasematching is necessary over longer distance. The solution to the problem of phasematching was proposed by

Bloembergen and coworkers in 1962 [16]. The method is called quasi-phase-matching (QPM) and relies on resetting of the phase mismatch to 0 every coherence length. After one coherence length of propagation, the phase mismatch becomes π. If the sign of the nonlinear susceptibility $\chi^{(2)}$ is changed at that location, an additional π phase shift is added to the nonlinear polarization ($\exp(-i\pi) = 1$), resetting the phase mismatch to 0. After another coherence length of propagation, another π of phase shift is accumulated and the sign of the nonlinear coefficient has to be changed again in order to reset the mismatch to 0. In such way, the power of the second harmonic wave is allowed to grow along the crystal quasi-quadratically (curve (c) in Fig. 2.2).

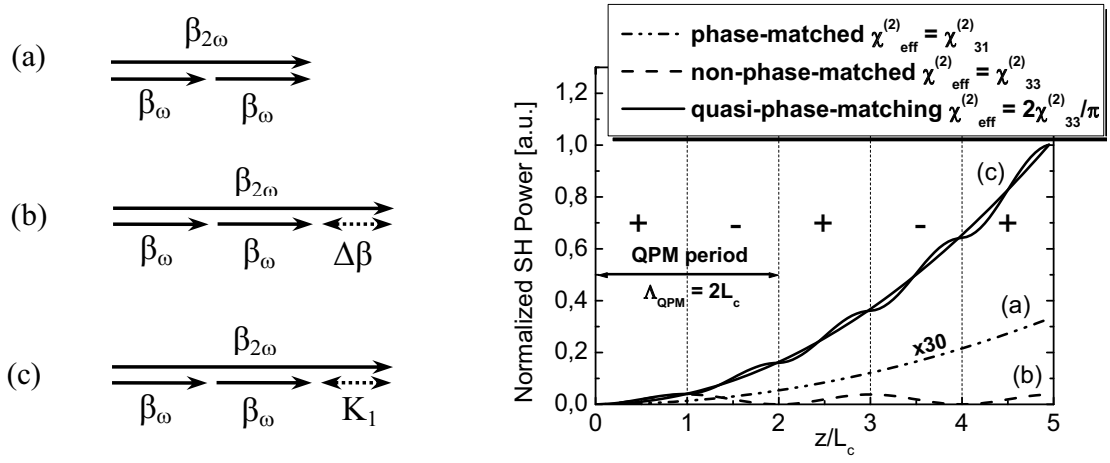

Fig. 2.2: Phasematching represented by β-diagrams (left), and SHG output power versus distance L normalized to the coherence length L_c (right) for; (a) quadratic growth in the case of birefringence phasematched SHG multiplied by 30 ($\chi^{(2)}_{31} \sim \chi^{(2)}_{33}/6$); (b) oscillatory behaviour in the non-phasematched case with β-mismatch Δβ; and (c) quasi-quadratic growth in the case of first-order quasi-phasematched SHG using a periodic sign reversal of the nonlinear susceptibility.

In uniaxial ferroelectric crystals such as lithium niobate, the sign of the nonlinear susceptibility is fixed with respect to the polar axis [17]. Therefore, a periodic sign reversal of the nonlinear susceptibility can be obtained by a periodic reversal of the direction of the polar axis (periodic poling) along the propagation direction. The resulting periodic pattern of the nonlinear susceptibility is often referred to as a "QPM grating" with the period Λ_{QPM}. With periodic poling, the $\chi^{(2)}$ grating has the functional form of a square wave in space. In the spatial Fourier domain, this square wave can have frequency components at only odd harmonics of the fundamental grating constant $K = 2\pi/\Lambda_{QPM}$:

$$K_m = \frac{m2\pi}{\Lambda_{QPM}},\ m = 1,3,5,\ldots \tag{2.2}$$

As shown in Fig. 2.2 (c), a harmonic K_m of the fundamental grating constant can be used for quasi-phasematching. Because the Fourier-series expansion coefficient of the m^{th} harmonic of a square wave is $2/(m\pi)$, the effective nonlinear coefficient of the medium for quasi-phase-matched optical wavelength conversion is [19]:

$$\chi_{eff}^{(2)} = \frac{2}{m\pi}\chi^{(2)},\ m = 1,3,5,... \tag{2.3}$$

Therefore, for strongest nonlinear mixing, it is desirable to use first-order quasi-phasematching (m = 1).

2.2 Second Order Nonlinear Optics

In a nonlinear medium the polarization can be written as:

$$\begin{aligned} &\vec{P} = \vec{P}_L + \vec{P}_{NL} \ \text{with} \\ &\vec{P}_L = \varepsilon_0 \chi^{(1)} \vec{E} \quad \text{linear polarization} \\ &\vec{P}_{NL} = \varepsilon_0 (\chi^{(2)} \vec{E}\cdot\vec{E} + \chi^{(3)} \vec{E}\cdot\vec{E}\cdot\vec{E} + \cdots \quad \text{nonlinear polarization} \end{aligned} \tag{2.8}$$

We are interested in the $\chi^{(2)}$ term which leads to three-wave interaction processes. The electromagnetic wave equation for a ferroelectric nonlinear medium can be derived from Maxwell equations by taking into account such a nonlinear polarization term $\vec{P}_{NL}$.

$$\nabla \times \vec{E} = -\frac{\partial \vec{B}}{\partial t} \tag{2.9a}$$

$$\nabla \times \vec{H} = \frac{\partial \vec{D}}{\partial t} \tag{2.9b}$$

$$\nabla \cdot \vec{D} = 0 \ \& \ \nabla \cdot \vec{B} = 0 \tag{2.9c}$$

Where $\vec{E}$ and $\vec{H}$ are the electric and magnetic fields respectively, $\vec{B} = \mu\vec{H}$ ($\vec{B} = \mu_0\vec{H}$ with $\mu_r = 1$ for a non magnetic medium like $LiNbO_3$) is the magnetic flux density and $\vec{D} = \varepsilon_0\varepsilon_r\vec{E} + (\vec{P}_L + \vec{P}_{NL})$ is the electric field displacement. Taking the curl of Eqn. 2.9a and inserting Eqn. 2.9b into its right-hand side, by neglecting the term $\nabla(\nabla.E)$ we arrive at [19]:

$$\nabla^2 \vec{E} + \varepsilon_0\varepsilon_r \mu_0 \frac{\partial^2 \vec{E}}{\partial t^2} = \mu_0 \frac{\partial^2 \vec{P}_{NL}}{\partial t^2} \tag{2.10}$$

as wave equation for a nonlinear medium where the nonlinear polarization ($\vec{P}_{NL}$) is the driving term.

Any $\chi^{(2)}$-based nonlinear process involves three fields at frequencies ω_1, ω_2, and ω_3 which are related to each other by the energy conservation ($\hbar\omega_3 = \hbar\omega_1 + \hbar\omega_2$) law. All the experiments presented in this dissertation, are based on type I (all the interacting waves has the same polarization) QPM nonlinear wavelength conversions. Thus, a single polarization (TM), co-polarized waves are considered for nonlinear interactions. Therefore, scalar magnitudes of P_{NL} can be expressed by:

$$\begin{aligned} P_{NL}(\omega_3) &= 2\varepsilon_0 d_0 d(x,y) d(z) E(\omega_1) E(\omega_2) \\ P_{NL}(\omega_2) &= 2\varepsilon_0 d_0 d(x,y) d(z) E(\omega_3) E^*(\omega_1) \\ P_{NL}(\omega_1) &= 2\varepsilon_0 d_0 d(x,y) d(z) E(\omega_1) E^*(\omega_2) \end{aligned} \qquad (2.11)$$

d_0 is the nonlinear coefficient in single-domain bulk medium and is related to the second order nonlinear susceptibility by $\chi^{(2)} = 2d_0$, d(x,y) is the normalized nonlinearity distribution in the transverse cross-section and ranges between 0 and 1 and d(z) is the normalized nonlinearity distribution in the propagation direction z, and is either +1 or -1. For quasi-phase-matched (QPM) structures which use a periodic axial modulation of the nonlinear coefficient to compensate for index dispersion, d(z) is a periodic function with a modulation period of Λ_{QPM} along the propagation and can be written as a Fourier series:

$$d(z) = \sum_m G_m \exp\left(\frac{-i 2\pi m z}{\Lambda_{QPM}}\right) \qquad (2.12)$$

where the Fourier coefficients are given by:

$$G_m = \frac{1}{\Lambda_{QPM}} \int_{-\Lambda_{QPM}/2}^{\Lambda_{QPM}/2} d(z) \exp\left(\frac{i 2\pi m z}{\Lambda_{QPM}}\right) dz \qquad (2.13)$$

In order to evaluate the QPM nonlinear optical interaction, Eqn. (2.12) was inserted into Eqn. (2.11). The total electric field can be developed as a superposition of waveguide modes of the order of m. It is a reasonable approximation to restrict the confined field to the guided modes, therefore:

$$E(r,t) = \frac{1}{2} \sum_m A_m(z) e^m(x,y) \exp i(\omega t - \beta_m z) + c.c. \qquad 2.14)$$

A_j represents the slowly varying amplitude of the electric field and $e^m(x,y)$ describes the field distribution within the waveguide cross section. Here, m designates the eigenmode of the order of m, which satisfies the Helmholtz equation [40] in the unperturbed waveguide. Substituting equation (2.14) into equation (2.10) under the slowly varying envelope approximation (SVEA), where the field amplitude changes slowly relative to the fast optical carrier frequency, second order derivatives of A_j with respect to the propagation direction z can be neglected, we arrive at:

$$\sum_m -i\beta_m \frac{dA_m}{dz}(z)e^m(x,y)\exp i(\omega t-\beta_m z)+c.c.=\mu\frac{\partial^2 P_{NL}}{\partial t^2} \qquad (2.15)$$

Multiplying equation (2.15) by $e^s(x,y)$ and integrating over the waveguide cross-section by taking into account the modes-orthogonality, $\iint e^l e^m(x,y)\,dx\,dy=\frac{2\omega\mu}{\beta_m}\delta_{lm}$, finally leads to [40]:

$$\frac{dA_s}{dz}(z)\exp i(\omega t-\beta_s z)+c.c.=\mu-\frac{i}{2\omega}\frac{\partial^2}{\partial t^2}\iint P_{NL}e^s(x,y)\,dx\,dy \qquad (2.16)$$

Equation 2.16 can be used to describe a multitude of interactions between guided modes. Assuming the coupling between a discrete combination of modes (e.g. the fundamental ones), equation (2.16) leads to the following set of first-order coupled differential equations for the field amplitudes in propagation direction [22], [23]:

$$\begin{aligned}
\frac{dA_3}{dz}&=-i\kappa_3 A_1 A_2\exp(i\Delta\beta z)-\frac{\alpha_3}{2}A_3\\
\frac{dA_2}{dz}&=-i\kappa_2 A_1^* A_3\exp(-i\Delta\beta z)-\frac{\alpha_2}{2}A_2\\
\frac{dA_1}{dz}&=-i\kappa_1 A_2^* A_3\exp(-i\Delta\beta z)-\frac{\alpha_1}{2}A_1
\end{aligned} \qquad (2.17)$$

where α_i are the power loss coefficients. The wavelength dependent phase mismatch in a QPM structure is compensated by the grating vector $K_{QPM} = 2\pi/m\Lambda_{QPM}$ and is expressed as:

$$\Delta\beta=2\pi\left(\frac{n_3}{\lambda_3}-\frac{n_2}{\lambda_2}-\frac{n_1}{\lambda_1}-\frac{2\pi}{\Lambda_{QPM}}\right)$$

κ is the effective coupling coefficient defined by:

$$\kappa_j = \frac{\pi d_{eff}\,\omega_j}{c\sqrt{2n_1n_2n_3\varepsilon_0 c}}\,\vartheta$$

$d_{eff} \equiv d_0 G_m$ is the effective nonlinearity for the QPM process. When the nonlinear coefficient is modulated with periodic sign reversal, the Fourier coefficient is $G_m = (2/m\pi).\sin(m\pi D)$, where the duty cycle $D = L_c/\Lambda_{QPM}$ is given by the length L_c of a reversed domain divided by the period Λ_{QPM} of domain reversal. The effective nonlinear coefficient for QPM of a first-order process (m = 1) with 50% duty cycle factor is; $d_{eff} = (2/\pi)d_0$. Throughout this dissertation the effective refractive indices of modes j as described by n_j instead of $n_{eff,\,j}$ for simplicity. Since the square of $A_j(z)$ is equal to the power of the corresponding wave (i.e. optical power $P_j(z) = |A_j(z)|^2$), the function $A_j(z)$ containing both amplitude and phase information describes the spatial evolution of the field envelope in the propagation direction z. The coupling coefficients κ_j contain a spatial modal overlap factor ϑ defined by

$$\vartheta = \int_{-\infty}^{\infty}\int d(x,y)\,e_1(x,y)\,e_2(x,y)\,e_3(x,y)\,dx\,dy$$

The inverse square of the overlap integral ϑ is commonly referred to the effective interaction area A_{eff} (i.e. $A_{eff} = 1/|\vartheta|^2$), which describes the strength of the overlap among the modes of the interacting waves and the transverse profile of the normalized nonlinearity.

The solutions of the above equations generally can only be expressed in integral formats and require numerical integration to obtain the results [19]. To study the sensitivity of the conversion efficiency as function of various parameters (wavelength, temperature, waveguide geometry, etc.), we can Taylor expand [24] the phase mismatch $\Delta\beta L$ as a function of an arbitrary parameter ξ as:

$$\Delta\beta L(\xi) = \Delta\beta L(\xi_0) + (\xi-\xi_0)\frac{d}{d\xi}\Delta\beta L(\xi) + (\xi-\xi_0)^2\frac{d^2}{d\xi^2}\Delta\beta L(\xi) + \cdots$$

At $\xi_0 = \xi$, the interaction is phasematched. We define the bandwidth $\Delta\xi_{3dB}$ as the 3 dB bandwidth that occurs when $\mathrm{sinc}^2(x) = 1/2$ at $x = \pm\ 0.443\ \pi$. When the first-order term in the Taylor expansion dominates the phase mismatch, the 3 dB bandwidth is linearly proportional to the inverse of the interaction length as:

$$\Delta\xi_{3dB} = 1.772\pi\left|\frac{d}{d\xi}\Delta\beta L\right|^{-1}$$

In this situation, the phasematching restricts the range of efficient wavelength conversion within a narrow wavelength range. When the first-order term is zero in the Taylor expansion, it is dominated by the second-order term, and the 3 dB bandwidth scales as the inverse square root of length:

$$\Delta\xi_{3dB} = \sqrt{\frac{3.544\pi}{L}\left|\frac{d^2}{d\xi^2}\Delta\beta\right|^{-1}} \tag{2.18}$$

Under certain circumstances, it is possible to design the waveguide geometry such that the first derivative of phasematching condition with respect to various parameters is equal to zero, resulting in a noncritical condition [25]. A more detailed description of tuning and tolerances of nonlinear optical parametric processes can be found in Refs. [26] and [19].

2.3 Second Harmonic Generation (SHG)

In second-harmonic generation (SHG), two photons of the fundamental wave λ_f are combined to generate a single SH photon at $\lambda_{sh} = \lambda_f/2$, satisfying energy conservation. The wavelength dependent phase mismatch incorporating the k vector $K_{QPM} = 2\pi/\Lambda_{QPM}$ of the QPM grating is given by $\Delta\beta_{SHG} = \beta_{sh} - 2\beta_f - K_{QPM}$. For SHG the set of coupled-mode equations 2.17 reduces to two equations [19]:

$$\frac{dA_f}{dz} = -i\kappa_f A_{sh}^* A_f \exp(-i\Delta\beta_{SHG} z) - \frac{\alpha_f}{2} A_f$$

$$\frac{dA_{sh}}{dz} = -i\kappa_{sh} A_f^2 \exp(i\Delta\beta_{SHG} z) - \frac{\alpha_{sh}}{2} A_{sh}$$

Solving this set of differential equations with the initial conditions $A_{sh}(0) = 0$ and $A_f(0) = (P_f)^{1/2}$ with undepleted fundamental or low conversion limit approximation, where the power in the fundamental wave does not significantly decrease due to frequency conversion or propagation losses, we get for an interaction length of L [21]:

$$P_{sh}(L) = \eta_{nor} P_f^2 L^2 \operatorname{sinc}^2\left(\frac{\Delta\beta_{SHG} L}{2}\right)$$

where $\eta_{nor} = (\kappa_{SHG}/2)^2$ is the normalized conversion efficiency (with respect to the square of the length L). It is given in units of %/(Wcm^2) and can reach values larger than 12 %/(Wcm^2) in current state-of-the-art Ti indiffused PPLN waveguide devices for the 1.5 μm band. In case of phasematching ($\Delta\beta_{SHG} = 0$), the SHG conversion effi-

ciency is given by $\eta_{SHG} = P_{sh}(L)/P^2_f = \eta_{nor}L^2$ and can reach values of 1000 %/W for a waveguide device with about 9 cm long QPM grating.

In Fig. 2.3 the calculated transmission SHG spectra of several waveguides with different lengths are shown as an example. The full-width-half-maximum (FWHM) of the $sinc^2$-shaped SHG characteristics is narrowing with increasing interaction length as expected from Eqn. 2.18.

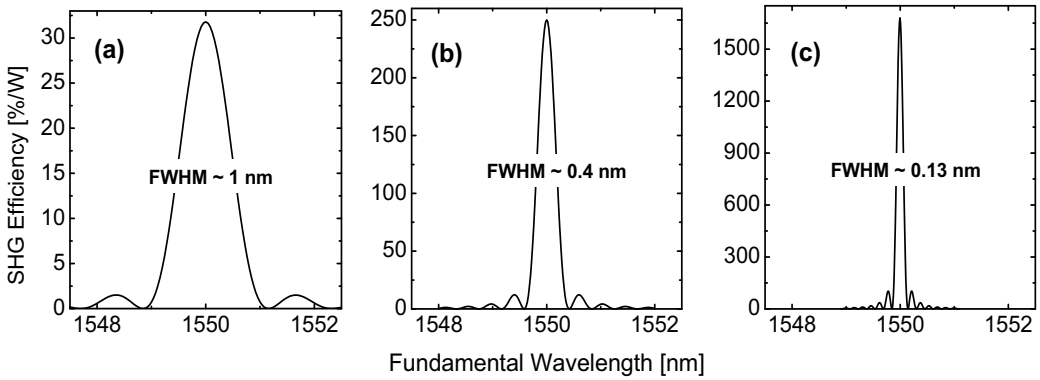

Fig. 2.3: Calculated SHG spectra versus fundamental wavelength for 1 cm (a), 3 cm (b), and 9 cm (c) long interaction lengths of PPLN waveguides. The FWHM of the SHG response is narrowing with increasing interaction length L.

2.4 Sum Frequency Generation (SFG)

In the sum frequency generation (SFG) process, the pump (λ_p) and the signal (λ_s) waves are combined to generate a sum frequency wave ($1/\lambda_{sf} = 1/\lambda_s + 1/\lambda_p$) at shorter wavelength with the wavelength dependent phase mismatch of $\Delta\beta_{SFG} = \beta_{sf} - \beta_p - \beta_s - K_{QPM}$. If A_1 is referred as pump, A_2 as signal and A_3 as sum frequency amplitudes, the coupled mode equations 2.17 become [19]:

$$\frac{dA_p}{dz} = -i\kappa_p A_s^* A_{sf} \exp(-i\Delta\beta_{SFG} z) - \frac{\alpha_p}{2} A_p$$

$$\frac{dA_s}{dz} = -i\kappa_s A_{sf} A_p^* \exp(-i\Delta\beta_{SFG} z) - \frac{\alpha_s}{2} A_s$$

$$\frac{dA_{sf}}{dz} = -i\kappa_{sf} A_p A_s \exp(i\Delta\beta_{SFG} z) - \frac{\alpha_{sf}}{2} A_{sf}$$

In the undepleted pump regime we have $dA_p/dz = 0$. Assuming zero phase mismatch ($\Delta\beta_{SFG} = 0$) and by applying the following initial conditions;

$$A_p(0)=\sqrt{P_p(0)},\ A_s(0)=\sqrt{P_s(0)},\ A_{sf}(0)=0$$

we arrive at the following analytical solution:

$$P_s(z)=P_s(0)\cos^2(\sqrt{\eta_{norm}P_p(0)}\,z),\ P_{sf}(z)=\frac{\lambda_s}{\lambda_{sf}}\sin^2(\sqrt{\eta_{norm}P_p(0)}\,z) \qquad (2.19)$$

where $\eta_{norm} \equiv \kappa_s\kappa_{sf}$ is the normalized SFG power efficiency in the low conversion limit.

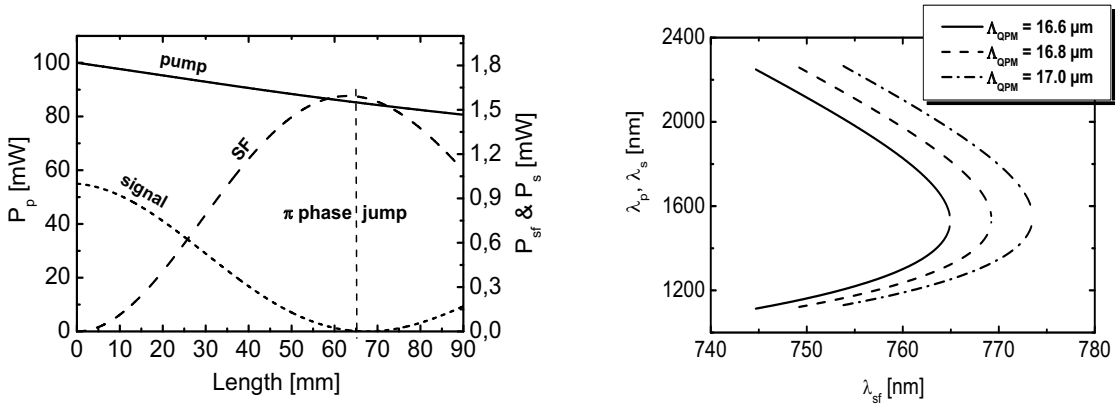

Fig. 2.4: Left: Calculated power evolution of the pump (λ_s = 1555 nm), signal (λ_s = 1545 nm) and SF (λ_s = 775 nm) waves along the 90 mm long PPLN waveguide during SFG process in a PPLN channel guide. Right: Phasematching curve for different micro domain periodicities (Λ_{QPM}).

In Fig. 2.4, as an example, the calculated power evolution of the interacting waves is plotted along a 90 mm PPLN waveguide. 100 mW of coupled pump power together with 1 mW of coupled signal power is assumed. The signal wave is depleted due to SFG. At 65 mm the signal power approaches zero; it rises again with increasing interaction length via difference frequency generation (DFG) of sum frequency and pump waves. This process induces a phase of π to the signal. More information and an interesting switching scheme are reported in Ref. [51]. Fig. 2.4, right, presents the calculated tuning characteristics for different micro-domain periodicities. For larger Λ_{QPM}, QPM wavelengths are shifted towards longer wavelengths.

2.5 Difference Frequency Generation

Difference frequency generation (DFG) is a three-wave-mixing process where a strong pump wave (λ_p) is combined with a (usually weak) signal wave (λ_s) to

generate a wavelength shifted idler wave ($1/\lambda_i = 1/\lambda_p - 1/\lambda_s$). For a continuous wave (cw) pump Eqn. 2.14 can be expressed as:

$$\begin{aligned}
\frac{dA_p}{dz} &= -i\kappa_p A_s A_i \exp(i\Delta\beta_{DFG} z) - \frac{\alpha_p}{2} A_p \\
\frac{dA_s}{dz} &= -i\kappa_s A_i^* A_p \exp(-i\Delta\beta_{DFG} z) - \frac{\alpha_s}{2} A_s \\
\frac{dA_i}{dz} &= -i\kappa_i A_p A_s^* \exp(-i\Delta\beta_{DFG} z) - \frac{\alpha_i}{2} A_i
\end{aligned} \tag{2.20}$$

Equations (2.20) represent useful formulas for describing QPM guided-wave DFG. In the limit of an undepleted pump and a lossless waveguide, one can get analytic solutions for DFG using the boundary condition $A_i(0) = 0$ [19]:

$$\begin{aligned}
A_s(L) &= A_s(0)\cosh(gL) \\
A_i(L) &= \sqrt{\frac{\lambda_s}{\lambda_i}} \frac{\sqrt{\eta_{norm} P_p(0)}}{g} \exp(-i\Delta\beta L/2) A_s^*(0) \sinh(gL)
\end{aligned} \tag{2.21}$$

The gain coefficient g is defined as:

$$g = \sqrt{\eta_{norm} P_p(0) - (\Delta\beta L/2)^2} \tag{2.22}$$

The above parametric process enables operation at arbitrarily low input signal powers, preserves signal phase information and reverses the sign of the signal phase ($A_i \propto A_s^*$). By calculating the power of the output idler wave (Eqn. 2.21), we obtain the power conversion efficiency of DFG defined as;

$$\eta_{DFG} = \frac{P_i(L)}{P_s(0)} = \frac{\lambda_s}{\lambda_i} \frac{\eta_{norm} P_p(0)}{g^2} \sinh^2(gL) \tag{2.23}$$

which in the low gain limit can be written as:

$$\begin{aligned}
\eta_{DFG} &\approx \frac{\lambda_s}{\lambda_i} \eta_{norm} L^2 P_p(0) \operatorname{sinc}^2\left(\frac{\Delta\beta_{DFG} L}{2}\right) \\
&\propto \frac{d_{eff}^2}{n^3} \frac{1}{A_{eff}} P_p(0) \operatorname{sinc}^2\left(\frac{\Delta\beta_{DFG} L}{2}\right).
\end{aligned}$$

This shows the relationship of conversion efficiency and material properties (d_{eff} and n), device geometry (A_{eff} and L), pump power, and the phase mismatch term

($sinc^2$ ($\Delta\beta L/2$)). The calculated power evolution of pump, signal and generated idler wave is presented in Fig. 2.5, left.

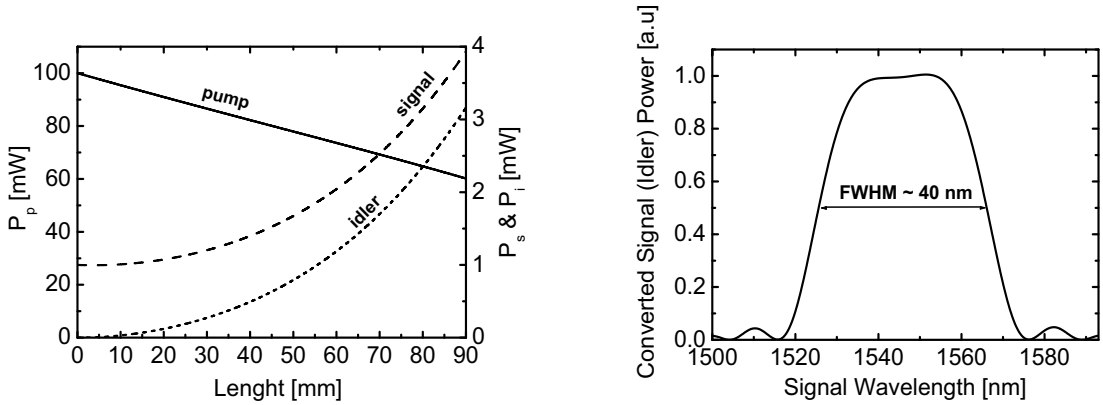

Fig. 2.5: Left: Calculated power evolution of pump (λ_s = 775 nm), signal (λ_s = 1545 nm) and idler (λ_i = 1555 nm) versus propagation length during DFG process. Right: Generated idler (or signal) power versus signal wavelength with about 40 nm operation bandwidth. A 90 mm long PPLN waveguide is assumed for the calculation.

To see the utility of a DFG-based wavelength converter for communication applications, consider a pump with a wavelength close to half that of the input signal. With $1/\lambda_p = 2(1/\lambda_s) - \Delta$, the output wavelength is $1/\lambda_i = 1/\lambda_s + \Delta$; that is, the output wavelength is shifted by an amount controlled by the offset of the pump wavelength. Another important property of a DFG-based wavelength converter results from the proportionality of the output wave to the complex conjugate of the input signal wave. If a chirped input signal spectrum E ($\omega_p/2 + \Delta$) is mixed with a pump at ω_p, the output spectrum is then E* ($\omega_p/2 - \Delta$), effectively reversing the chirp on the input signal. This function allows complete "mid-span" correction of chromatic dispersion in any arbitrarily dispersed fiber links [15], [18].

A DFG process is always accompanied by amplification of the input signal; this phenomenon is called optical parametric amplification (OPA). One higher energy (shorter wavelength) pump photon decays to generate two lower energy (longer wavelength) photons: one idler photon and one additional signal photon (see Fig. 2.5, left). DFG is the main parametric process for converting data signals in the C-band. If the pump wavelength is chosen to be at the degeneracy point of the phasematching curve (see Fig. 2.4, right), DFG/OPA is a broad band process. As an example, the calculated bandwidth of DFG in a 90 mm long PPLN waveguide is shown in Fig. 2.5, right.

2.6 Cascaded Second Order Nonlinear Optical Wavelength Conversion

Nonlinear wavelength conversion can also be carried out using a $\chi^{(2)}$:$\chi^{(2)}$ process [52, 53, 54] where both, fundamental and signal, are within the same band. The interaction involves the cascading of SHG and DFG (cSHG/DFG) or SFG and DFG (cSFG/DFG). The second process enables a tuning of the generated idler with fixed signal but tuneable control wavelength. In the following a brief explanation of these interactions is presented.

Cascaded Second Harmonic Generation and Difference Frequency Generation (cSHG/DFG)

We can classify the cSHG/DFG processes as co-propagating simultaneous cSHG/DFG or separated sequential SHG and DFG in a counter-propagating scheme. In the second scheme the generated SH wave is reflected by an endface mirror and mixes with a signal wave coupled to the waveguide counter directionally. A schematic plot of these processes is shown in Fig. 2.6.

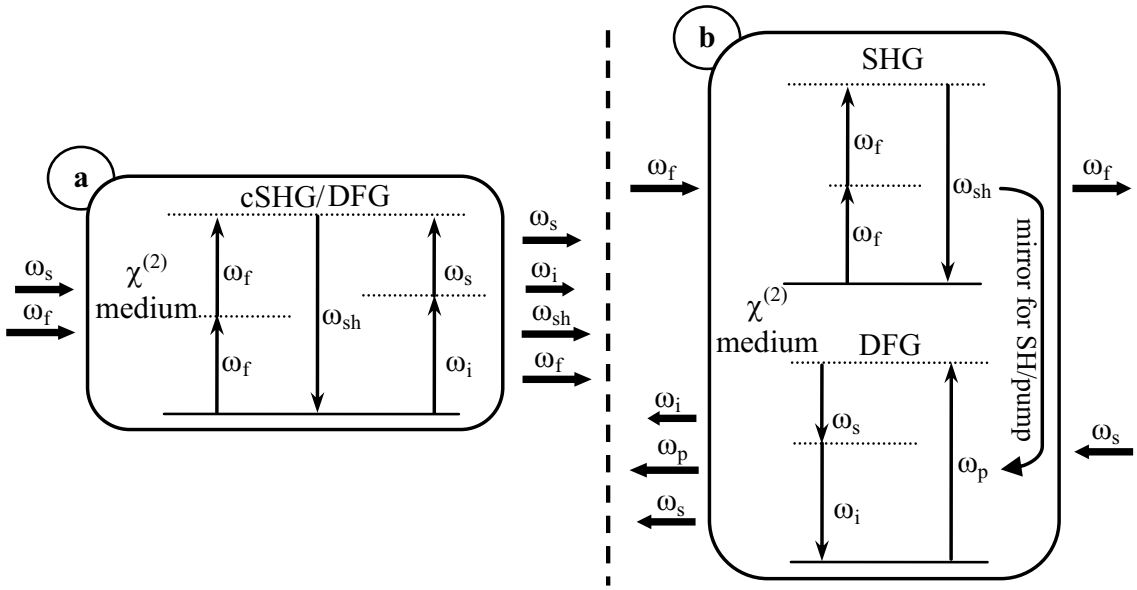

Fig. 2.6: Left: Scheme of cSHG/DFG-based wavelength conversion. Right: separated SHG/DFG-based wavelength conversion in a counter-propagation scheme.

In cSHG/DFG, the coupled fundamental wave (λ_f) generates a quasi-phase-matched SHG wave ($\lambda_{sh} = \lambda_f/2$). Simultaneously, the generated SH wave is mixed (as a pump for DFG) with the input signal wave (λ_s) to generate a wavelength-shifted

output idler ($1/\lambda_i = 1/\lambda_{sh} - 1/\lambda_s$). Since all the input waves are within the same band ($\lambda_f \approx \lambda_s \approx \lambda_i$ and $\lambda_{sh} = \lambda_f/2$), QPM guaranties the selective mode excitation of the pump (SH) wave [11].

The coupled-mode equations describing the co-propagating simultaneous cSHG/DFG can be expressed as [19]:

$$\begin{aligned}
\frac{dA_f}{dz} &= -i\kappa_f A_{sh}^* A_f \exp(-i\Delta\beta_{SHG} z) - \frac{\alpha_f}{2} A_f \\
\frac{dA_{sh}}{dz} &= -i\kappa_{sh} A_f^2 \exp(i\Delta\beta_{SHG} z) - i\kappa_{sh} A_i A_s \exp(i\Delta\beta_{DFG} z) - \frac{\alpha_{sh}}{2} A_{sh} \\
\frac{dA_s}{dz} &= -i\kappa_s A_i^* A_{sh} \exp(-i\Delta\beta_{DFG} z) - \frac{\alpha_s}{2} A_s \\
\frac{dA_i}{dz} &= -i\kappa_i A_{sh} A_s^* \exp(-i\Delta\beta_{DFG} z) - \frac{\alpha_i}{2} A_i
\end{aligned} \qquad (2.24)$$

where the phase mismatch is determined by $\Delta\beta_{SHG} = \beta_{sh} - 2\beta_f - K_{QPM}$ for SHG and $\Delta\beta_{DFG} = \beta_{sh} - \beta_s - \beta_i - K_{QPM}$ for DFG. For such a parametric process a significant depletion of the fundamental radiation is required to generate sufficient SH power (pump for DFG). In general, a numerical analysis is used to solve these four coupled mode equations [24]. To get some insight into the conversion process, we derive the simplest analytic solution by assuming that the depletion of the cw-fundamental and waveguide propagation losses can be ignored. The analytical solution for this case yields the conversion efficiency $\eta_{cSHG/DFG}$:

$$\eta_{cSHG/DFG} \approx \frac{1}{4} \eta_{norm} L^4 P_f^2$$

The conversion efficiency depends on the length of the device raised to the power of four due to the cascaded process; thus it is important to have a long device to achieve significant conversion efficiency. In practice, owing to the fundamental depletion and waveguide propagation losses, the dependence on the length is less than the fourth power. The properties and bandwidth of cSHG/DFG are similar to those of directly pumped DFG, since the idler is actually generated through the DFG process. The above description ignores the possible direct interaction of fundamental and signal waves via sum-frequency generation. In general, it will happen only when the input signal is tuned too close to the fundamental wavelength (i.e. within the narrow sum-frequency bandwidth < 0.2 nm for a 90 mm long PPLN waveguide). The complete equations for describing such interactions are given in the next section.

The separated sequential cSHG/DFG interaction also involves a SHG process and a DFG process, but both processes do not happen simultaneously since counter-propagating fundamental and signal waves are used. A schematic plot of the counter propagation process is shown in Fig. 2.6 right. In such a process, the fundamental wave is converted to a SH wave, then the generated SH wave is reflected from the end face mirror of the waveguide and used as the pump for the DFG process in backward direction. The coupled-mode equations can be written as:

For SHG:

$$\begin{aligned}\frac{dA_f}{dz} &= -i\kappa_f A_{sh}^* A_f \exp(-i\Delta\beta_{SHG} z) - \frac{\alpha_f}{2} A_f \\ \frac{dA_{sh}}{dz} &= -i\kappa_{sh} A_f^2 \exp(i\Delta\beta_{SHG} z) - \frac{\alpha_{sh}}{2} A_{sh}\end{aligned} \tag{2.22}$$

And for DFG:

$$\begin{aligned}\frac{dA_{sh}}{dz} &= -i\kappa_{sh} A_i A_s \exp(i\Delta\beta_{DFG} z) - \frac{\alpha_{sh}}{2} A_{sh} \\ \frac{dA_s}{dz} &= -i\kappa_s A_i^* A_{sh} \exp(-i\Delta\beta_{DFG} z) - \frac{\alpha_s}{2} A_s \\ \frac{dA_i}{dz} &= -i\kappa_i A_{sh} A_s^* \exp(-i\Delta\beta_{DFG} z) - \frac{\alpha_i}{2} A_i\end{aligned} \tag{2.23}$$

By solving the SHG and DFG equations separately, we can get a solution for the cSHG/DFG process with counter propagating beams. In the limit of undepleted pump and a lossless waveguide, one gets a stationary solution by use of the boundary condition [55]. The power conversion efficiency can be expressed as:

$$\eta_{DFG} = \frac{P_i(L)}{P_s(0)} = \frac{\lambda_s}{\lambda_i} \frac{\eta_{norm} P_{sh}}{g^2} \tanh^2 \sqrt{\eta_{norm} L^2 P_{sh}} \sinh^2(gL)$$

One major advantage of using counter-propagating beams is that the full length of the device is used twice and thus the interaction is more efficient than in the co-propagating scheme.

The performance of the counter-propagating scheme in comparison with the co-propagating scheme can be assessed with the modelling results presented in Fig. 2.7. The left diagram shows the evolution of fundamental, SH, signal and idler power levels along the propagation direction for cSHG/DFG assuming propagation losses of 0.1 dB/cm around 1.55 μm wavelength and 0.2 dB/cm at the SH wavelength for a 90 mm long PPLN channel guide. The right diagram shows the conversion efficiencies for counter-propagating separated SHG and DFG and co-propagating

cSHG/DFG compare as a function of the length of a PPLN waveguide. At 100 mW of coupled fundamental power the expected improvement of the counter-propagating approach compared to the co-propagating scheme is ~ 5 dB.

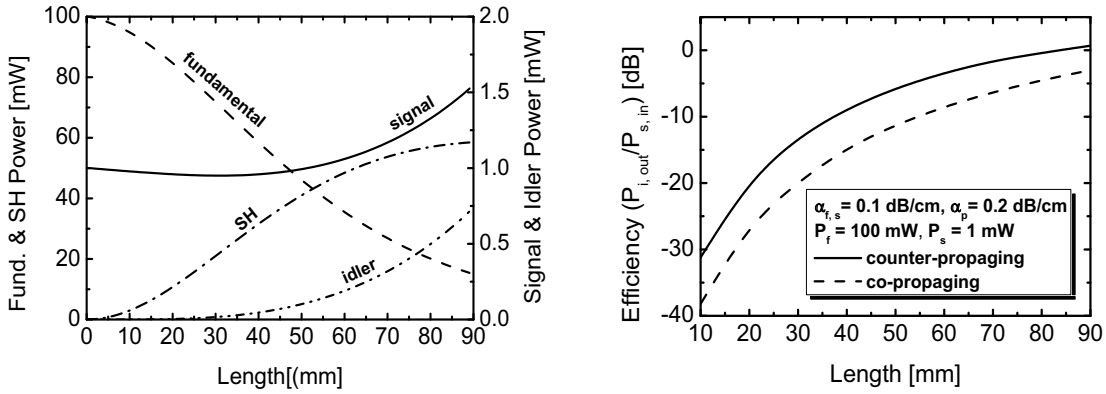

Fig.2.7: Left: Calculated evolution of the fundamental (λ_f = 1550 nm), SH (λ_{sh} = 775 nm), signal (λ_s = 1560 nm), and generated idler (λ_i = 1540.1 nm) power levels in a cSHG/DFG process along a 90 mm PPLN waveguide for 100 mW and 1 mW of coupled fundamental and signal powers, respectively. Right: calculated efficiency of wavelength conversion using a co- and counter-propagating scheme versus PPLN waveguide length.

Cascaded Sum Frequency Generation/Difference Frequency Generation (cSFG/DFG)

Wavelength conversion by cSFG/DFG in PPLN waveguides is greatly desirable in the future optical networks to construct a much more flexible communication system. Since for cSHG/DFG the small acceptance bandwidth for SHG, defined by the QPM condition, restricts the fundamental wavelength tolerance, it is difficult to implement tuneable wavelength conversion. To overcome this restriction, cascaded sum and difference frequency generation (cSFG/DFG) was proposed in recent years [27], [28].

Fig. 2.8 shows the operation principle and the potential for tuneable-in tuneable-out all optical wavelength conversion exploiting the cSFG/DFG approach. An input signal wave (λ_s) interacts with a pump wave (λ_p) and generates the sum frequency (SF) wave ($1/\lambda_{sf} = 1/\lambda_s + 1/\lambda_p$) via SFG. The generated SF wave together with a tunable control wave (λ_c) then generates a tuneable wavelength shifted idler ($1/\lambda_i = 1/\lambda_{sf} - 1/\lambda_c$) via DFG.

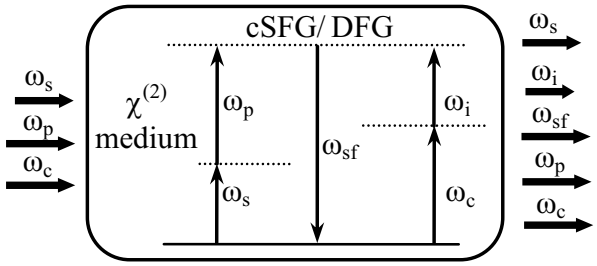

Fig. 2.8: Scheme of tuneable wavelength conversion by cSFG/DFG in a Ti:PPLN channel guide. The signal (ω_s) wave and the tuneable pump wave (ω_p) generate a SF (ω_{sf}) wave. The tuneable control (ω_c) wave together with the SF wave generate the tuneable wavelength converted idler (ω_i) wave via DFG.

The coupled-mode equations describing cSFG/DFG can be expressed as:

$$\begin{aligned}
\frac{dA_p}{dz} &= -i\kappa_p A_{sf} A_p^* \exp(-i\Delta\beta_{SFG} z) - \frac{\alpha_p}{2} A_p \\
\frac{dA_s}{dz} &= -i\kappa_s A_{sf} A_p^* \exp(-i\Delta\beta_{SFG} z) - \frac{\alpha_s}{2} A_s \\
\frac{dA_{sf}}{dz} &= -i\kappa_{sf} A_p A_s \exp(i\Delta\beta_{SFG} z) - i\kappa_{sf} A_i A_c \exp(i\Delta\beta_{DFG} z) - \frac{\alpha_{sf}}{2} A_{sf} \\
\frac{dA_c}{dz} &= -i\kappa_c A_i^* A_{sf} \exp(-i\Delta\beta_{DFG} z) - \frac{\alpha_c}{2} A_c \\
\frac{dA_i}{dz} &= -i\kappa_i A_{sf} A_c^* \exp(-i\Delta\beta_{DFG} z) - \frac{\alpha_i}{2} A_i
\end{aligned} \tag{2.24}$$

where wavelength dependent phase mismatch is defined by $\Delta\beta_{SFG} = \beta_{sf} - \beta_p - \beta_s - K_{QPM}$ for SFG and $\Delta\beta_{DFG} = \beta_{sf} - \beta_c - \beta_i - K_{QPM}$ for DFG. For such a parametric process, significant depletion of the signal wave is required to generate sufficient SF (pump for DFG) power.

A numerical analysis is used in general to solve these five coupled mode equations [24]. In Fig. 2.9, as an example, the evolution of pump, signal, SF, control and idler power levels along a 90 mm long PPLN waveguide has been calculated for P_p = 60 mW and P_c = 70 mW coupled pump and control wave powers, respectively.

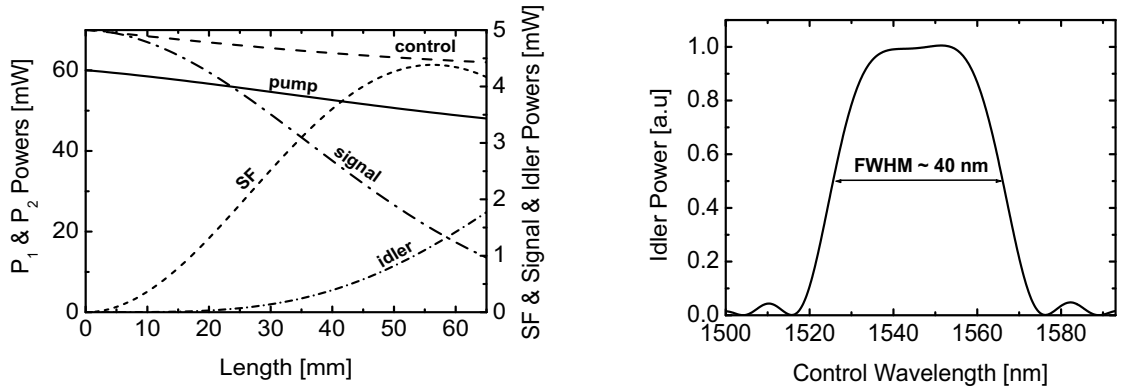

Fig.2.9: Left: Calculated power level evolution of pump (λ_p = 1545 nm), fixed signal (λ_s = 1555 nm), SF (775 nm rang), control (λ_c = 1560 nm), and tuneable idler (λ_i = 1540 nm) waves along a 90 mm PPLN waveguide for 60 (70) mW of coupled pump and control power levels, respectively. Right: Generated idler power versus control wavelength. The operation bandwidth is about 40 nm.

2.6 Summary

In this chapter, we have developed coupled-mode equations for QPM guided-wave nonlinear wavelength conversion, including SHG, SFG, and DFG and for cascaded second-order nonlinear wavelength conversion such as cSHG/DFG and cSFG/DFG. We have also discussed their simplified solutions to illustrate the dependence on several important parameters. The use of DFG requires a pump (~780 nm) at roughly half of the signal wavelength for frequency mixing within the 1.5 μm band. However, by use of cascaded $\chi^{(2)}$:$\chi^{(2)}$ processes a fundamental (pump and control for cSFG/DFG) wavelength within the 1.5 μm band is allowed: it involves the cascading of SHG and DFG.

3. Titanium Indiffused Periodically Poled Lithium Niobate Waveguides: Fabrication & Characterization

Interaction of confined electromagnetic waves in a long nonlinear optical waveguide can increase the nonlinear wavelength conversion efficiency by orders of magnitude, as compared to bulk media [35]. Therefore suitable materials with appropriate micro-structured nonlinearity for quasi-phasematching (QPM) in homogeneous low loss waveguides are required. In this work, $LiNbO_3$ is chosen as a substrate to demonstrate efficient all optical wavelength converter (AOWC). By improvements in periodic poling and waveguide preparation techniques, devices with second harmonic generation (SHG) efficiency of ~1000 %/W were developed for this work. This chapter describes the fabrication of titanium indiffused in congruent lithium niobate (CLN) straight (section 3.1) and bent (section 3.3) waveguides. The waveguide samples have been prepared in the technology lab of the Applied Physics/Integrated Optics group of Prof. Sohler. Their linear optical characterization for telecommunication applications are presented as well. The poling technique to fabricate periodically poled lithium niobate (PPLN) is mentioned briefly in section 3.2. The photorefraction effect is discussed in section 3.4 of this chapter.

3.1 Titanium Indiffused Waveguide Fabrication

The waveguide fabrication by metal indiffusion was demonstrated for the first time in 1974 [29]. Indiffusion of metallic Titanium into a lithium niobate substrate ($Ti:LiNbO_3$) is the most widely used waveguide fabrication method around the world and the required technology is well established [30], [31]. In contrast to proton exchanged waveguides, $Ti:LiNbO_3$ waveguides can guide both, TE and TM polarisations, and the nonlinear properties of the substrate materials after Ti indiffusion are preserved. Waveguides with propagation losses as low as only 0.03 dB/cm have been fabricated for this work.

Fig. 3.1 presents the fabrication steps of a $Ti:LiNbO_3$ channel waveguide. The only difference to fabricate $Ti:LiNbO_3$ waveguides for this work as compared with Ref. [24] is the diffusion temperature and time. In order to avoid reverse poling

during indiffusion into a + Z surface, the temperature is reduced by 30 °C to 1030 °C over a longer (13.2 hrs.) diffusion time [32].

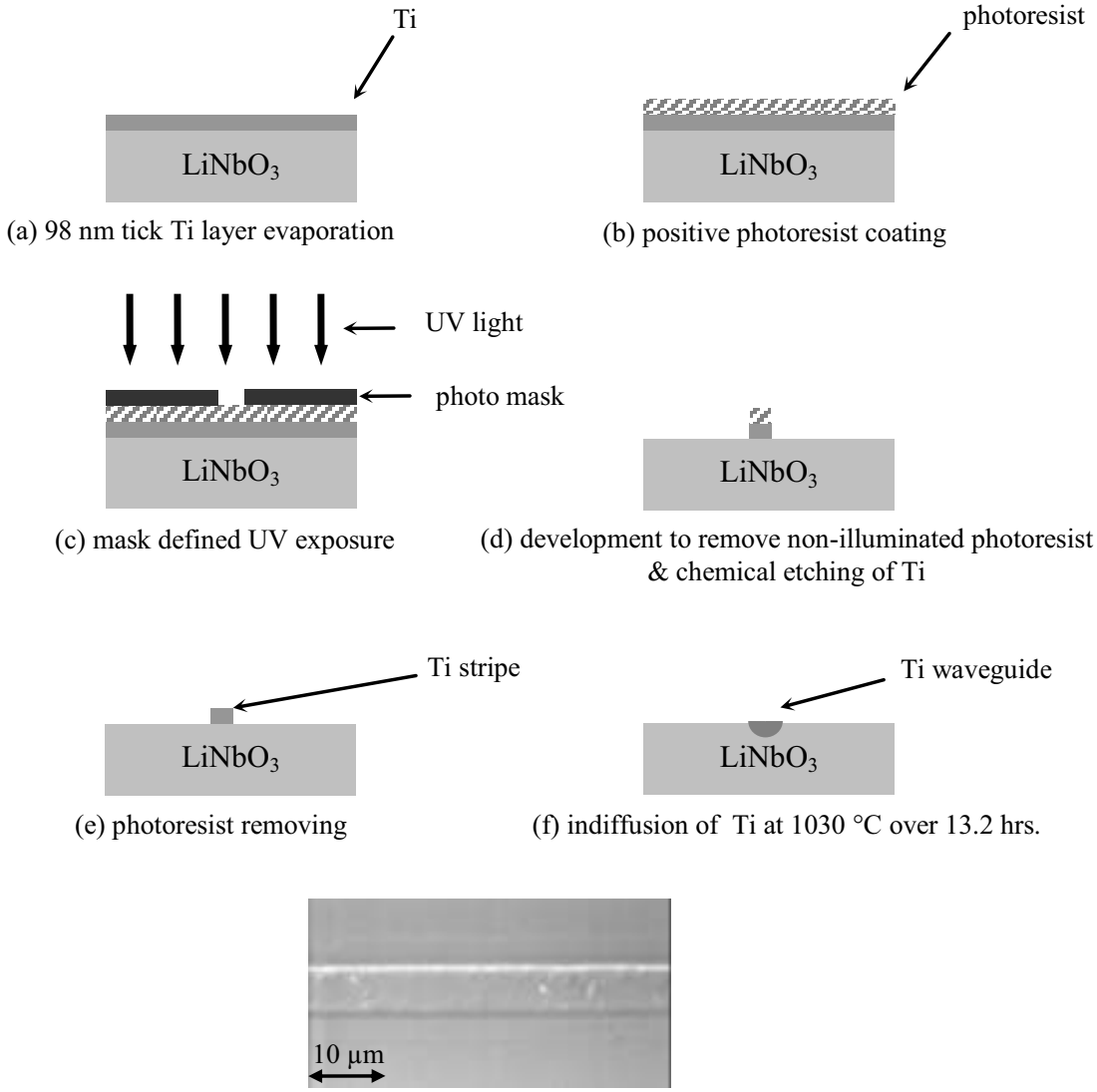

Fig. 3.1. Sketch of different steps to fabricate Ti:$LiNbO_3$ channel waveguides.

In order to fabricate waveguides single mode in the telecommunication band a Ti thickness of about 100 nm is required [24]. Therefore, after cutting the 12 mm wide piece from a 4 inches diameter $LiNbO_3$ wafer, the – Z surface of the $LiNbO_3$ sample was e-beam coated by about 100 nm of Ti. Photolithographically delineated 5, 6 and 7 µm wide Ti stripes are then indiffused to the – Z surface of the sample at 1030 °C over 13.2 hours in an argon atmosphere. Subsequently, post diffusion follows at the

same temperature in oxygen to reoxidize the material. The fabricated waveguides have to be tested under the optical microscope to verify the quality as compared to the chromium mask used for the fabrication (Fig. 3.1g). To enable near field intensity distribution (mode size) and scattering loss measurements, the waveguide sample is cut rectangular and endface polished. Characterization results obtained from an 88 mm long sample, Pb293z, are presented in Fig. 3.2.

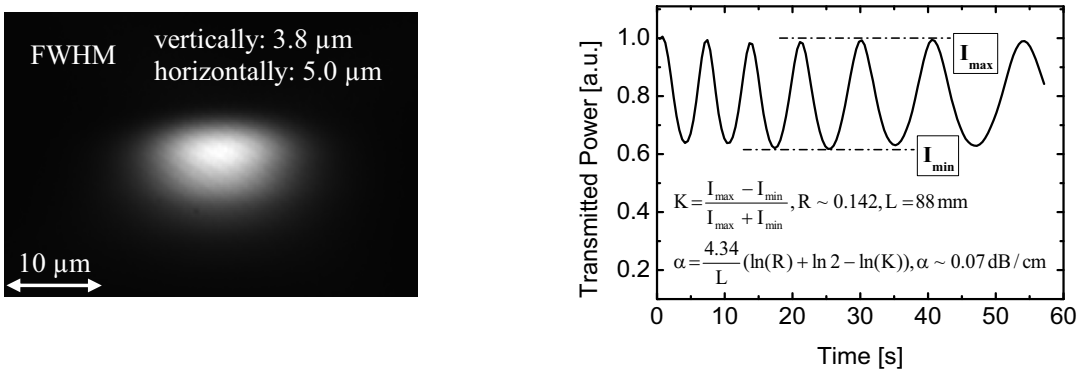

Fig. 3.2: Left: Measured near field intensity distribution of a TM-mode at 1550 nm wavelength in a 7µm wide Ti:$LiNbO_3$ channel waveguide. Right: Transmitted power through a Ti:$LiNbO_3$ waveguide versus time when its temperature is changing continuously. Due to the known endface reflectivities (14.2 %), the contrast K of the measured resonances allows to evaluate the attenuation coefficient α [34]. The equations to obtain the loss coefficient are given as inset.

3.2 Electric Field Periodic Poling

A detailed description of the electric field poling of Ti:$LiNbO_3$ waveguide samples can be found in Ref. [24]; therefore, it will not be explained in detail here. The different poling steps in order to get an appropriate periodically poled lithium niobate (PPLN) waveguide are summarized in Fig. 3.3. The poling process always starts from the + Z face of $LiNbO_3$ and the waveguides are made in the – Z face. Therefore, to get a homogeneous periodic microdomain structure in the waveguides, a two step electric field poling technique has been developed [24], [33]. The spontaneous polarization of the whole substrate was reversed in the first step (Fig. 3.3b); in this way waveguides are located in the + Z face where poling electrodes were fabricated. Thus, the domain structure can be precisely defined in a surface layer including the waveguides. A lithographically defined periodic photoresist structure is formed on the + Z face of the sample surface. In order to have a homogeneous distribution of the applied electric field, the liquid electrodes of LiCl dissolved in isopropylalcohol were used. Thereafter, by application of a high voltage

to exceed the coercive field strength of $LiNbO_3$ of about 21-22 kV/mm [35], periodic poling was accomplished. Monitoring of the displacement current due to the reversed poling is an essential tool to control the process. The poling process was stopped, when the charge Q ($Q = 2P_{spon} \times A_{pol}$ where $P_{spon} \sim 80$ μC/mm [36] is the spontaneous polarization of LN and A_{pol} is the area of the inversion region) was transferred to the sample to compensate the inversion of the spontaneous polarization. The charge Q was adjusted to get a 50/50 duty cycle of the domain pattern. By this technique homogeneous periodically poled gratings of periods around 16 μm for samples up to 95 mm long were achieved. Finally, thermal annealing at ~ 400 °C over 2 hours [37] is performed to reduce as much as possible the optical losses induced by mechanical stress near the domain walls.

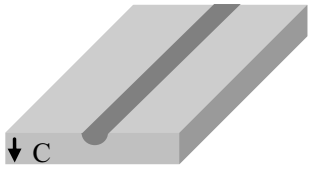

(a) Ti:$LiNbO_3$ channel waveguide fabricated on the – Z surface of the $LiNbO_3$ substrate

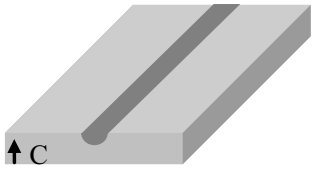

(b) homogenous spontaneous polarization reversal (Ti:$LiNbO_3$ on the + z surface)

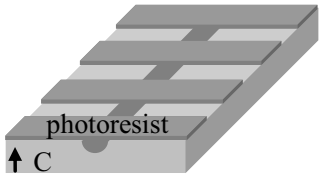

(c) photolithographically defined photoresist structure

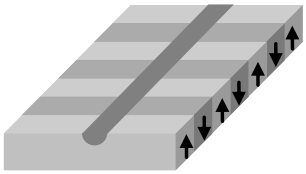

(d) electric field poling and photoresist removing

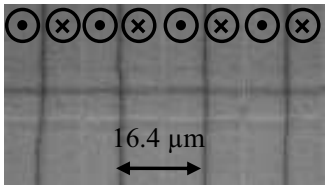

(f) Ti:PPLN waveguide after slight etching of the surface under the microscope

Fig. 3.3: Sketch of different steps to fabricate PPLN waveguides.

3.3 Ti:PPLN Bent Waveguides

The efficiency of nonlinear parametric processes strongly depends on the interaction length as it has been shown in chapter 2. Therefore, a fabrication of long waveguides is of great interest. The state of the art of crystal growth of $LiNbO_3$ allows making optically polished crystal wafers up to 4 inches of diameter. Therefore, the maximum interaction length for straight waveguides in such a wafer after cutting and polishing is about 95 mm. Though such an interaction length is much larger in comparison with bulk optics, longer waveguides would allow to demonstrate even more efficient nonlinear integrated optical devices. With appropriate low bending losses the waveguides [38] the interaction length twice as large as that of straight waveguides was realized.

Because of the weak index difference in Ti indiffused waveguides, the bending radius has to be rather large to avoid bending losses [39]. Therefore, bent waveguide fabrication has to be done in the whole $LiNbO_3$ wafer. The waveguide fabrication process is the same as for straight waveguides but using a different mask. The mask consists of 17 U shaped waveguides parallel to each other. The two straight parts of the waveguides have ~ 37 mm length and the radius of curvature varies from 20 to 36 mm. In this way, the last waveguide length in the outer side can exceed 18.5 cm. Although the fabrication of the waveguide itself is straightforward, a poling of the bent section of the waveguides with a continuous rotation of the domain structure was not possible.

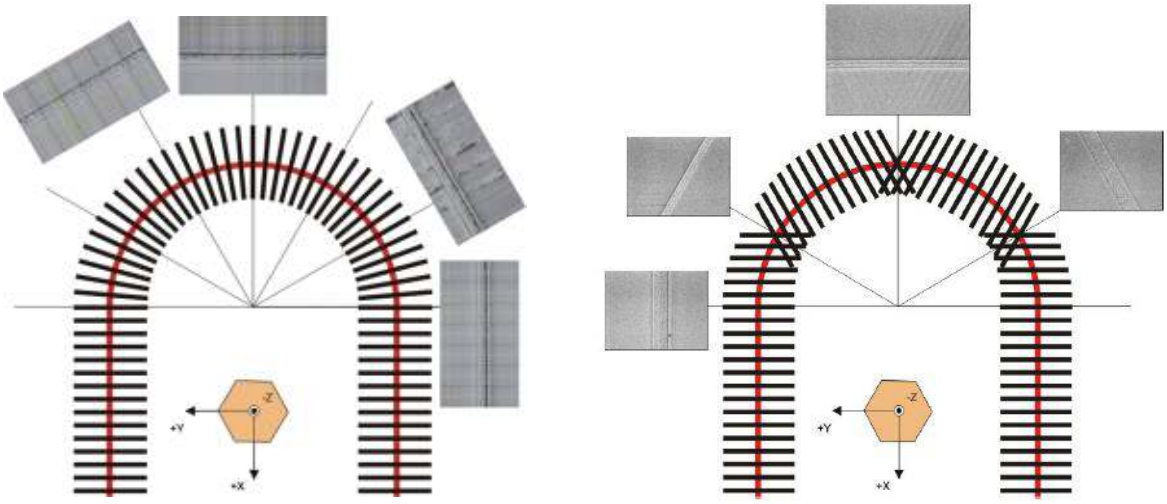

Fig. 3.4: Schematic diagram of the waveguide and periodic poling orientation relative to the crystallographic axes: Left: Periodic poling oriented perpendicular to the waveguide and corresponding pictures after the poling. Right: Periodic poling oriented under angle to the waveguide parallel to the crystallographic axes and corresponding pictures after the poling.

The samples with continuous periodic domains followed by the bent waveguide have shown burned areas near the domain walls in the bending section of the waveguide (Fig. 3.4 left). The poling process is stopped and doesn't continue through the whole 0.5 mm crystal (Fig. 3.4 right). Therefore an inhomogeneous profile of the walls on the surface does not allow reaching proper domain periodicity and therefore phase matching condition. Further work has shown that the growth of domains with walls parallel to the main crystallographic axis is preferred. Therefore, recent developments with periodical poling oriented all the time parallel to the crystallographic axis was used (Fig. 3.4 right). Fig. 3.5 presents the characterization results obtained from such a bent waveguide sample. Waveguide losses for a smaller radius of the curvature are larger due to increased bending losses. They become smaller for the outer waveguides approaching the losses of straight waveguides at a radius larger than 30 mm (Fig. 3.5 right).

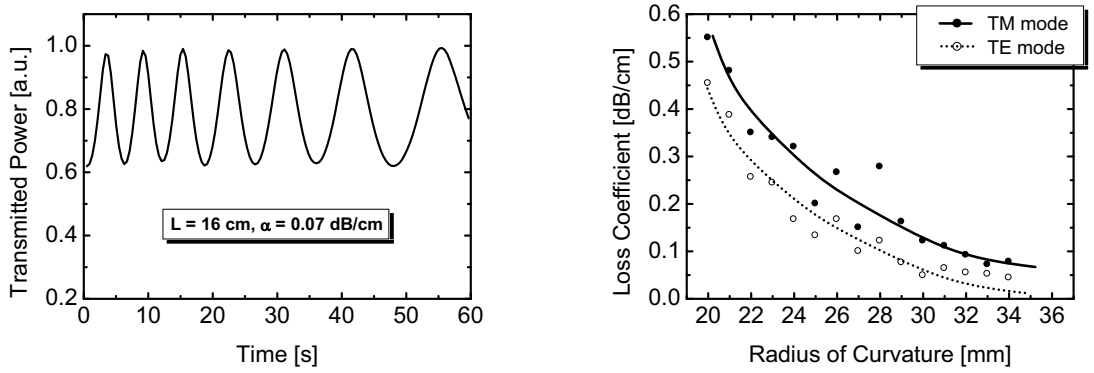

Fig. 3.5: Characterization of a bent waveguide at 1550 nm wavelength. Left: Transmitted power through a 16 cm long bent waveguide versus time when its temperature is changing continuously. Right: Measured losses in the bent waveguides vs. radius of curvature.

3.5 Summary

A brief description of the basic Ti:PPLN waveguide fabrication process including key parameters for high quality nonlinear waveguides has been presented in this chapter. In case of long bent waveguides, an important parameter for device optimization has been discussed. Their linear optical characterization results have been presented.

4. Second Harmonic Generation (SHG)- and Difference Frequency Generation (DFG)-Based Wavelength Converters

This chapter summarizes the results of SHG in single-pass Ti:PPLN waveguides (section 4.1) and matched waveguide resonators (section 4.2). Then results of directly pumped DFG-based wavelength conversion are presented in section 4.3.

4.1 SHG in Straight Ti:PPLN Waveguides

Measured and calculated SHG results of three different Ti:PPLN waveguide samples are presented in this section. The results of their linear optical characterization are summarized in table 4.1. The end-faces of the investigated samples were antireflection coated for both, SH and fundamental wavelengths, not only to avoid Fabry-Perot interference effects, but also to get a better coupling efficiency between a fiber and the Ti:PPLN waveguide.

sample name	length [mm]	waveguide width [μm]	Λ_{QPM} [μm]	TM loss [dB/cm]	TM mode size [μm]
Pb808zB	10	7	16.6	0.11	4.8 × 3.2
Pb645z	30	6	16.4	0.03	4.6 × 3.0
Pb293z	88	7	16.4	0.07	5.2 × 3.8

Table 4.1: The results of the linear optical characterization of three different Ti:PPLN waveguide samples.

The experimental setup to demonstrate SHG in a single-pass Ti:PPLN waveguide is shown in Fig. 4.1. A tuneable external cavity laser (ECL) served as fundamental. After polarisation controlling (PC), it was fiber butt-coupled to the Ti:PPLN waveguide. The generated SH wave was measured using a silicon detector that is sensitive only for SH. To obtain a stable temperature of the whole waveguide, the sample was mounted on a copper base plate; its temperature was controlled within 0.1 °C. The residual fundamental radiation was measured behind the sample using an InGaAs photo-detector (PD).

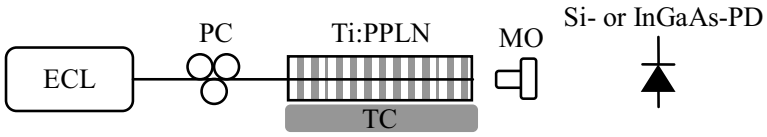

Fig. 4.1: Experimental setup to investigate single-pass SHG in a Ti:PPLN straight waveguide; ECL- external cavity laser, PC- polarisation controller, TC- temprature controlling unit, PD- photo detector, MO- microscope objective.

The low power (non-depleted fundamental) SHG responses of the waveguide samples described above are presented in Fig. 4.2. From the SH-full width half maximum (FWHM) an effective interaction length can be determined. Therefore FWHM of the $sinc^2$ shaped SHG characteristics are narrowing with increasing interaction length as explained in chapter 2. The comparison between measured and calculated results is presented in Fig. 4.2, d. The large discrepancy between measured and calculated even for homogeneous waveguides can be speculated to the quality of the PPLN grating (e.g. duty cycle) and/or reduced nonlinearity of the substrate itself.

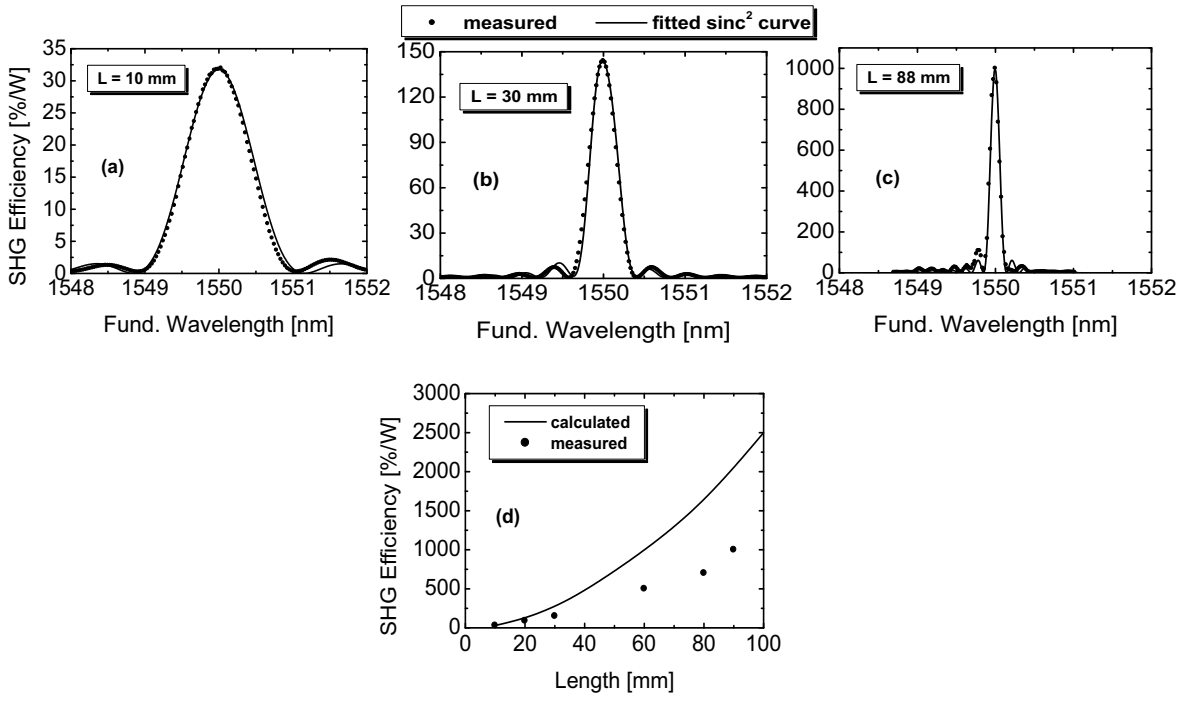

Fig. 4.2: Measured SHG spectra versus fundamental wavelength for 10 mm (a), 30 mm (b), and 88 mm (c) long interaction lengths of Ti:PPLN waveguides. Diagram on (d): Calculated and measured SHG efficiency versus interaction length L.

Ti:PPLN waveguides have high susceptibility to the photorefraction effect. This effect degrades the waveguide performance for high power SHG. In the next section photorefraction effect is introduced briefly.

Photorefraction Effect

In 1966, Ashkin et al. [41] observed optically-induced inhomogeneities of the refractive index in $LiNbO_3$ and $LiTaO_3$. This light-induced index change is known as photorefraction effect (PRE). Depending on the application pursued this effect can be either very useful (holographic applications [42]) or undesirable (optical damage in high-power photonic devices).

In an integrated AOWC device index inhomogeneities caused by the PRE can drastically deteriorate the device performance. Waveguides, which are single-mode at a wavelength around 1550 nm (e.g. fundamental wave for SHG process), can guide several transverse modes at the half of the input wavelength (second harmonic wave). The Ti:PPLN is more susceptible to the PRE at the wavelength range below 1 µm. Thus with an intense SH, the index of refraction can be locally perturbed. In this way, in addition to the change in transverse mode(s) of propagation, phasematching condition can also be effectively perturbed. As a consequence, QPM condition is no longer fulfilled to continue the parametric process (here SHG). Because of the now changed intensity profile, the index perturbation also changes, which again affects the modes of propagation and phasmatching condition and so on. Therefore, photorefraction prevents efficient conversion if it is not appropriately mitigated.

In 1969, Chen postulated that photorefraction arises from the redistribution of light-induced free carriers causing index changes (Δn) by the linear electro-optic effect from the space-charge field E_{SC} [43].

$$\Delta n = \frac{1}{2} r n^3 E_{SC} \tag{1.4}$$

Here “r” represents the electro-optic coefficient of the photorefractive material and “n” is the refractive index of the material. This simple model successfully explains photorefraction in various materials and experimental conditions.

Free carriers are a result of photoionization of deep levels. The transport properties of ferroelectrics are unusual in that, there is a photogalvanic term in addition to the usual drift and diffusion term. Ref. [44] observed constant currents along the ferroelectric axis in $LiNbO_3$ when the sample was illuminated. This bulk photovoltaic effect is also known as the photogalvanic effect and results in a source term directed along the polar axis in the constitutive relation for the current density:

$$\vec{J} = \sigma \vec{E}_{SC} + \kappa I \hat{z} \tag{2.4}$$

Here $\vec{J}$ is the current density vector, σ is the conductivity (assumed to be isotropic), κ is the photogalvanic coefficient, I is the intensity of the light and $\hat{z}$ is a unit vector along the polar axis. In this relation, the diffusion term is neglected. This space charge field induces a change in the refractive index through the electro-optic effect (Eqn. 1.4). In typical congruent lithium niobate these space charge fields can reach values in excess of 10 kV/cm. The electro-optic coefficient of PPLN is close to 30 pm/V, and thus these space charge fields can easily cause enough scattering to render a 1-mm-long crystal useless. Moreover, the performance of nonlinear devices can degrade with time since these charges can accumulate due to the long dielectric lifetimes observed in PPLN.

The conductivity in a PPLN crystal can be divided to dark conductivity σ_d and photo conductivity σ_{ph} [45]:

$$\sigma = \sigma_d + \sigma_{ph} \Rightarrow \vec{E}_{SC} = -\frac{\kappa}{(\sigma_d + \sigma_{ph})} \vec{I} \tag{3.4}$$

It has been shown that many defects, both impurities and native defects; alter photoconductivity and photogalvanism of photorefractive materials [46], [47]. In particular, magnesium doping [48], [49] to enhance the photo-conductivity σ_{ph} and raising the temperature [50] to increase the dark-conductivity σ_d have been shown to be effective in reducing the susceptibility to photorefractive damage.

Here Ti:PPLN waveguides are operated at elevated (> 150 °C) temperature to enhance the dark conductivity and thus reducing the photorefractive susceptibility.

High Power SHG in Ti:PPLN Waveguides

As mentioned above, one of the ways to mitigate the photorefraction effect (PRE) is to increase the dark conductivity by raising the temperature above 150 °C. In this section, high power SHG in a Ti:PPLN channel guide is investigated at different operating temperatures.

The 80 mm long and 7μm wide Ti:PPLN channel guide used for this experiment, has a micro-domain periodicity of 16.5 μm. Its propagation losses around 1550 nm are ~ 0.1 dB/cm. Fig. 4.3 presents the SHG-results. The SHG conversion efficiency of ~ 700 %/W was measured at 1.1 mW coupled fundamental power (see Fig. 4.3, left). The measured half-width $\Delta\lambda_{FWHM}$= 0.14 nm obtained from the SHG curve

corresponds to an effective interaction length of 77 mm. The SH power generated with different fundamental powers at different operating temperatures of the Ti:PPLN waveguide is plotted in Fig. 4.3, right. The measured (points) SHG power follows the theoretical prediction (solid line), at low coupled fundamental powers for all operating temperatures. This indicates that the perturbation of the refractive index by photorefraction is small and does not significantly change the quasi-phase-matching condition for SHG. When the coupled fundamental power was increased, the measured SHG can no longer follow the theoretical response especially at lower operation temperature. This means that the refractive index is perturbed significantly by the photorefraction effect, thus the QPM condition is no longer valid for existing fundamental wavelength. By increasing the temperature of the Ti:PPLN waveguide, its resistance to the photorefraction effect can be increased. The highest SH power of ~ 80 mW was achieved at ~ 200 °C with a coupled fundamental power of ~ 300 mW.

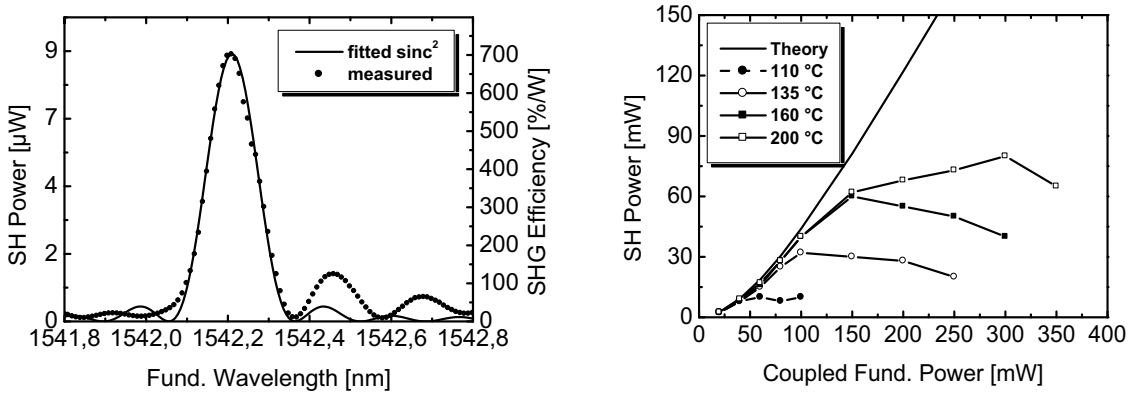

Fig. 4.3: Left: Measured and calculated SHG spectra versus fundamental wavelength of an 80 mm long Ti:PPLN channel guide for 1.1 mW coupled fundamental power at room temperature. Its 0.14 nm FWHM corresponds to 77 mm effective interaction length. Right: High power SHG: by increasing the operation temperature the photorefractive damage decreases due to an increased dark conductivity.

Fig. 4.4, left, shows the measured SHG characteristics as SH power versus fundamental wavelength for different coupled fundamental power levels at an operating temperature of 200 °C. As the fundamental power is increased, on one hand, the phasematching wavelength shifts to shorter wavelengths due to photo-refraction effect, and on the other hand due to the power depletion of the funda-mental wave the shape of the SHG curve is changed. A sinc^2 shape of the SHG curve is true only for non-depleted approximation. As the power of the generated SH wave increases, more depletion happens for the power of the fundamental wave leading to shrinking of the SHG curve [51]. This can be obtained by a solution of the coupled mode equations for the SHG process taking into account the power depletion of the fundamental wave (non-depleted regime). The diagram on the right of the Fig. 4.4

shows depletion of the fundamental power versus coupled fundamental power. The calculated SHG responses versus fundamental wavelength are presented as inset for three different depletions of 5 %, 40 % and 60 % respectively. The central portion of the SHG curve is narrowing and side-lobes are growing.

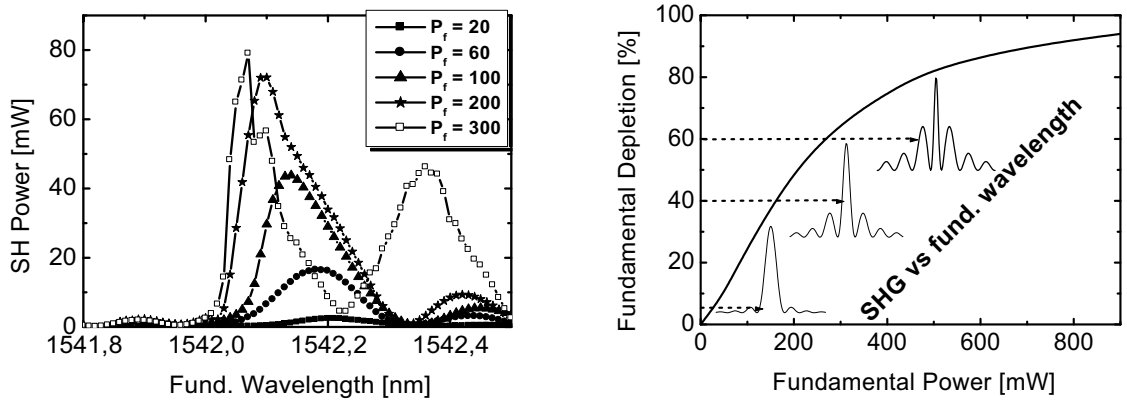

Fig. 4.4: Left: Measured SHG curves versus fundamental wavelength for different coupled fundamental power levels at an operating temperature of 200 °C. Blue shift of the phasematching wavelength is due to photorefraction effect. Phasematching curve is narrowing for higher depletion of the fundamental power. Right: Calculated depletion of the fundamental power versus coupled fundamental power. The SHG responses versus fundamental wavelength of a photorefraction effect free and homogeneous Ti:PPLN waveguide is presented as inset for different fundamental depletions of 5 %, 40 % and 60 % respectively.

4.2 Efficient SHG in Ti:PPLN Matched Waveguide Resonators

Second harmonic generation (SHG) in waveguide resonators has been investtigated in detail many years ago [52], [53]; at that time phase matching was usually achieved by exploiting the birefringence of the waveguide material. This was a strong limitation for the possible wavelength combinations of a three wave nonlinear second order interaction. Moreover, it was not possible to exploit the largest nonlinear coefficient. With the advent of periodically poled substrate materials quasi phase matching (QPM) became possible [19]. In the meantime single pass SHG and other parametric interactions have been demonstrated in periodically poled materials with excellent efficiencies for wavelengths in different spectral ranges from the UV to the infrared [54], [55]. Moreover, SHG in waveguide resonators exploiting QPM is investigated in fiber ring resonator [56] or doubly resonant [57] operation with relatively low conversion efficiency.

Standard Ti:PPLN channel guides of excellent quality were used to investigate resonant SHG. Their low propagation losses, even down to 0.03 dB/cm around λ =

1550 nm, allow the development of relatively high Q waveguide resonators as already exploited e.g. in different types of optical parametric oscillators [38], [58].

The theory of SHG in (Fabry-Perot-type) matched waveguide resonators has been presented in Ref. [53]. The key results will be mentioned here again, to highlight the advantages of SHG in waveguide resonators. The main advantage is the large intracavity enhancement of the fundamental power, if low loss waveguides and appropriate mirrors are used. This enhancement can be described by a resonance factor f with [53]:

$$f = \frac{1 - R_f}{\left[1 - (R_f R_r)^{1/2} \exp(-\alpha_f L)\right]^2}$$

where R_f and R_r are the power reflectivities of the front and rear mirror of the resonator, respectively (see Fig. 4.5); α_f is the loss coefficient describing the propagation loss of the fundamental wave; L is the sample length. Figure 4.5 shows the operation principle of SHG in a non-resonant waveguide (single-pass, Fig. 4.5, left) and SHG in a matched waveguide resonator (Fig. 4.5, right). Mirrors have high reflectivites in the C-band to provide fundamental wave enhancement waveguide resonator.

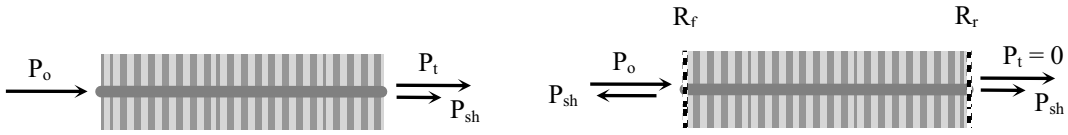

Fig. 4.5: Left: Operation principle for single-pass (nonresonant) SHG. Right: Operation principle of SHG in a matched waveguide resonator.

If no transmitted fundamental power is needed R_r can be set to 1. Then R_f is determined by the condition for maximum power enhancement or maximum f yielding:

$$R_{fm} = R_r \exp(-2\alpha_f l)$$

Such a front mirror reflectivity (R_{fm}) leads to zero reflected fundamental power at resonance; all the input fundamental power is used for intracavity power enhancement limited by (scattering) losses alone. The maximum enhancement factor of such a "matched" resonator is given by:

$$f_m = \frac{1}{1 - R_{fm}} > 1$$

This power enhancement leads in the nondepleted pump approximation to a corresponding enhancement of the conversion efficiency for SHG:

$$\eta_{res} = \eta_{non-res} f^2$$

with the single pass, nonresonant SHG efficiency $\eta_{non\text{-}res}$. In Fig. 4.6 left, the calculated resonant SHG efficiency η_{res} for symmetric and matched resonators are shown as function of the resonator length L. Fig. 4.6 right is the calculated enhancement factor for different propagation loss values of a 65 mm long waveguide. Matched resonator shows three times more improvement in comparison with symmetric resonator. These results predict that η_{res} depends only weakly on the length of the resonator (left diagram), but strongly on the propagation losses α_f (right diagram). It can be seen that even two orders of magnitude improvement of the SHG efficiency can be expected in comparison with single-pass nonresonant SHG.

The 65 mm long single mode Ti:PPLN channel waveguide used in this experiment has a 16.6 μm micro-domain periodicity allowing QPM SHG at 1531 nm fundamental wavelength at room temperature. The end faces of the waveguide sample have been polished perpendicular to the waveguide axis and dielectric mirrors of special properties have been prepared by vacuum-deposition.

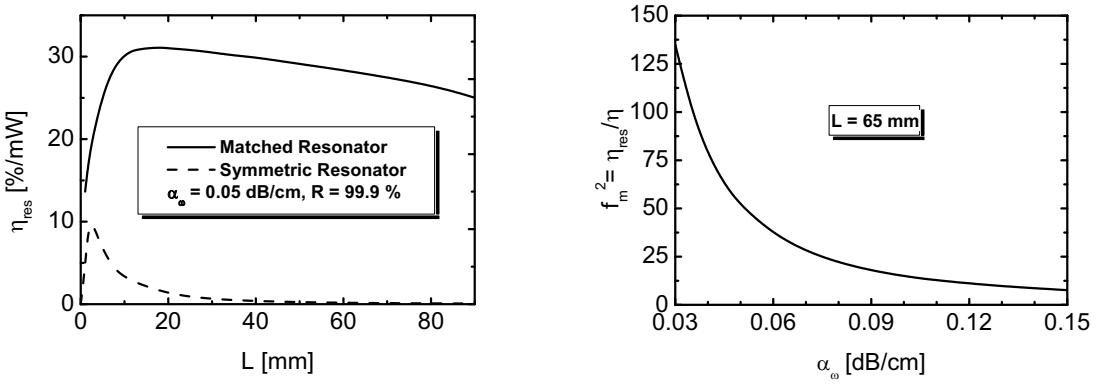

Fig. 4.6: left: The calculated resonant SHG efficiency η_{res} for symmetric and matched resonators as function of the resonator length L with propagation loss value of 0.05 dB/cm. Right: improvement of the resonant SHG efficiency η_{res} in comparison to nonresonant efficiency η (square of the enhancement factor f_m) for given propagation loss α_f of the waveguide.

On one hand, both input and output mirrors should have a negligible reflectivity at 765 nm (generated SH) wavelength, but a high reflectivity around 1530 nm. To be specific, according to theoretical results the reflectivity of the input (output) mirror should be about 70% (> 99%) to get a matched resonator for most efficient SH-generation by maximum intracavity fundamental field enhancement. Modeling calculations show that 6 pairs of SiO_2 and TiO_2 layers will form dielectric multilayer mirrors of the required spectral properties. Fig. 4.7 presents the measured transmission of input and output mirrors. The measured reflectivities for the input

mirror are ~ 3 % around λ_{sh} = 765 nm and ~ 70% around λ_f = 1530 nm. The corresponding data for the output mirror are 3 % and 99 %.

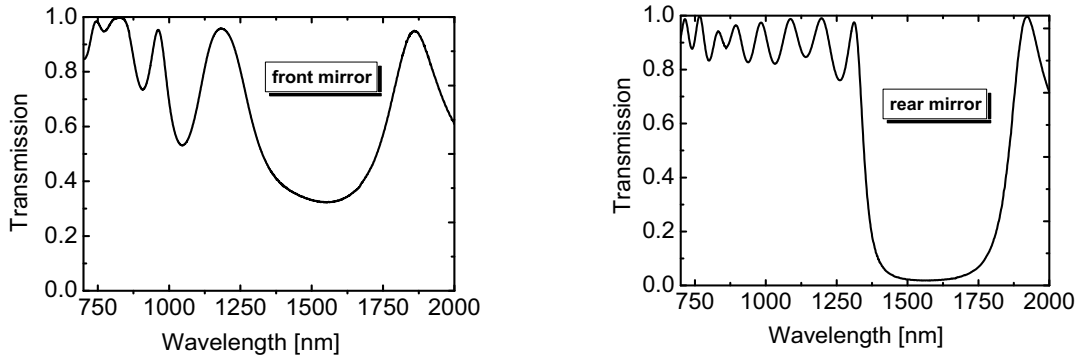

Fig. 4.7: Measured transmission spectra of the input (left) and output mirror (right) of the matched waveguide resonator.

The experimental setup to investigate SHG in the matched Ti:PPLN waveguide resonators is shown in Fig. 4.8. The sample is mounted on a thermoelectric cooler/heater, which allows a temperature stabilization of about ± 1°C. A semiconductor Extended Cavity Laser (ECL) is used as tunable coherent light source of about 150 kHz instantaneous line-width. It can be continuously tuned in a small wavelength range enabling to sweep over some cavity resonances. The light is fed into the sample via a fiber circulator to monitor the reflected fundamental power by a InGaAs-photodiode. The generated SH output power is measured by a Silicon photodiode, which is sensitive at the SH-wavelength only.

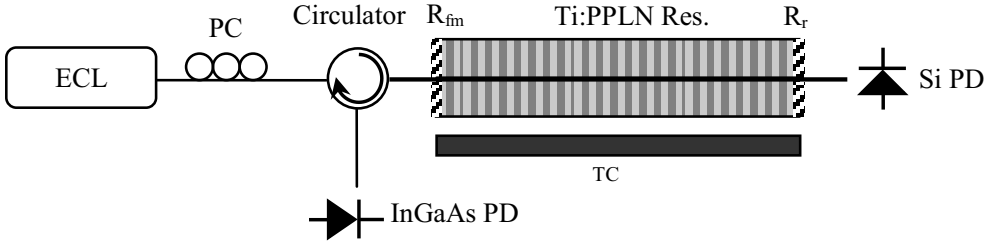

Fig. 4.8: Sketch of experimental setup: ECL-tunable semiconductor Extended Cavity Laser, PC-polarization controller, R_{fm} and R_r- dielectric mirrors of the matched waveguide resonator, TC-Thermoelectric Cooler/Heater, PD- photo diode.

The SHG response of the waveguide in single pass configuration has been measured before appropriate dielectric mirror have been deposited. Fig. 4.9 shows the measured SHG spectrum around the phasematching wavelength at room temperature. Due to inhomogeneities, which might arise from inhomogeneities of the

substrat or/and of the fabrication process, not a $sinc^2$ response is observed. The calculated $sinc^2$ function with 0.23 nm FWHM corresponds to a 46 mm effective interaction length. With 0.5 mW of coupled fundamental power, 1.2 µW of generated SH power is obtained which corresponds to an efficiency of η = 480 %/W.

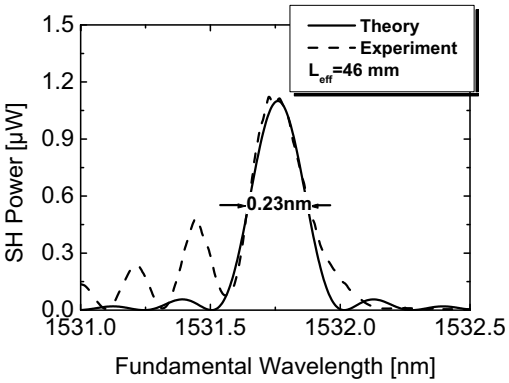

Fig. 4.9: Measured nonresonant SHG response of a 65 mm long Ti:PPLN waveguide as SH power versus fundamental wavelength. The 0.23 nm FWHM of the main peak corresponds to a 46 mm effective interaction length.

Fig. 4.10 presents the measured and calculated reflected fundamental power versus fundamental wavelength around the expected phasematching wavelength of 1531 nm from the matched waveguide resonator; the input power was 0.5 mW. The simulated results are given using experimentally determined waveguide parameters (R_{fm} = 74.1%, R_r = 98.6%, α_ω = 0.08 dB/cm, L = 65 mm). As predicted for almost matched resonators the reflected power nearly drops to zero in a resonance due to maximum fundamental power enhancement. The agreement of theoretical and experimental results is relatively good; only the measured drop in the resonances is somewhat smaller than calculated. The reasons might be the imperfection of the dielectric mirror reflectivities.

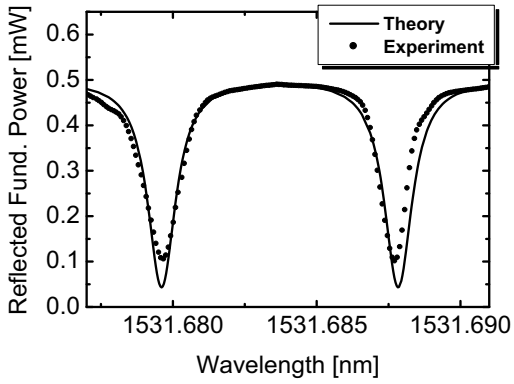

Fig. 4.10: Measured and calculated reflected fundamental power versus wavelength for an input power of 0.5 mW.

In Fig. 4.11 the generated SH-power (at $\lambda_{2\omega}$ ~ 765 nm) is shown as function of the wavelength of the fundamental radiation. Again, the fundamental power in front of the waveguide resonator is 0.5 mW. SHG can be observed in a large number of cavity resonances (left diagram). The envelope of the SH-power reflects the phase

match properties of the waveguide similar to the nonresonant operation. The wavelength of the laser can be stabilized to a single resonance by a proper feedback circuit to the laser control (see next chapter).

The results of SHG in the two neighbouring resonances of highest efficiency is presented in Fig. 4.11 right. With only 0.5 mW of fundamental power, measured in front of the waveguide resonator (not coupled), a SH power of 25.8 µW was generated in forward direction. This corresponds to a record conversion efficiency of the device of 10300 %/W or 10.3 %/mW in reasonable agreement with the theoretical simulation (~ 13 %/mW) which is one order of magnetude larger than what has been reported in Ref. [53]. This impressive efficiency can even be doubled by using an appropriate input mirror of high reflectivity and appropriate phase adjustment for the SH wave. A further improvement should be possible with a doubly resonant device taking into account the phase relation between fundamental and SH waves.

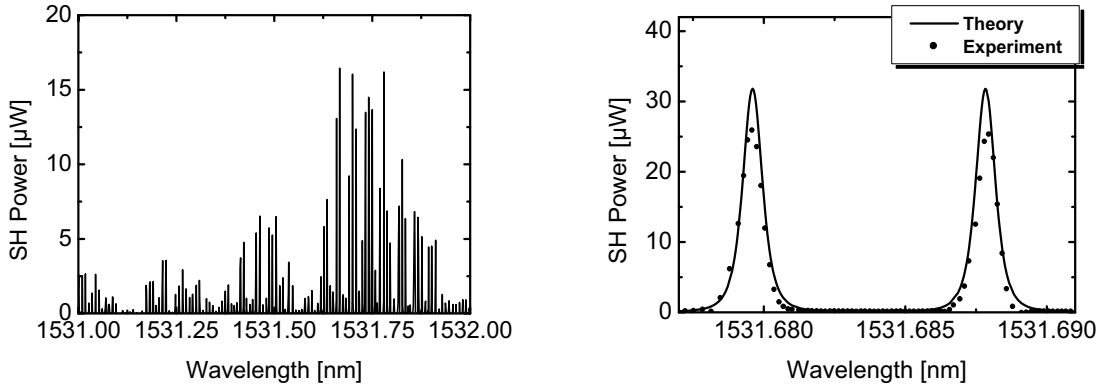

Fig. 4.11: Left: Measured SH power emitted in forward direction from a matched Ti:PPLN waveguide resonator versus fundamental wavelength around phase matching wavelength. Right: Measured SH-power emitted in forward direction from a matched Ti:PPLN waveguide resonator versus fundamental wavelength around the two resonances of highest efficiency, fundamental power is 0.5 mW.

4.3 Directly Pumped DFG-based wavelength conversion

In DFG-based wavelength conversion, the input signal and the generated output (idler) waves must be at significantly longer wavelength than the pump wave preserving energy conservation. For operation in the C-band, the pump wave for DFG with $\lambda_p \sim 775$ nm can be generated externally either by SHG or by an appropriate laser (e.g. Ti:Sapphire laser). Directly pumped DFG (dDFG) requires selective spatial mode excitation in a waveguide which is multimode at the pump wavelength.

Therefore, an efficient selective excitation is hard to achieve without additional means, e.g. a wavelength selective directional coupler [59], [60].

To investigate dDFG-based wavelength conversion of a signal in the C-band, a 83 mm long Ti:PPLN-waveguide (Pb232z) with 16.6 µm domain period was used. The sample was heated up to 182 °C to avoid photorefraction mainly caused by the pump wave at ~ 780 nm. The experimental setup is shown in Fig. 4.12. A Ti:Sapphire (TiSa-) laser was used as the pump source. Its line-width was narrowed to a few MHz using intracavity etalons. The signal source was a distributed feedback (DFB) diode laser operated at 1554 nm. Bulk and fiber-optic wave-plates were used to adjust the polarization of both lasers. Pump and signal beams were multiplexed using a dichroic mirror. To achieve the necessary spot size for a selective excitation of the TM_{00} pump mode, expansion optics (EO) was inserted which allowed varying the illuminated aperture of the input 20× microscope objective (MO) and in this way the effective numerical aperture. To optimize the TM_{00} pump mode excitation the near field pattern at the waveguide end face was imaged to a video camera using a microscope objective of the same type as for the input. Alternatively, the output was coupled into a fiber and launched to an optical spectrum analyzer (OSA) for spectral investigation (see Fig. 4.12).

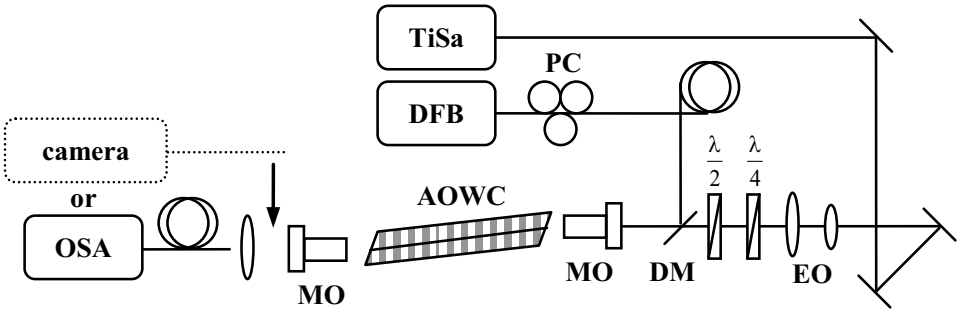

Fig. 4.12: Sketch of the setup for directly pumped DFG-based wavelength conversion; TiSa- Ti:Saphire laser, DFB- distributed feedback diode laser, PC- fiberoptic polarization controller, EO- expansion optics, DM- dichroic mirror, MO- 20× microscope objective, AOWC- all optical wavelength converter, OSA- optical spectrum analyzer

An output spectrum is shown in Fig. 4.13 on the left. With only 4.2 mW of coupled pump power a wavelength conversion efficiency of -16 dB has been obtained. The conversion efficiencies for this approach have been modelled as it is shown in Fig. 4.13 on the right. A conversion efficiency of -14.3 dB theoretically requires about 4 mW of (coupled) pump power for the dDFG-process. Grating stabilized, pigtailed diode laser should therefore be possible as pump sources also for the dDFG scheme.

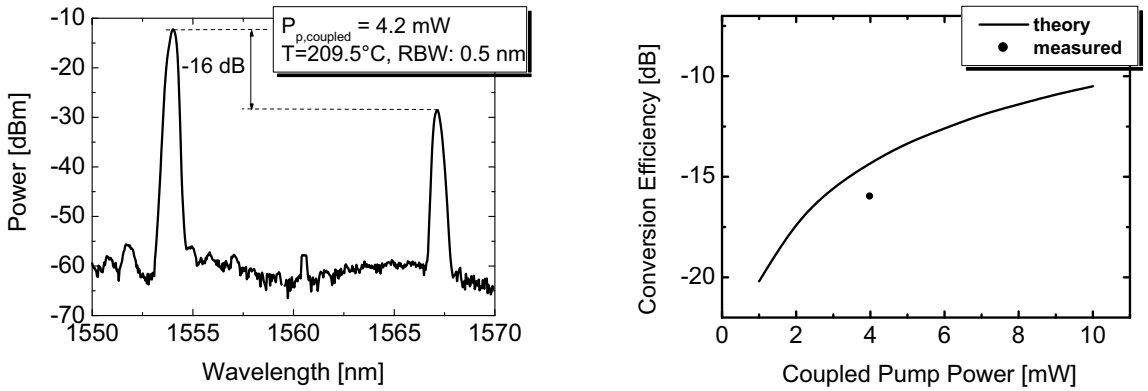

Fig. 4.13: Left: Optical spectrum of the directly pumped DFG-based wavelength conversion. Right: Calculated (line) and measured (dot) wavelength conversion efficiencies versus coupled pump power for directly pumped DFG-based wavelength conversion.

Although, the result of dDFG is promising, the stable selective coupling of TM_{00} mode of the pump wave to the waveguide is quite difficult. Therefore, any environmental effect causes the change in coupling of the pump wave in phase matched mode, which then transfers to the power fluctuation of the out coupled wavelength shifted idler wave. This was the main motivation to investigate the cascaded SHG/ DFG-based wavelength conversion (see chapter 5).

4.4 Summary

Single-pass SHG in straight waveguides with an SHG efficiency of ~ 1030 %/W was achieved in an 88 mm long Ti:PPLN waveguide sample.

The photorefractive damage for a Ti:PPLN waveguide is investigated. Experimental results proved that by raising the operation temperature, photorefraction effect is decreasing due to an increased dark conductivity. In high power operation (> 300 mW coupled fundamental power) the photoconductivity dominates the dark conductivity. In such a case due to strong time varying space-charge fields, the SH power was not stable. The best SH power obtained at 200 °C with 300 mW coupled fundamental power was ~ 90 mW.

SHG in Ti:PPLN waveguide resonators for the fundamental wavelength has been investigated. Theoretical modelling helped to identify matched resonators as optimum devices for maximum conversion efficiency. Based on these results corresponding Ti:PPLN resonators with appropriate dielectric mirrors have been developed. In a device of 65 mm length a record conversion efficiency of 10.3 %/mW has been achieved with 0.5 mW fundamental power at λ_f = 1531 nm.

Directly pumped DFG-based wavelength conversion has been investigated. At low pump power levels of only 4.2 mW a conversion efficiency of -16 dB has been achieved. However, directly pumped DFG requires a selective excitation of one transverse pump mode, as waveguides are multimode at the pump wavelength around ~775 nm. Therefore, special wavelength division multiplex (WDM-) couplers are needed for on-chip integration.

5. Cascaded Second Harmonic Generation/Difference Frequency Generation (cSHG/DFG)-Based Wavelength Converters

In directly pumped difference frequency generation (DFG)-based wavelength conversion, it is difficult to excite selective mode of the pump wave. On the other hand, by an internal generation of the pump wave via cascaded second harmonic generation and DFG (cSHG/DFG) a phasematched pump (SH) mode can be excited selectively [11], [61], [62].

In this chapter, results of cSHG/DFG-based wavelength conversion are presented. They comprise modelling and experimental achievements of Ti:PPLN straight waveguides for wavelength conversion exploiting the cascaded $\chi^{(2)}$:$\chi^{(2)}$ three wave interaction processes (section 5.1). The theoretical investigations of temporal shape and induced chirp of the converted data pulses in a cSHG/DFG-based wavelength converter and the experimental data obtained during system experiments in the HHI (see appendix B) are also presented in this chapter. As the group velocity dispersion (GVD) between signal and generated idler are small, the broadening and chirping for input pulses of ~ 1.4 ps halfwidth is negligible. Even a polarization insensitive ultra-fast wavelength conversion was realized [13] (see appendix B).

Afterwards, wavelength conversion using new device configurations, which have been developed and investigated with the objective to improve the wavelength conversion efficiency, is discussed. According to the theory, this should be possible for a given fundamental power by; the use of a counter-propagating scheme with separated SHG and DFG (section 5.2); an increase of the interaction length using either long bent waveguide (section 5.3) or a double-pass scheme in a folded waveguide structure (section 5.4).

5.1 cSHG/DFG-Based Wavelength Conversion in Ti:PPLN Straight Waveguides

Efficient wavelength converters for C-band (1535- 1565 nm) operation with PPLN waveguides, require a pump power of about 50-100 mW in the wavelength range of 750-800 nm. This is a less convenient laser source compared to the well developed 1550 nm sources for telecommunication applications. Moreover, a selective excitation of a single spatial mode of the pump wavelength in a monomode waveguide in the C-band (multimode for pump wave) can complicate the practical operation of the device. However, the pump wave can be generated internally by Second Harmonic Generation (SHG) of a "fundamental" wave in the 1.55 μm band with simultaneous QPM for SHG and DFG. This attractive mode of operation is also known as cascaded SHG/DFG or cSHG/DFG. A schematic diagram of the operation principle with the different input and output waves is shown in Fig. 5.1, left. This approach has the advantage, that reliable, relatively cheap tunable semiconductor lasers can be used as fundamental wavelength sources for the λ ~ 1550 nm range. If necessary, the power level can be boosted using an erbium doped fiber amplifier (EDFA). Moreover, a selective excitation of one spatial mode only of the SH-wave is guaranteed by the phase matched SHG-process itself.

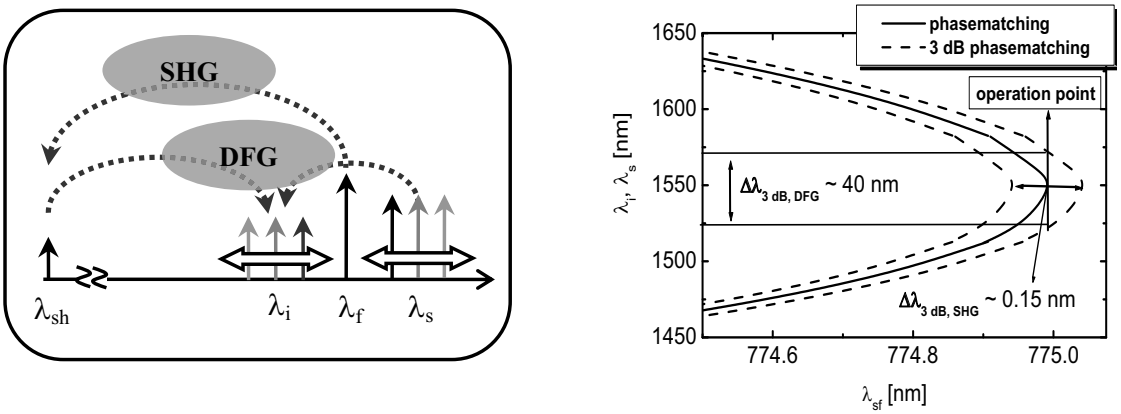

Fig. 5.1: Left: Schematic diagram of cSHG/DFG-based wavelength conversion in a Ti:PPLN channel guide. The fundamental wave (λ_f) generates its second harmonic (λ_{sh}) as pump wave for the DFG-process. The idler (λ_i) is the wavelength-shifted signal (λ_s) wave. Right: Phasematching condition for cSHG/DFG process. The SHG process is quasi-phasematched and within its 3 dB bandwidth of ~ 0.15 nm, DFG process is possible with a larger bandwidth of ~ 40 nm.

In this section, we demonstrate cSHG/DFG-based wavelength conversion in Ti:PPLN straight channel guides. In a cSHG/DFG process with co-propagating waves the pump wave for DFG process can be generated by quasi-phase matched SHG of the input fundamental wave (λ_f). The generated pump wave ($\lambda_{sh} = \lambda_f/2$) is

simultaneously mixed with the input signal wave (λ_s) to generate a wavelength-shifted idler ($1/\lambda_i = 2/\lambda_f - 1/\lambda_s$) by DFG. Cascaded processes in PPLN can also be considered as an analogue to the four-wave-mixing (FWM) process used in third-order nonlinear materials. The effective $\chi^{(3)}$ of such processes in PPLN is two orders of magnitude larger than that of silica glass. Therefore, efficient devices can be made with much shorter PPLN waveguides compared to FWM-based devices with (highly nonlinear) fibers. Moreover, such a device is immune to parasitic effects such as stimulated Brillouin scattering (SBS) [63], and has a better noise figure compared to FWM in semiconductor optical amplifiers [64].

Polarization-Dependent Wavelength Converter

Different polarizations in a PPLN waveguide have different effective index of refraction. Therefore, cSHG/DFG-based wavelength conversion in PPLN waveguides is inherently polarization dependent.

The Ti:PPLN waveguide used in this experiment is 93 mm long, has a QPM period of 16.3 µm and a waveguide width of 7 µm. Its propagation losses (for TM-polarisation) at 1550 nm wavelength are ~ 0.1 dB/cm. The waveguide is mounted on a copper base plate to enable homogeneous heating and a precise temperature control. Its end faces are angle polished under 5.8° and AR coated to avoid Fabry-Perot effects. Monomode PM-fiber pigtails with angled and AR coated ferrules are aligned to the Ti:PPLN waveguide using built-in micromanipulators [the main concept and design of the fiber coupled and temperature stabilized packaged device has been developed by H. Suche]. A special temperature controller has been developed and built by our electronic workshop allowing stabilization within 0.1 °C up to temperatures > 200°C. Fig. 4.4 shows the packaged wavelength converter. The optimized fiber-to-fiber insertion loss is ~ 6 dB.

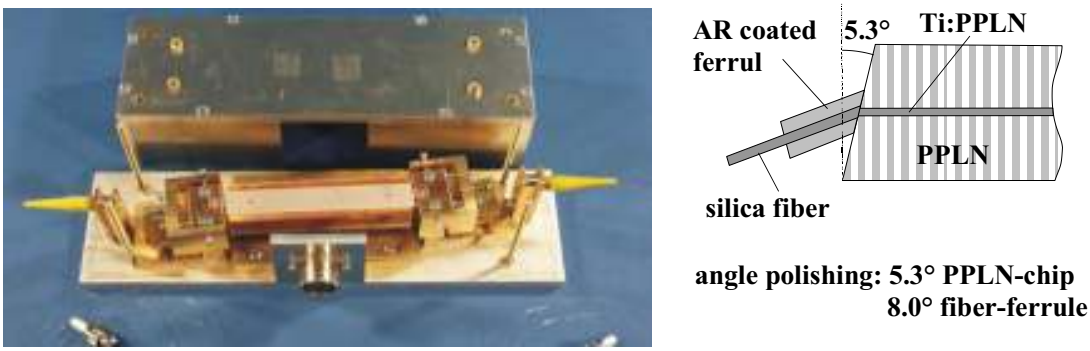

Fig. 5.2: Left: Photograph of the packaged and pigtailed wavelength converter. Right: Schematic drawing of fiber pigtailed waveguide endface.

The experimental setup for investigation of the device is sketched in Fig. 5.3, left. Light from a DFB-laser served as signal (λ_s = 1552 nm) and a tunable external cavity laser (ECL) (λ_f = 1480- 1640 nm) was used as fundamental. Both beams are combined after polarization control using a 3 dB coupler. Both waves can be amplified using an erbium-doped fiber amplifier (EDFA). 1540 nm has been used as fundamental wavelength requiring T = 207°C for phase matched SHG and cascaded DFG with a signal of 1552 nm wavelength. A variable optical attenuator (VOA) allows to vary the signal power.

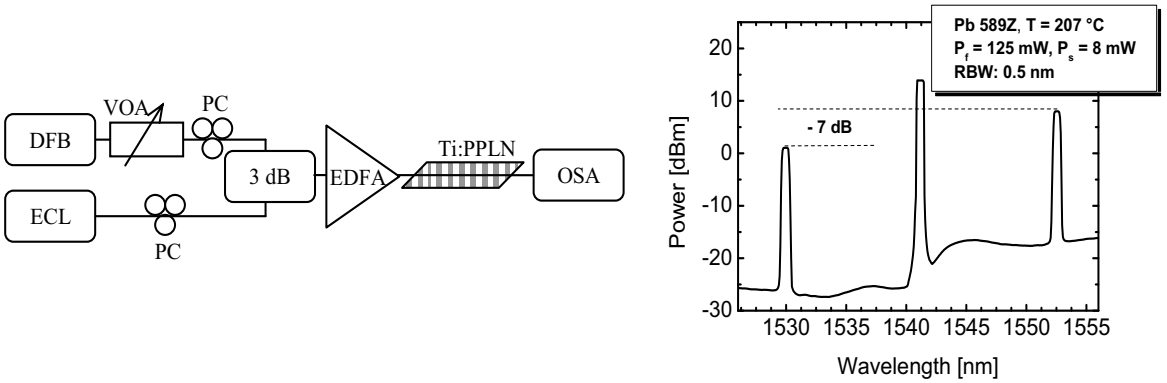

Fig. 5.3: Left: Setup to investigate cSHG/DFG-based wavelength conversion in a Ti:PPLN-waveguide. Right: Optical spectrum at the output of the packaged and pigtailed, polarization dependent wavelength converter.

With 125 mW of coupled fundamental power a conversion efficiency of -7dB has been achieved; the generated idler power was + 1dBm. This result is in good agreement with predicted theory (-5 dB). The packaged device has been tested in a system experiment by Heinrich Hertz Institute (HHI) in Berlin and demonstrated the potential of practical operation [13].

Polarization-Independent Wavelength Converter

To overcome the constraint that cSHG/DFG is inherently polarization-dependent a polarization diversity scheme in which the two polarization components of the input signal are converted independently is needed [65]. To provide identical quasi-phase-matching (QPM) and differential group delay (DGD) for the two components it is ideal to utilize the same waveguide twice. This has been accomplished using a polarization maintaining ring configuration with contra-directional single-pass conversion of the two polarization components in the same waveguide. In this way DGD equalization between the two converted polarization components is automatically provided [13]. In Fig. 5.4 the setup for polarization independent

wavelength conversion is sketched. A 4-port circulator and a tuneable fibre optic Bragg grating (FBG) of 0.5 nm reflection bandwidth (FWHM) are used to multiplex fundamental (ECL) und signal (DFB-laser) waves with very low loss. A fibre optic polarization beam splitter (PBS) with PM-pigtails is used to split fundamental and signal waves into their TM and TE components. The TM components are launched from the left into the converter, whereas the TE components are rotated by 90°, following the rotation of the fibre, and launched as TM waves from the right.

By a proper adjustment of the polarization of the fundamental wave equal powers are launched from both sides into the converter leading to equal conversion efficiencies for both polarization components of the signal wave. The PBS is used again to recombine the polarization components of the transmitted and converted signals and to feed them into an optical spectrum analyzer (OSA). It is important to note that the optical path lengths for clockwise and counter-clockwise operation are identical thus avoiding any polarisation mode dispersion (PMD) effects by the wavelength converter. Waveguide and packaging of the polarization independent wavelength converter are very similar to those of the polarization dependent configuration. The domain period of the waveguide has been slightly increased to 16.4 µm to achieve phase matching for SHG at the fundamental wavelength of 1545 nm (center of the C-band for telecommunications) at more moderate temperatures (~ 180°C).

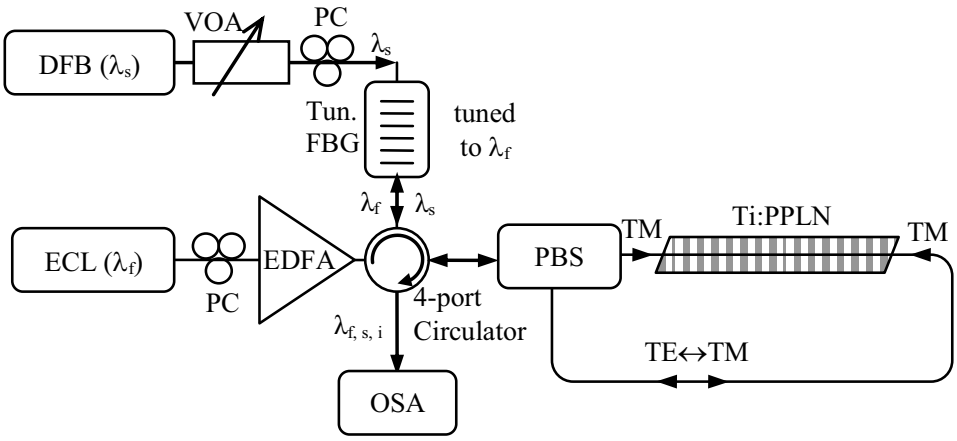

Fig. 5.4: Schematical diagram of the experimental setup for polarization insensitive wavelength conversion using a ring configuration to achieve polarization diversity.

Before closing the fibre loop, both single polarization conversion efficiencies (from left-to-right and from right-to-left) have been measured and optimized to achieve maximum conversion in the polarization independent configuration (see Fig. 5.5, left; due to asymmetric fibre coupling losses different efficiencies might arise). With about 150 mW of coupled fundamental power almost identical single polarization conversion efficiencies of -10 dB for both directions have been achieved.

For the polarisation insensitive configuration the wavelength conversion efficiency dropped to -13.2 dB due to the splitting of both, fundamental and signal powers (Fig. 5.5, right). To confirm a polarization insensitive operation the signal polarization was arbitrarily scrambled and the generated idler power was simultaneously recorded versus time (Fig. 5.5 right inset). The maximum resulting variations of the idler power were about ± 0.5 dB. This result is in good agreement with predictions. Using this device a number of additional (system) experiments have been performed in the labs of Heinrich Hertz Institute (HHI) Berlin (described in appendix B).

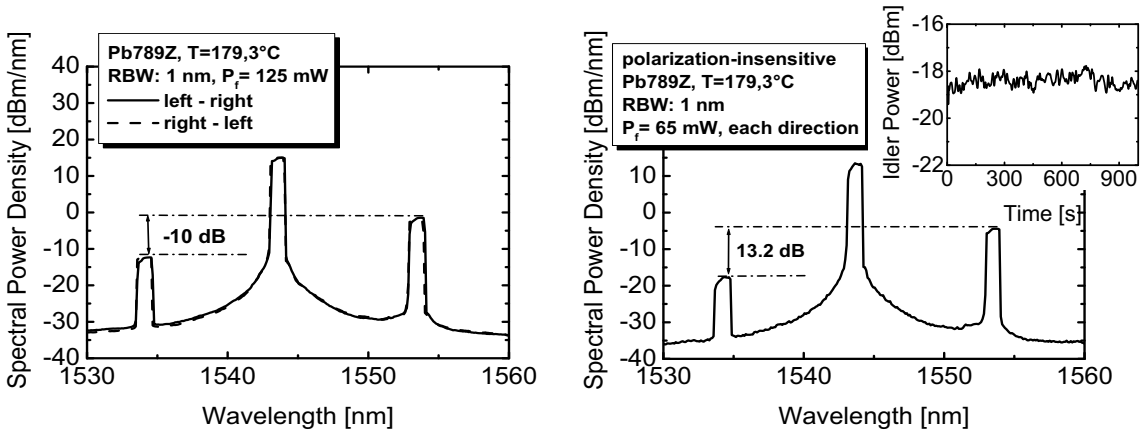

Fig. 5.5: Left: Measured optical output spectra for single polarization operation with propagation from left to right and vice-versa. Right: Spectrum for polarization-insensitive wavelength conversion via cSHG/DFG in the packaged and fiber pigtailed device. Inset: Idler (converted signal) output power versus time (OSA with zero span).

cSHG/DFG-Based Wavelength Conversion of Short Signal Pulses

In this section cSHG/DFG-based wavelength conversion of short signal pulses in a Ti:PPLN waveguide is discussed. To explore the limitations of this process for the conversion of ~ 1.4 ps signal pulses, as used in high data rate transmission experiments with of 320 Gb/s RZ/DQPSK data (see appendix B), wavelength conversion of a train of short signal pulses of ~ 1.4 ps halfwidth was investigated theoretically and experimentally.

Propagation and interaction of short optical pulses in a dispersive medium like $LiNbO_3$ is affected by group velocity dispersion (GVD), leading to temporal walk off, thereby changing the shapes of the interacting pulses. These effects require the consideration of temporal first and second order derivatives in the governing equations. The split step integration in time and frequency domains is used to solve

the coupled amplitude equations in the slowly varying envelope approximation [19]. Fig. 5.6 shows the temporal evolution of the shapes of signal and generated idler pulses after transmission through three successive sections (20 mm, 40mm and 60 mm) of a 60 mm long homogeneous Ti:PPLN waveguide. Since the signal source (λ_s = 1551 nm) in the system experiment (320 Gb/s) is a 1.4 ps FWHM pulse train with the average power of 32 mW, a Gaussian input signal pulse of 100 mW peak power is assumed. The cw power level of the fundamental wave at λ_f = 1546.2 nm was 55 mW.

The simulation results, presented in Fig. 5.6, show negligible pulse broadening (and walk off) for the transmitted signal; also the pulse peak power remains nearly constant as propagation losses are partly compensated by parametric amplification (Fig. 5.6, left). The idler pulse (λ_i = 1541.4 nm) strongly grows with increasing interaction length; by comparing its peak power after 60 mm interaction length with the peak power of the input signal pulse, an internal conversion efficiency of ~ -11 dB can be deduced. Moreover, the shape of the idler pulse at the output is practically identical with the shape of the signal pulse at the input (Fig. 5.6, right). In other words, the wavelength conversion by cSHG/DFG in a 60 mm long Ti:PPLN waveguide induces only negligible distortions of 1.4 ps long pulses.

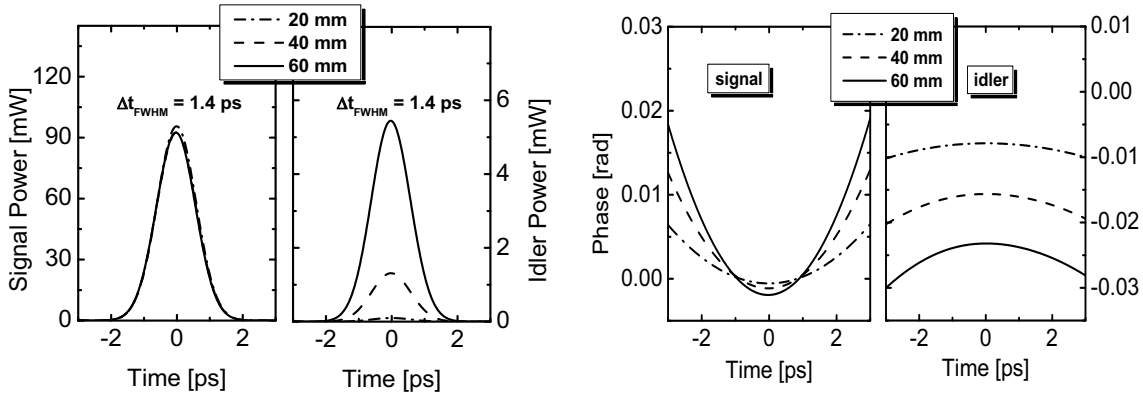

Fig. 5.6: Left: Calculated evolution of signal (λ_s = 1551 nm, left) and idler ((λ_i = 1541.4 nm, right) pulses for cSHG/DFG-based wavelength conversion over a distance of 60 mm long effective interaction length are shown after 20 mm (dashed-dotted), 40 mm (dashed) and 60 mm (solid), respectively. The distortions of signal and idler pulses are negligible. Right: calculated phases of the transmitted signal and idler pulses. A time-dependent phase chirp with the maximum amplitude of less than 0.008 rad was observed.

A very weak, almost parabolic phase chirp of less than 0.008 rad for signal and idler pulses are predicted leading to a very small positive frequency chirp for the signal and a negative (phase conjugation) for the idler pulses (Fig. 5.6, right).

The corresponding experimental results are shown in Fig. 5.7. A small broadening of transmitted signal and idler pulses was observed. The original pulse width of 1.65 ps (FWHM, after some dispersive components (see Fig. B.1) in front of the Ti:PPLN channel guide) is broadened to 1.75 ps for the signal and 1.8 ps for idler pulses, respectively, behind the Ti:PPLN waveguide.

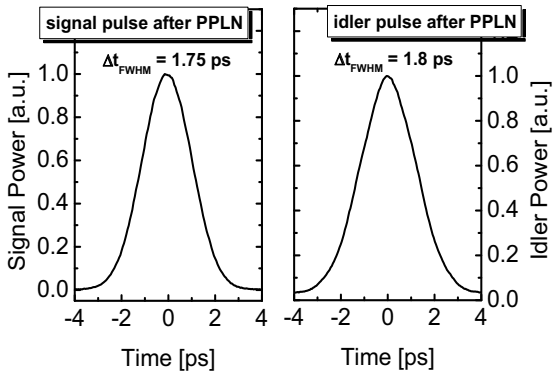

Fig. 5.7: Measured transmitted signal (left) and generated idler (right) pulses behind the Ti:PPLN waveguide [13]. A small broadening of the wavelength shifted pulse is observed. In comparison with the input signal pulse of 1.65 ps FWHM also a small broadening of the transmitted signal pulse was observed.

Moreover, as presented in Fig. 5.8 on the left, the propagation of even shorter pulses of 140 fs halfwidth was theoretically investigated. In this case, a more significant broadening of the signal pulses (λ_s = 1551 nm) to ~200 fs, after transmission through the 60 mm long Ti:PPLN waveguide, was evaluated; this is mainly attributed to GVD. On the other hand, the wavelength shifted idler pulses (λ_i = 1541.4 nm) broaden (parameter dependent) to ~150 fs only; this is again mainly a consequence of the GVD of the waveguide broadening the signal pulses but narrowing the idler pulses after spectral inversion. As presented in Fig. 5.8 on the right, in contrast to the signal pulse, the idler pulse get the negative phase chirp (spectral inversion or phase conjugation) leading to the narrowing of the pulse instead of broadening. In addition, this partial compensation is influenced by the parameters of the nonlinear wavelength conversion in the device. And further propagation in the waveguide without nonlinear interaction (i.e. in a waveguide section without periodic domain grating) should lead to restored idler pulses at the output very similar to the input signal pulses. In other words, it should be possible to design PPLN wavelength converters even for very short pulses, which induce practically no pulse distortions and, therefore, do not lead to a limitation of the bit rate in communication systems. We anticipate that ultra-fast PPLN wavelength converters can be designed for bit rates surpassing 3 Tbit/s.

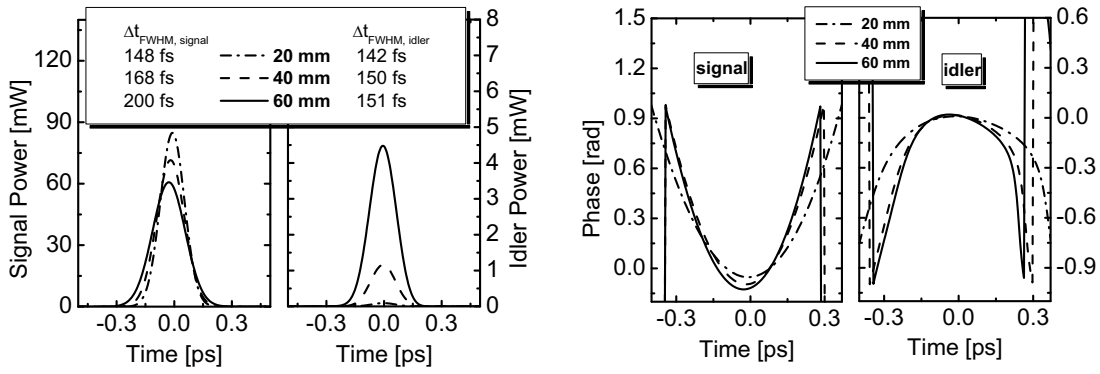

Fig. 5.8: Left: Calculated transmission of the signal and generated idler pulses behind the Ti:PPLN waveguide for 140 fs pulse width. Broadening of the signal pulse up to 200 fs is not observed for the wavelength shifted idler pulse due to phase conjugation effect accompanied by parametric wavelength conversion. Right: Calculated phases for transmitted signal and idler pulses. In contrast to the signal pulse, the phase of the idler pulse has a negative curvature due to phase conjugation leading to a narrowing of the idler pulse while propagating along the waveguide.

5.2 Separated SHG and DFG in a Counter-Propagation Scheme

There is a way to improve the efficiency for wavelength conversion described above. In contrast to the conventional approach of co-propagating signal and fundamental waves as sketched in Fig. 5.9, left, SHG and DFG can be completely separated by exploiting the Ti:PPLN waveguide in forward and in backward directions (Fig. 5.10, above). In this approach the fundamental wave is coupled to the waveguide from the right, generating a phase matched SH wave with its maximum at the left end face. Here a dichroic mirror selectively reflects the SH wave propagating to the right with nearly constant (maximum) amplitude. The signal wave is coupled from the left interacting via DFG with the strong SH (pump) wave. In the conventional approach, both, signal and fundamental waves are coupled to the waveguide from the left (see Fig. 5.9, left); SHG and DFG happen simultaneously during co-propagation to the right. The SH-wave achieves its maximum at the right end face; therefore, also the "local" efficiency of DFG grows during propagation to the right, but yields at the output an idler wave of significantly smaller amplitude. Using both approaches wavelength conversion was investigated with the same sample launching the same fundamental power of 70 mW either from the left through the mirror to the waveguide (Fig. 5.9) or from the right (Fig. 5.10). In both cases the signal is coupled from the left and co- or counter-propagates with the fundamental wave. A conversion efficiency of -20 (-15) dB was observed for the co-propagating (counter-propagating) scheme. This is a significant improvement of the wavelength conversion efficiency by 5 dB.

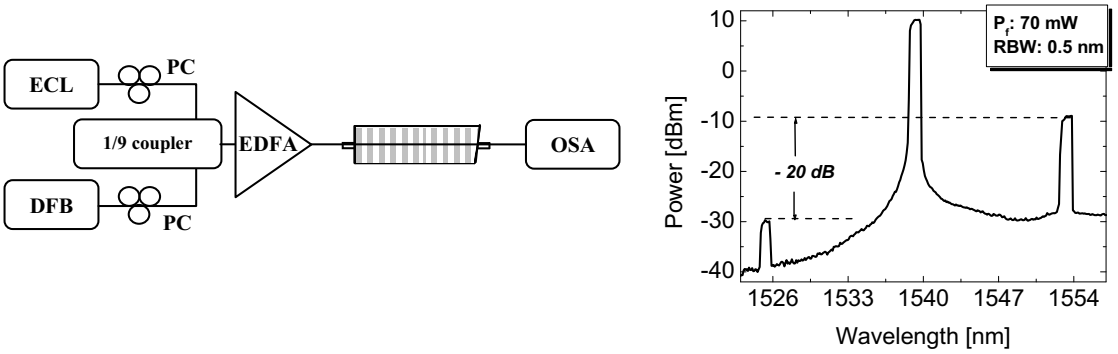

Fig. 5.9: Left: Experimental setup to investigate co-propagating (conventional) cSHG/DF-based wavelength conversion. Right: Measured optical output spectrum for in a scheme.

The residual fundamental power observed in the counter-propagating approach is due to the small mirror reflectivity of about 8% at the fundamental wavelength (Fig. 5.9, lower left). Due to the small amount of power reflection, the noise level in such a configuration (counter-propagating scheme) can be significantely reduced. The noise level in the counter propagating approach is about 10 dB lower than of that in conventional co-propagating scheme (compairing the two spectra in the Figs. 5.9 and 5.10).

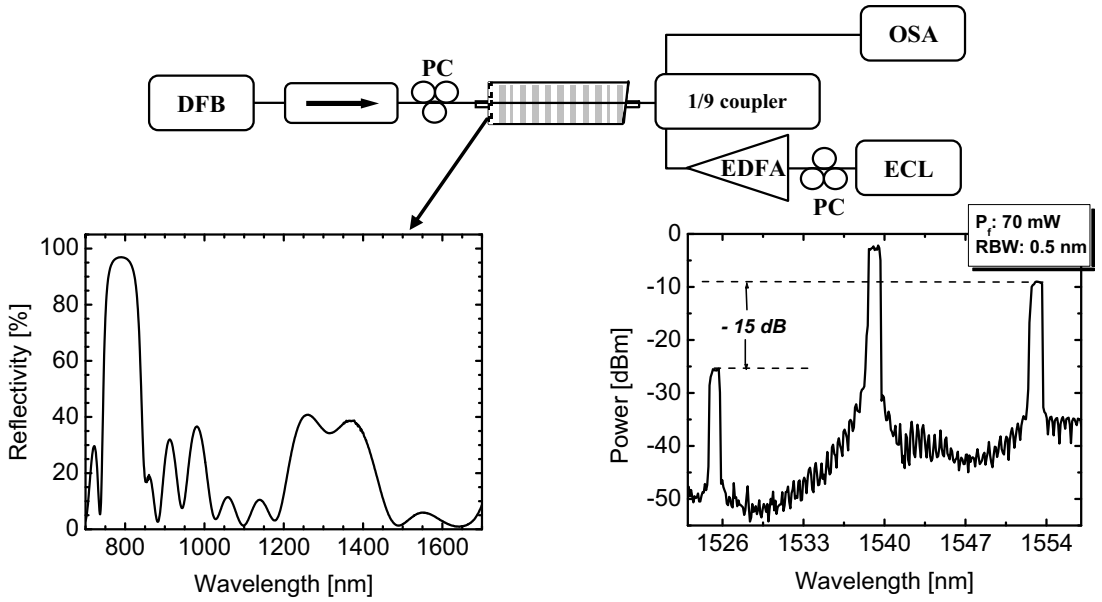

Fig. 5.10: Above: Schematic diagram of experimental setup to investigate counter-propagating cSHG/DF-based wavelength conversion. Lower left: Measured reflectivity of endface couted mirror. Lower right: measured optical output spectrum for wavelength conversion via cSHG/DFG in a Ti:PPLN waveguide with counter-propagating fundamental- and signal waves.

The wavelength conversion efficiency has also been calculated for both approaches as function of the fundamental power (Fig. 5.11, left) and of the

interaction length (Fig. 5.11, right), respectively. As expected, the counter-propagating scheme yields a significant improvement. For an effective interaction length of 37.5 mm, as in our experiment, a 5 dB difference is found by the theory as well; however, the conversion efficiencies are about 6 dB higher than measured. The results of the right diagram in Fig. 5.8 underline again the large potential for an improvement of the conversion efficiency by increasing the length of the devices.

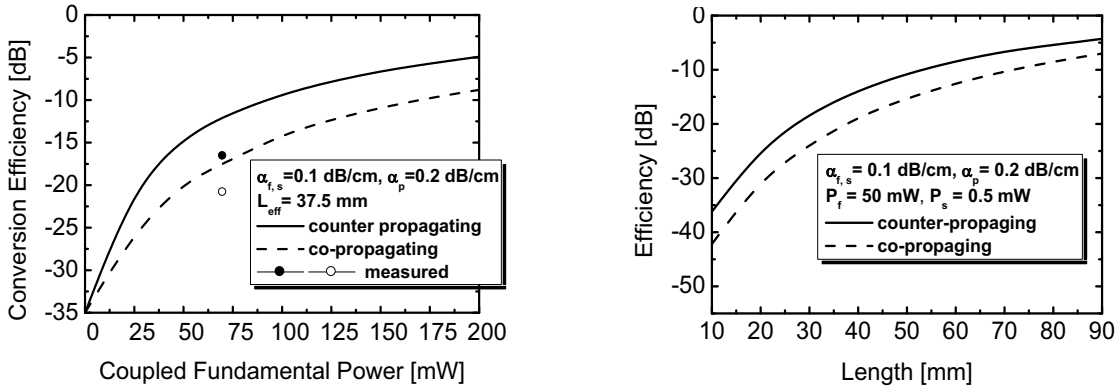

Fig. 5.11: Left: Calculated (solid) and measured (dashed) conversion efficiencies versus coupled fundamental power for co-propagating cDFG (dashed) and counter-propagating bDFG (solid) signal and fundamental waves, respectively.

5.3 cSHG/DFG-Based Wavelength Conversion in Bent Waveguides

The conversion efficiency of cSHG/DFG wavelength converters critically depends on the interaction length. In the limit of negligible depletion at low power levels of the fundamental wave the efficiency grows with the length proportional to L^4 (see chapter 2). Although, at higher power levels with a considerable depletion of the fundamental wave (as in our devices) this growth is weaker, still a remarkable improvement of the conversion efficiency can be expected by increasing the interaction length. Consequently, the fundamental power level can be reduced significantly in a longer device to obtain the same efficiency. Therefore, two approaches have been introduced and experimentally investigated to increase the interaction length. One way is to make a long waveguide by bending the waveguide structure. By this way, waveguides with a length up to 180 mm are realized. The fabrication of these devices and their linear optical characterization have been described in chapter 3.

Bent waveguides allow to double or even triple the interaction length and, therefore, to increase the conversion efficiency, if quasi phase matching can be

maintained over the whole physical length. Fig. 5.12 shows the SHG reponse obtained from such a bent waveguide.

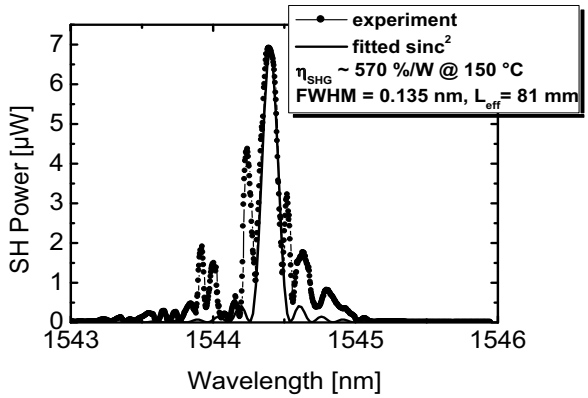

Fig. 5.12: Measured quasi-phase matching curve for SHG in a 155 mm long bent Ti:PPLN waveguide at 150°C.

The setup for the investigation of cSHG/DFG-based wavelength conversion in bent waveguides is sketched in Fig. 5.13. The investigated waveguide has a length of 155 mm; its propagation losses at $\lambda \sim 1550$ nm are only 0.09 dB/cm.

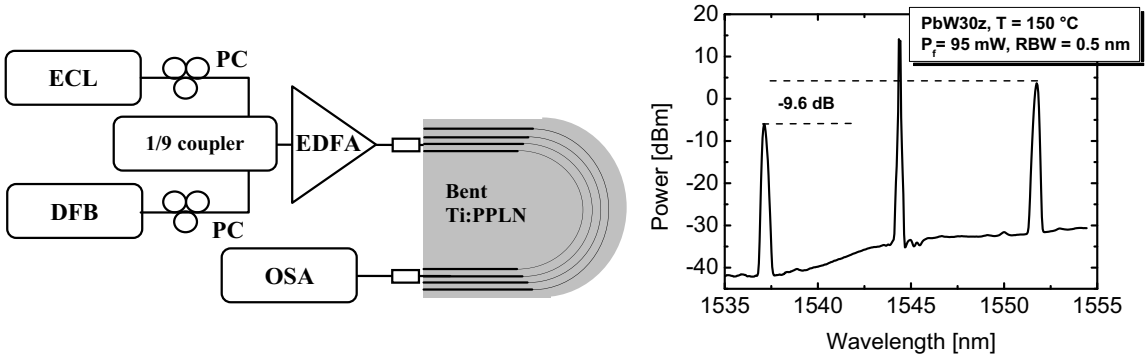

Fig. 5.13: Left: Experimental setup for cSHG/DFG-based wavelength conversion in a bent Ti:PPLN waveguide. Right: Measured optical output spectrum for wavelength conversion via cSHG/DFG in a bent Ti:PPLN-wavguide of 155 mm length.

A measured output optical spectrum is shown in Fig. 5.13 right. Though we had learned from the SHG analysis that the extremely stringent requirements for phase matching over such a long interaction length can hardly be fulfilled, a remarkably high wavelength conversion efficiency of -9.6 dB has been achieved with 95 mW of coupled fundamental power; theory predicts - 4.3 dB. It is evident that with improvements of waveguide and material homogeneity this difference can be made significantly smaller.

5.4. cSHG/DFG-Based Wavelength Conversion in Double-Pass Configuration

The second way of increasing the interaction length consists of using a folded waveguide structure by reflecting all the interacting waves from one end face of the waveguide using an appropriate (broadband) dielectric mirror. Since the realization of long homogeneous PPLN waveguides is difficult, the use of a folded structure where the interacting waves are reflected back into the same waveguide to double the interaction length is an alternative scheme. Fig. 5.14 shows the schematic drawing of the double-pass scheme using a PPLN waveguide. In any nonlinear parametric process, the steady energy transfer requires a well defined phase relation between the interaction waves. Therefore, in cSHG/DFG-based wavelength conversion, this phase relation between fundamental and SH waves on one hand and SH, signal and idler waves on the other hand have to be maintained after the reflection for the second pass through the waveguide. Due to the dispersive properties of a dielectric mirror, not only the reflectance amplitude but also the reflectance phase is wavelength dependent. Therefore, the phase relation between waves interacting via the nonlinear polarization can drastically change. This can lead to a depletion of the converted wave during the second pass rather than a continuation of the conversion process performed during the first pass through the waveguide. Therefore, an efficient phase control scheme is needed to utilized the double-pass for efficiency improvements.

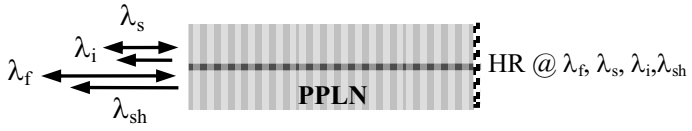

Fig. 5.14: Double-pass configuration with a broadband dielectric mirror deposited on the PPLN waveguide end face.

Phase control schemes have already been reported in the literature for the SHG process alone. For a bulk optical approach Imeshev et al. have used a wedged periodically poled crystal and adjusted the propagation length between mirror and nonlinear crystal for phase control by a lateral movement of the crystal [66]. Hsu and Yang have used a Bragg grating to compensate the relative phase change of the propagating waves in a Ti:PPLN waveguide upon reflection [67]. Huang et al. used phase modulation to tune the phase relation in an unpoled dispersive section of an electro-optic waveguide [68].

In this section, simultaneous phase control for SHG and DFG in a cSHG/DFG-based wavelength conversion in a folded double-pass Ti:PPLN waveguide configuration with a broadband dielectric mirror on one end face of the guide is investi-

gated. To adjust the phase relation between the interacting waves after reflection three different approaches have been investigated which will be discussed in detail.

According to the theoretical background mentioned in chapter 2, in the slowly varying envelope approximation [69] the interaction of the four waves in a cSHG/DFG process, fundamental, SH, signal, and idler waves, is described by first order coupled differential equations of the complex amplitudes:

$$\begin{aligned} A_f &= |A_f| \exp(i\varphi_f) \text{ for fundamental} \\ A_{sh} &= |A_{sh}| \exp(i\varphi_{sh}) \text{ for SH} \\ A_s &= |A_s| \exp(i\varphi_s) \text{ for signal} \\ A_i &= |A_i| \exp(i\varphi_i) \text{ for idler} \end{aligned} \tag{5.1}$$

To provide a steady conversion from the fundamental to the SH wave and growth of signal and idler waves at the expense of the SH pump, the following phase relations (Eqs. 5.2) have to be maintained, simultaneously:

$$\begin{aligned} \varphi_{sh} - 2\varphi_f &= \frac{\pi}{2} \text{ for SHG} \\ \varphi_{sh} - \varphi_s - \varphi_i &= \frac{\pi}{2} \text{ for DFG} \end{aligned} \tag{5.2}$$

For double-pass cSHG/DFG-based wavelength conversion operated in the C-band, both conditions can be simultaneously fulfilled to a good approximation. For such a phase controlled condition simulations predict (as in the waveguide of twice the length) an almost exponential increase of signal and idler powers with the interaction length using sufficient fundamental power (Fig. 5.15, left). For a coupled fundamental power level of 200 mW and a device length of 35 mm the calculated wavelength conversion efficiency of the double-pass configuration surpasses that of the single pass version by ~ 10 dB (Fig. 5.15, right).

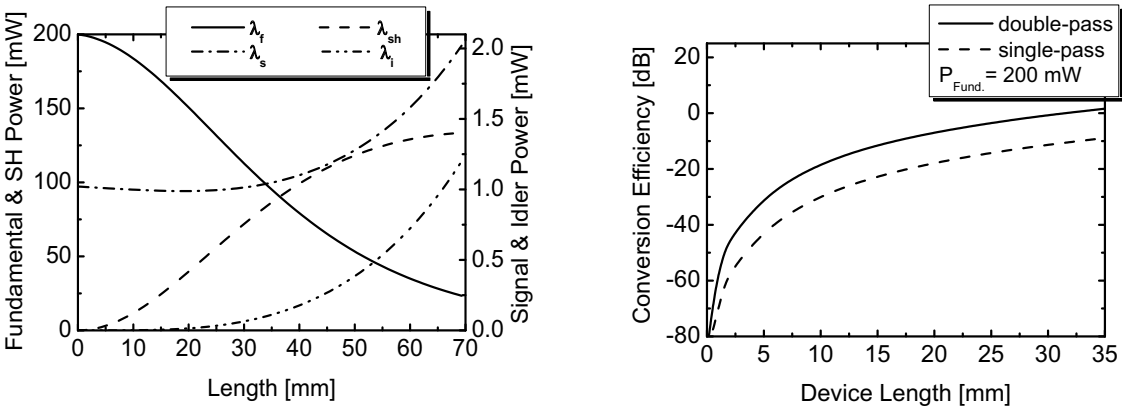

Fig. 5.15: Left: Simulated evolution of cSHG/DFG: power levels versus interaction length for 200 mW of coupled fundamental power. Right: Comparison of calculated cSHG/DFG conversion efficiencies in single- and double-pass devices for 200mW of coupled fundamental power versus device length.

For a specifically designed (15 layer) broadband dielectric mirror reflecting all interacting waves involved in the cSHG/DFG process, the calculated wavelength dependent phase shifts modulo 2π for fundamental ($\Delta\varphi_f$), signal ($\Delta\varphi_s$), and idler ($\Delta\varphi_i$) waves and the SH ($\Delta\varphi_{sh}$) wave are shown in Fig. 5.16 versus wavelengths in the C-band and around 775 nm, respectively. In both wavelength ranges, the wavelength dependence phase shifts are almost linear with different slopes.

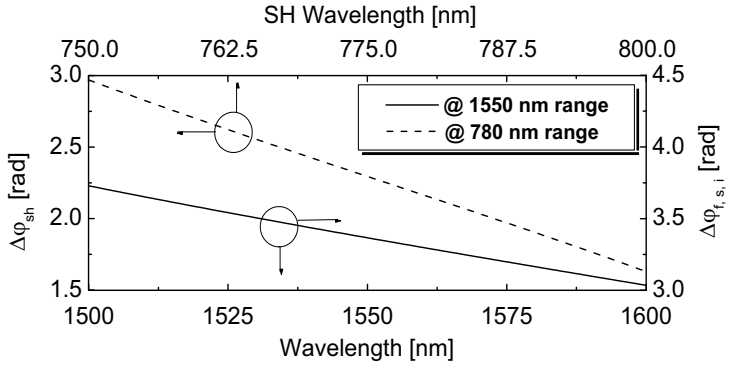

Fig. 5.16: Calculated phase shifts $\Delta\varphi_{f,\,s,\,i}$ and $\Delta\varphi_{sh}$ for fundamental, signal, idler, and second harmonic waves induced by an broadband dielectric mirror versus wavelength in the ~ 1550 nm (lower scale) and ~ 775 nm (upper scale) range, respectively.

To maintain a steady energy transfer by the SHG and DFG processes after reflection, the changes of the phase differences by reflection (Eqs. 5.3) have to be compensated:

$$\begin{aligned} \Delta\varphi_{SHG} &= \Delta\varphi_{sh} - 2\Delta\varphi_f \text{ for SHG} \\ \Delta\varphi_{DFG} &= \Delta\varphi_{sh} - \Delta\varphi_s - \Delta\varphi_i \text{ for DFG} \end{aligned} \tag{5.3}$$

Since signal and idler wavelengths are located symmetrically with respect to the fundamental wavelength and all wavelengths are in a narrow band, their phase shifts can be approximated by:

$$2\Delta\varphi_f \approx \Delta\varphi_s + \Delta\varphi_i$$

which consequently is leading to:

$$\Delta\varphi_{DFG} = \Delta\varphi_{sh} - \Delta\varphi_s - \Delta\varphi_i \approx \Delta\varphi_{sh} - 2\Delta\varphi_f = \Delta\varphi_{SHG} \tag{5.4}$$

Therefore, a phase compensation $\Delta\varphi_{comp}$ can indeed be achieved for both processes, SHG and DFG, simultaneously. The following conditions have to be fulfilled:

$$\Delta\varphi_{SHG} + \Delta\varphi_{comp} \approx \Delta\varphi_{DFG} + \Delta\varphi_{comp} = 0 \text{ or } m2\pi \tag{5.5}$$

In order to control the phase relationship between the interacting waves after reflection, three different phase compensation schemes are introduced and were experimentally investigated.

Fig. 5.17 shows the experimental setup to investigate double-pass cSHG/DFG with the different phase control schemes. A tuneable external cavity laser (ECL) was used as fundamental source; a fixed wavelength DFB-laser served as signal source. Polarization controlled (PC) signal and fundamental waves were combined by a 3 dB coupler and boosted by an erbium doped fiber amplifier (EDFA). The light was butt coupled to the temperature stabilized waveguide. Single-pass wavelength conversion spectra were investigated using an optical spectrum analyzer (OSA) in forward direction. In backward direction, double-pass cSHG/DFG spectra were recorded using a circulator and an OSA.

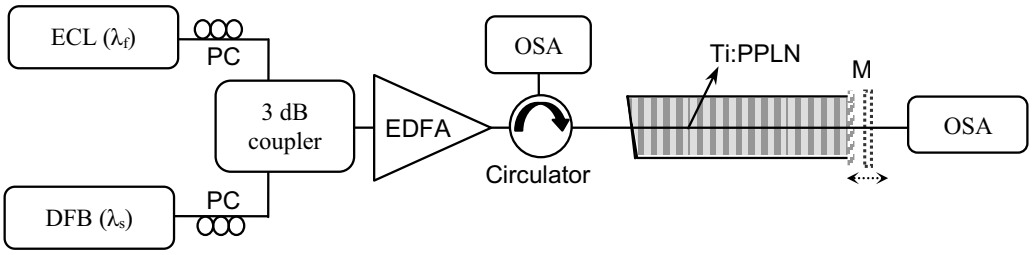

Fig. 5.17: Experimental setup to investigate double-pass cSHG/DFG: ECL - external cavity laser; DFB – distributed feedback laser; PC – fiber optical polarization controller; EDFA - erbium doped fiber amplifier; OSA – optical spectrum analyser; M – dielectric mirrors, deposited on waveguide end face and movable, respectively.

a. Phase control with dichroic mirrors of adjustable spacing

In this phase control scheme different interacting waves in two different wavelength ranges are reflected by two sequential dichroic mirrors: The first mirror, which is directly deposited on the polished waveguide end face, selectively reflects the SH wave (780 nm range) and transmits fundamental, signal, and idler waves (Fig. 5.18, solid graph). Its measured transmittance is only ~ 2% for the SH, but more than 98% for fundamental, signal, and idler waves. The second mirror is an external one and its separation from the first one can be adjusted; it reflects fundamental, signal and idler waves (C-band) only. This broadband mirror has a high reflectivity (more than 98%) fundamental, signal, and idler waves but it is highly transparent for the SH-wave (Fig. 5.18, dashed graph).

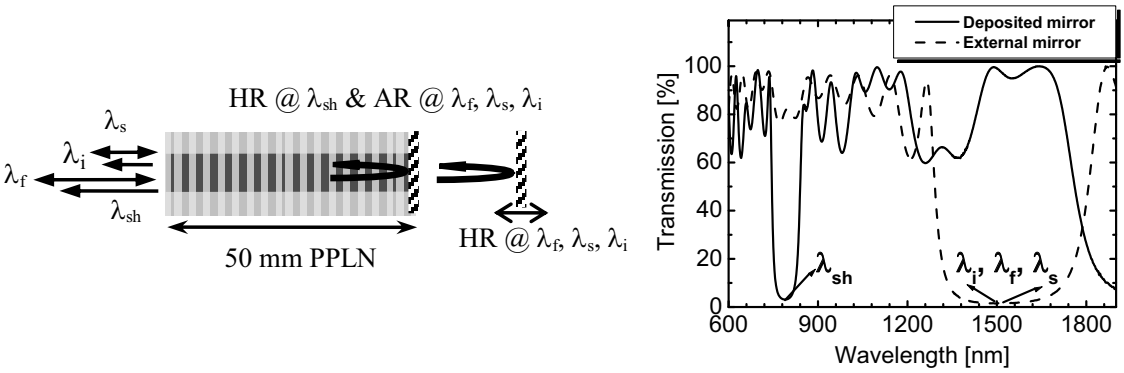

Fig. 5.18: Left: Double-pass configuration using two dichroic mirrors. AR – anti reflection coated; HR – high reflection coated. Right: Measured transmission versus wavelength of the mirror deposited on the waveguide end face (solid) and of the external moveable mirror (dashed).

By controlling the separation Δz of the external mirror to the waveguide end face within half a fundamental wavelength, the phase relationship between the

reflected SH wave and the fundamental, signal, and idler waves can be adjusted according to:

$$\Delta\varphi_{comp} = 2\pi\left(\frac{2\Delta z}{\lambda_f}\right) \tag{5.6}$$

This leads to maximum power transfer from the fundamental to SH, signal, and idler waves. The coupling loss back into the waveguide is negligible as long as the mirror separation is smaller than a wavelength (the Rayleigh range for a wavguide with 7 µm width is about 20 µm).

Using this scheme an improvement of cSHG/DFG-based wavelength conversion of 7.5 dB has been achieved in comparison to the single-pass configuration for the same device of 50 mm length. In Fig. 5.19 the experimental results for SHG (left diagram) together with the cSHG/DFG wavelength conversion spectra (right diagram) are shown. The improvement of 7.5 dB agrees reasonably well with the theoretically predicted 10 dB for an effective interaction length of 35 mm derived from the single-pass SHG characteristic.

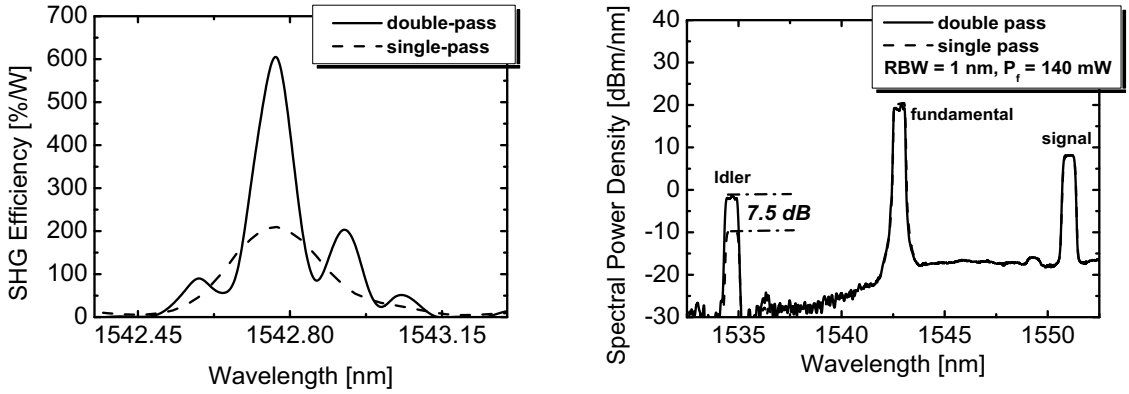

Fig. 5.19: Left: Measured single- and double-pass SHG efficiency versus fundamental wavelength. Right: Measured spectra for single- and double-pass wavelength conversion by cSHG/DFG. Device temperature was 190 °C in both experiments.

b. Exploiting the Dispersion of $LiNbO_3$ within an Unpoled Waveguide Section L

In this case the waveguide is not completely periodically poled but has an unpoled section just in front of the broadband dielectric mirror. In this case the deposited mirror reflects both, fundamental and SH wavelength ranges (Fig. 5.20, right). This phase controlling scheme has been realized by two different configurations:

i. An unpoled, several mm long section of the waveguide in front of the end face mirror allows to adjust the phase differences of the interacting waves by a small wavelength shift of the fundamental wave (higher order approach)

ii. The same adjustment can be achieved by a very short waveguide section of appropriate length, corresponding to a fraction of half a domain period. Waveguide sections of slightly different lengths before the end face mirror were fabricated by tilting a homogeneous domain grating over a set of waveguides. Then the channel leading to optimum phase compensation can be selected (zero order approach).

i. Higher Order Approach, Allowing Wavelength Tuning

If the unpoled waveguide section has a length of several mm (Fig. 5.20, left), the phase relation between the interacting waves can easily be changed within 2π by slightly tuning the fundamental wavelength within the acceptance bandwidth of the QPM-condition (0.3 nm in our device for the single-pass). Therefore, the wavelength dependent phase shifts by reflection from the dielectric mirror can be fully compensated.

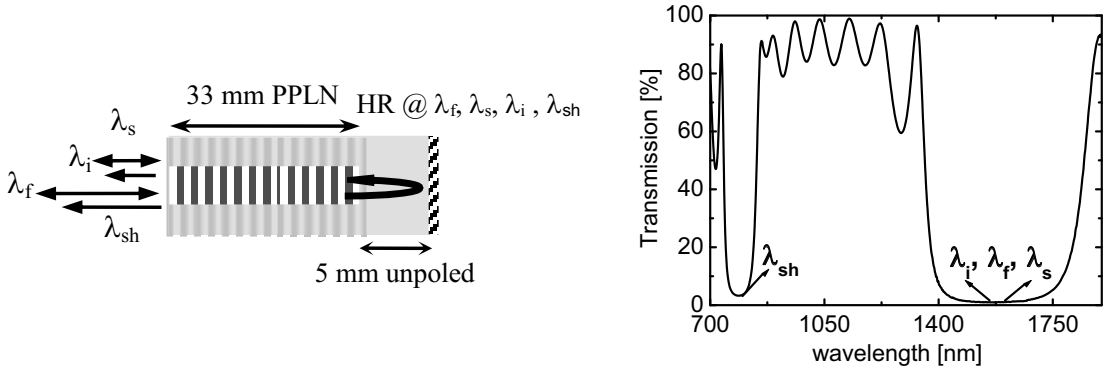

Fig. 5.20: Left: Operating scheme. Right: Measured transmission of the broadband dielectric mirror deposited on the polished waveguide end face.

In the 5 mm long unpoled waveguide section used in our experiments, a total relative phase change $\Delta\varphi_{\text{dispersion}}$ of about $1000(2\pi)$ is induced by:

$$\Delta\varphi_{\text{dispersion}} = \Delta\varphi_{\text{dispersion,sh}} - 2\Delta\varphi_{\text{dispersion,f}} \tag{5.7}$$

It strongly depends on the fundamental wavelength yielding a slope of:

$$\frac{\mathrm{d}(\Delta\varphi_{\text{dispersion}})}{\mathrm{d}\lambda_{\text{f}}} = 10\pi/\text{nm} \tag{5.8}$$

Therefore, a very small tuning of the fundamental wave is sufficient to adjust phase compensation. In our experiment a wavelength change of only 29 pm resulted in a 5 dB improvement of the double-pass SHG efficiency compared to the single-pass result. This was the basis to get nearly 9 dB improvement of signal to idler conversion efficiency for cSHG/DFG-based wavelength conversion (Fig. 5.21) which is in good agreement with predicted theory (10 dB).

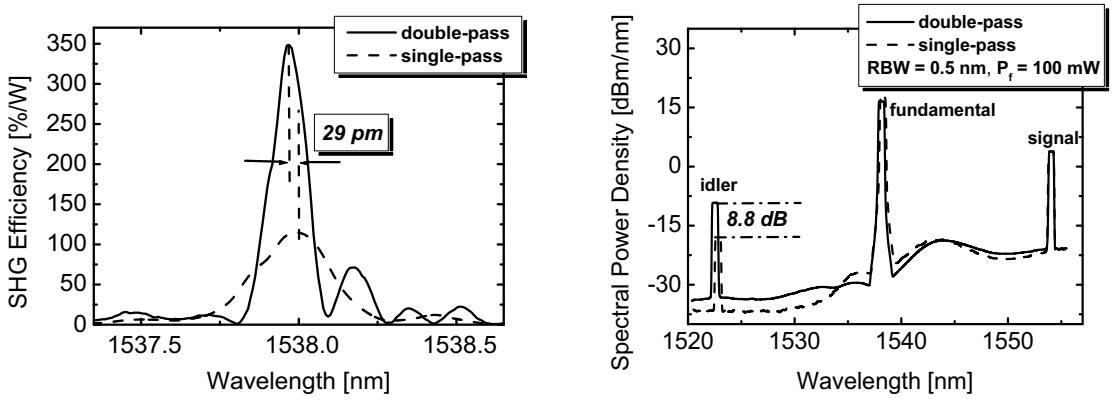

Fig. 5.21: Left: Measured single- and double-pass SHG efficiencies versus the fundamental wavelength. Right: Measured spectra for single- and double-pass wavelength conversion by cSHG/ DFG. Device temperature was 190 °C in both experiments.

ii. Zero Order Approach, Selecting the Right Section Length

Similar to the approach discussed in the former section the dispersion within a fraction (L) of half a domain period ($\Lambda/2 = L_c$) can be utilized to adjust the phase relation after reflection of the interacting waves. By slightly tilting the periodically poled domain grating with respect to the mirror the channel within a batch of parallel waveguides can be selected for which the phase adjustment (Eqn. 5.9) is fulfilled:

$$\Delta\varphi_{comp} = \Delta\varphi_{SHG\,or\,DFG} - \frac{2\pi L}{L_c} \tag{5.9}$$

The operating scheme to investigate double-pass cSHG/DFG wavelength conversion in a Ti:PPLN waveguide with tilted domain grating together with the condition for the compensation of the change in phase relation is shown in Fig. 5.22, left. Waveguides with different fractions of the final domain period in front of the mirror have been investigated clearly showing the dependence of the SHG efficiency on the length of this last domain fraction (Fig. 5.22, right).

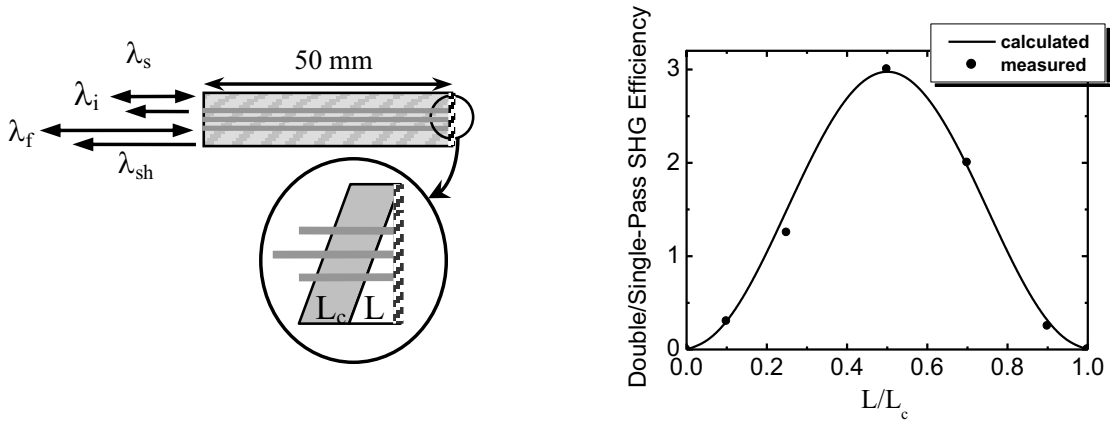

Fig. 5.22: Left: Schematic drawing of the Ti:PPLN-waveguide sample with a tilted domain grating (L indicates the wedged domain fraction, L_c is the width of a complete domain). Right: Measured and calculated double-pass SHG efficiency with respect to the single-pass efficiency for waveguides with different fractions $L/L_c$of the last domain.

Fig. 5.23 shows the measured SHG-efficiency for both, single- and double-pass (left diagram), and the experimental results of the corresponding cSHG/DFG-wavelength conversion (right diagram). About 5 resp. 8 dB of improvement were measured for the double-pass SHG resp. wavelength conversion efficiency compared to the single-pass. As this compensation scheme is of zero order we can expect a large compensation bandwidth which is suitable for multi-wavelength conversion in WDM-systems.

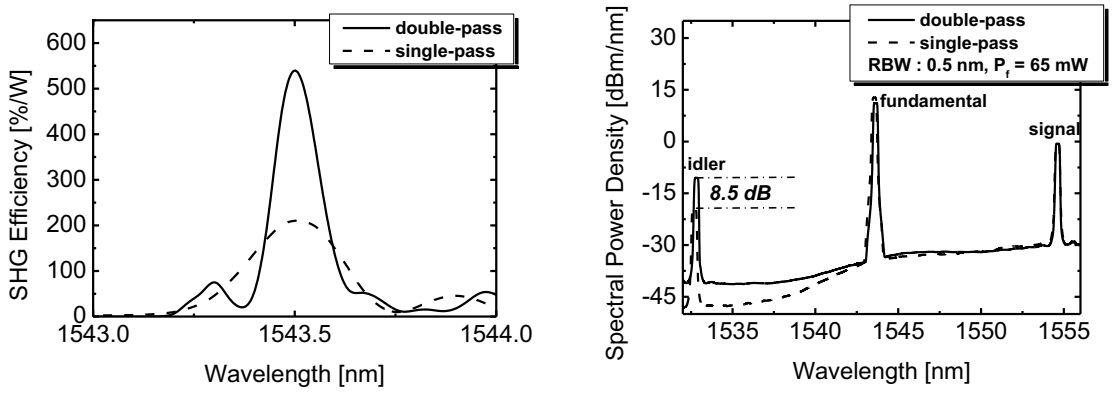

Fig. 5.23: Left: Measured single- and double-pass SHG-efficiencies versus the fundamental wavelength. Right: Measured spectra for single- and double-pass wavelength conversion by cSHG/DFG. Device temperature was 190 °C in both experiments.

The noise level of the double-pass with respect to the single-pass towards the idler is increased (see Figs. 5.21 and 5.23 rights). Since cSHG/DFG-based wavelength conversion has a large bandwidth covering whole C-band in our

experiments, the amplified spontaneous emission (ASE) of boosted fundamental wave by EDFA between fundamental and signal wavelength can also be wavelength converted. However, for the lower single-pass conversion efficiency the level of converted ASE spectral power density is low enough to be hidden by the ASE of the EDFA itself close to the fundamental wavelength. At larger wavelength separation from the fundamental towards the idler the ASE level of the amplifier is low enough to observe the converted ASE from the signal side.

5.5 cSHG/DFG-Based Wavelength Conversion in a Ti:PPLN Waveguide Resonator for the SH Wave

To improve the wavelength conversion efficiency in a cSHG/DFG process, the fundamental and/or the SH-wave can be enhanced in an appropriate waveguide resonator [57], [70]. The enhancement of the fundamental wave requires narrowband grating mirrors for fundamental only, in the waveguide itself. As their fabrication is difficult, the resonant enhancement of the SH-wave for cSHG/DFG-based wavelength conversion has been investigated in this section to reach reasonably high pump power levels with low external fundamental power.

To investigate SH-wave resonant cSHG/DFG, a 30 mm long Ti:PPLN channel waveguide is used. Its micro-domain periodicity was Λ = 16.5 μm. The challenge was to develop such a Ti:PPLN waveguide with the extremely high homogeneity and low loss required to get a resonant QPM interaction along the whole waveguide length. The low loss (0.03 dB/cm around 1550 nm) Ti:PPLN waveguide sample was coated using vacuum deposition on both polished end faces. The coated dielectric mirrors provide a high reflectivity of ~ 96 % at the pump wavelength around 770 nm and almost perfect transmission at the fundamental signal and idler wavelengths around 1550 nm. Modeling calculations show that 7 pairs of SiO_2 and TiO_2 layers will form dielectric multilayer mirrors of the required spectral properties. Fig. 5.24, left, presents the measured reflectivity spectrum (spectral reflectivity) of the mirrors.

The transmission through the waveguide cavity was measured over several resonances using a narrow linewidth TiSa-laser (λ_{sh} =765 nm) and temperature tuning (see Fig. 5.24, right). From the transmission curve a finesse of about 11 can be estimated. For the reflectivities mentioned above this finesse figure is consistent with a TM waveguide loss of 0.03 dB/cm only.

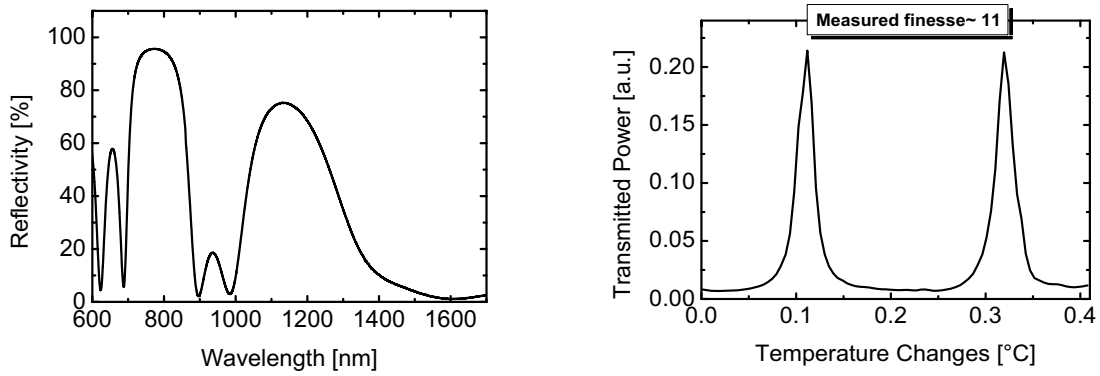

Fig. 5.24: Left: The mirror reflectivities at 765 nm are 93.5 and 92.1%, respectively. Right: Measured normalized transmission at 765 nm wavelength (TM-polarized) of a Ti:PPLN-waveguide cavity with dielectric mirrors versus temperature change.

To record the quasi phase matching curve an external cavity laser (ECL) for $\lambda_f \approx$ 1550 nm was used as the fundamental source. The result is shown in Fig. 5.25, on the right. The shape of the phase matching curve (Fig. 5.25, left) appears as envelope of the successive SHG-resonances.

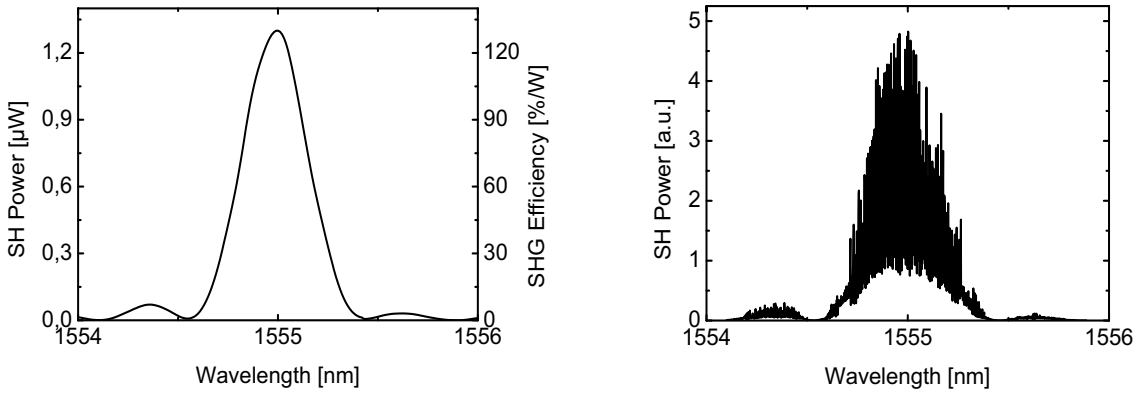

Fig. 5.25: Measured SH power versus fundamental wavelength for non-resonant (left) and resonant (right) SHG in the waveguide sample discussed above for a 6 µm Ti:PPLN-waveguide. The fundamental wavelength was scanned in steps of 1 pm for resonant SHG.

Wavelength conversion via cSHG/DFG has been investigated with the setup sketched in Fig. 5.26. To achieve a stable pump power level by resonant SHG a stabilization of the SHG-resonance via a precise control of the cavity length or the fundamental frequency is required. We decided to control the fundamental frequency and to temperature-stabilize the waveguide cavity. The control loop is used to stabilize the SH-power within the resonator. For this purpose a control loop is built

up as depicted in Fig. 5.26 on the left. An external cavity laser is used as the fundamental source. A function generator is used to slightly dither its frequency via piezo-fine tuning of its cavity length. The generated SH-power is detected using a Si-PIN-photodiode and a lock-in amplifier synchronized to the dithering frequency. The lock-in output is superimposed to the dithering signal using a bias-tee. The output of the bias-tee tunes the ECL-frequency until the peak of the SHG- resonance is reached.

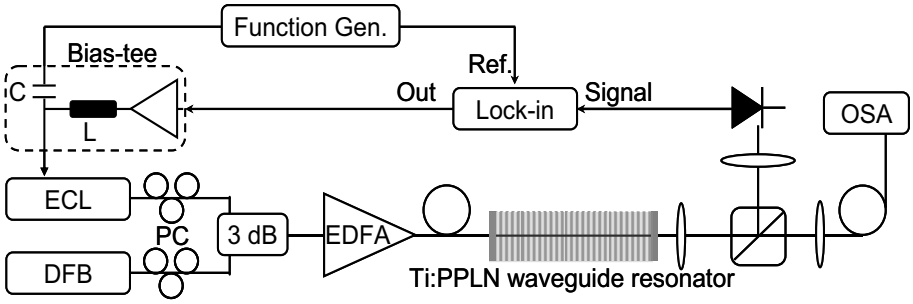

Fig. 5.26: Experimental setup to investigate wavelength conversion via cSHG/DFG with resonantly enhanced SH-wave as pump of the DFG process with simultaneous stabilization of the SH-power via a feedback loop for the control of the fundamental (ECL-) wavelength.

The ECL was operated at λ_f = 1554.9 nm (fundamental wavelength); the DFB-laser diode emitted at λ_s = 1551 nm (signal wavelength). Polarization controlled fundamental and signal waves were multiplexed using a 3 dB coupler, boosted by an EDFA and butt-fiber coupled to the Ti:PPLN-waveguide cavity serving as cSHG/DFG-based wavelength converter. Collimation optics together with a beam splitter were used to extract a control signal and to simultaneously investigate the output spectrum with an optical spectrum analyzer (OSA). The Ti:PPLN-waveguide cavity was heated to 210°C to avoid photorefraction.

In Fig. 5.27, left, the controlled SH-power out of the waveguide cavity has been recorded over 1 hour. The power varies within ± 7 %. With about 50 mW of coupled fundamental power a wavelength conversion efficiency of -20 dB was observed (see Fig. 5.27, right). This value is in good agreement with simulated results of -18 dB. This corresponds to about 10 dB improvements in the wavelength conversion efficiency in comparison with the non-resonant (conventional) cSHG/DFG-based wavelength conversion. At higher fundamental power levels the control scheme to stand in one particular resonance condition of the cavity failed due to strong onset of photorefractive damage.

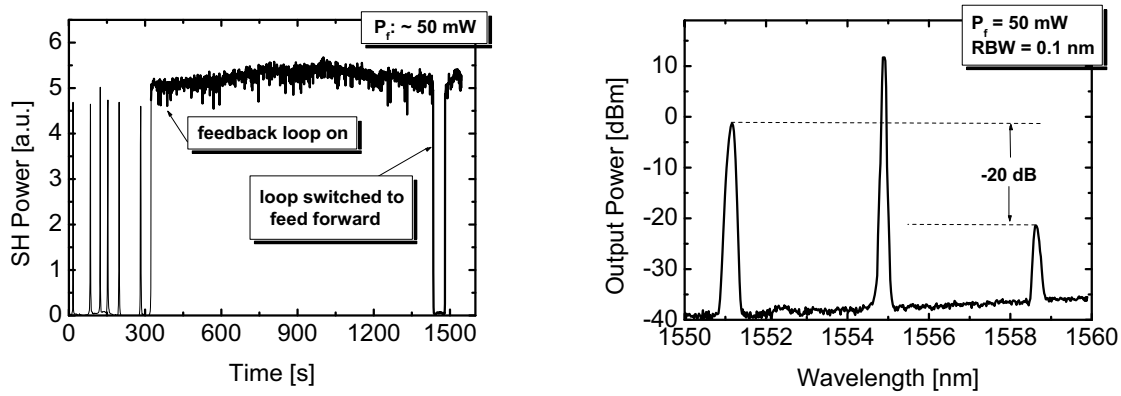

Fig. 5.27: Left: SH-power versus time for 50 mW of coupled fundamental power. When the feedback loop is closed stabilaization scheme runs to stand in a resonance peak. In feed forward it pushes to a deep (out of resonance). Right: Measured optical output spectrum for wavelength conversion via cSHG/DFG in an Ti:PPLN-waveguide cavity with resonantly enhanced SH-wave as pump of the DFG process.

5.6 Summary

Polarisation dependent and independent cSHG/DFG-based wavelength conversion in straight Ti:PPLN waveguides are reported. The performance of such devices has been investigated in system experiments in detail; they are described in chapter appendix B. In the polarization independent device wavelength conversion is done in a polarization diversity scheme. The same waveguide is used for both polarizations in bidirectional operation in a ring configuration. In this way polarisation mode dispersion (PMD) is automatically avoided by group delay equalization of the two converted polarization components. A conversion efficiency of -7 dB has been achieved for the polarisation dependent device (-13 dB in for polarisation independent one), which could be more enthusiastic for many applications (see appendix B).

Theoretical and experimental investigations of the temporal shape and chirp of the converted data pulses show only very little broadening and chirping indicating the potential for wavelength conversion of even much higher data rates. This is confirmed by modeling calculations of signal and idler pulse evolution of even shorter halfwidth. They reveal that pulse broadening of the signal pulses induced by group velocity dispersion can already be compensated to a large degree in the device itself as a consequence of the spectral inversion of the wavelength shifted idler. Therefore, the ultra-fast Ti:PPLN wavelength converters can be designed for bit rates surpassing 3 Tbit/s.

Conversion with counter-propagating signal and pump waves has been shown to yield a significant improvement of the conversion efficiency. Unfortunately, this approach is not suited for polarization independent conversion.

Also bent waveguides of long nonlinear interaction length should allow combining improved conversion efficiency with polarisation insensitivity using the same diversity scheme. However, in practice the expected improvement could not be achieved due to insufficient control of quasi phase matching along the whole waveguide length.

Double-pass SHG respectively cascaded SHG/DFG for wavelength conversion in the C-band of optical telecommunications has been reported. To optimize the wavelength conversion efficiency in the double-pass configuration three different schemes for compensating wavelength dependent phase shifts upon reflection have been investigated. More than 5 dB improvement of the SHG-efficiency compared to the single-pass has been achieved. This is close to the 6 dB predicted for a lossless waveguide and an undepleted fundamental wave. Using the cascaded SHG/DFG-based wavelength conversion ~ 9 dB improvement of the efficiency compared to the single pass configuration has been obtained in reasonably good agreement with the predicted 10 dB for undepleted small signal conversion.

The SH-wave resonator enhances the intracavity SH power. Therefore significant reduction of the required input fundamental power level can be expected. Based on this scheme, an improvement of ~10 dB for cSHG/DFG-based wavelength conversion efficiency has been achieved with 50 mW of coupled fundamental power in a 30 mm long Ti:PPLN. However, operation was limited to relatively small fundamental power levels (< 50 mW) due to the onset of photorefractive instabilities destroying the cavity stabilization. This approach requires damage resistant waveguides to achieve good stabilization of a SH resonance. Moreover, coupled cavity effects may deteriorate a stable bidirectional operation for polarization independent conversion.

6. Cascaded Sum and Difference Frequency Generation (cSFG/DFG)-Based Wavelength Converters

Tuneable wavelength converters which can cover the whole C-band (1535 nm – 1565 nm) is desirable for future optical networks in order to construct much more flexible communication systems. Cascaded second harmonic generation and difference frequency generation (cSHG/DFG) in a periodically poled $LiNbO_3$ (PPLN) waveguide is an attractive method, owing to the large bandwidth and modulation format transparency. However, for conventional cSHG/DFG-based wavelength converters, due to the limited SHG bandwidth (typically ~ 0.2 nm), the SH (pump) wave tolerance is very small. Therefore, realization of tuneable wavelength conversion of a fixed signal wave over the whole C-band is impossible. To overcome such restriction, cascaded sum and difference frequency generation (cSFG/DFG) was proposed in recent years [71], [72], [73]. In this chapter an experimental investigation of tuneable cSFG/DFG-based wavelength conversion in Ti:PPLN straight waveguides is presented. In addition, the temporal evolutions of the pulsed signal and idler propagating along the PPLN waveguide are simulated to show the capability of such a device for practical applications in a communication system.

6.1 cSFG/DFG-Based Wavelength Conversion in Ti:PPLN Waveguides

Fig. 6.1 illustrates the operation principle of cSFG/DFG-based tuneable wavelength conversion. The input signal wave (λ_s) is mixed with the pump wave (λ_p) to generate a SF (λ_c) via SFG. With the interaction of the SF and control waves (λ_c) via DFG, the idler wave (λ_i) can be generated. Since the signal wave is involved to generate the required pump (SF) wave for the DFG process, the information carried by the signal wave is successfully copied to the idler wave. Therefore, tuneable wavelength conversion from a fixed signal to any idler wavelength can be achieved.

When SFG occurs between signal and pump, the idler wavelength is given by $1/\lambda_i = 1/\lambda_s + 1/\lambda_p - 1/\lambda_c$. Therefore, for a fixed signal wavelength, tuneable idler wavelength can be obtained by tuning the control wavelength (Fig. 6.1a). In addition,

if the signal wavelength is changed, the pump wavelength can be tuned to get a constant idler wavelength (Fig. 6.1b). Therefore, by proper wavelength adjustments of pump and control waves, fixed-in/tuneable-out, tuneable-in/fixed-out functions can be performed using cSFG/DFG-based wavelength converters. In this chapter, in order to realize tunable wavelength down- or up-conversions, SFG of pump and signal waves is studied.

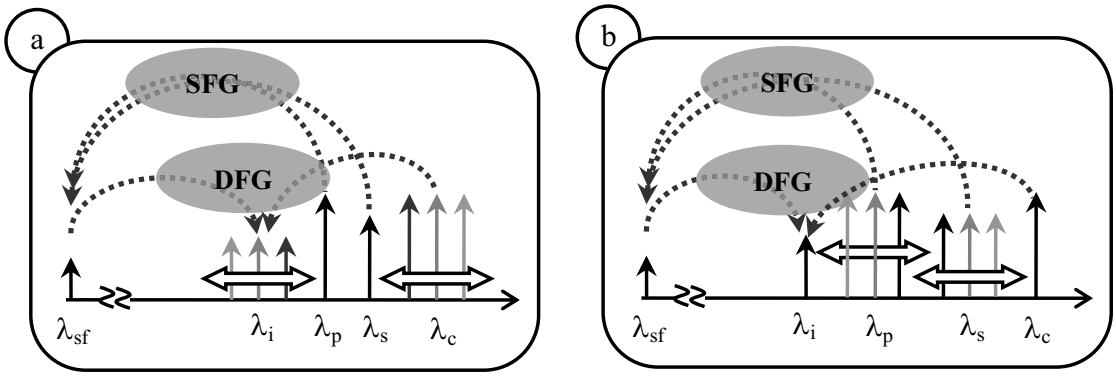

Fig. 6.1: The operation principle of tuneable cSFG/DFG-based wavelength conversion for fixed-in/tuneable-out (a) and tuneable-in/fixed-out (b) wavelengths.

Polarization-Dependent Tuneable Wavelength Converter

The generated idler wavelength (λ_i) is governed by the following expression:

$$\frac{1}{\lambda_i} = \frac{1}{\lambda_s} + \frac{1}{\lambda_p} - \frac{1}{\lambda_c} \tag{6.1}$$

From Eqn. 6.1, for a fixed input signal wavelength, the pump wavelength has to be adjusted to meet the QPM condition for the SFG process: then the output idler wavelength can be tuned by simply tuning of the control wavelength.

The packaged Ti:PPLN waveguide sample used in this experiment is the same used for the demonstration of the cSHG/DFG-based wavelength converters described in the previous chapter. The experimental setup for the investigation of cSFG/DFG-based tuneable wavelength conversion is sketched in Fig. 6.2 left. Light of a DFB-laser served as signal source (λ_s = 1556 nm). In order to provide flexible tuneability of the wavelength converter, two tunable extended cavity lasers (ECL) (λ_f = 1480 – 1640 nm) served as the pump and control wave sources, respectively. The control and the signal waves were combined by a 3 dB coupler. The pump wave was boosted by an erbium doped fiber amplifier (EDFA) and butt coupled to the tempe-

rature stabilized Ti:PPLN waveguide through another 3 dB coupler. The polarization of all three input waves was controlled using a fiber-optical polarization controller (PC). The output spectra were recorded using an optical spectrum analyzer (OSA). The phase matched SFG at temperature of T = 193°C was met by λ_p = 1543 nm as pump wavelength and λ_s = 1556 nm as signal wavelength.

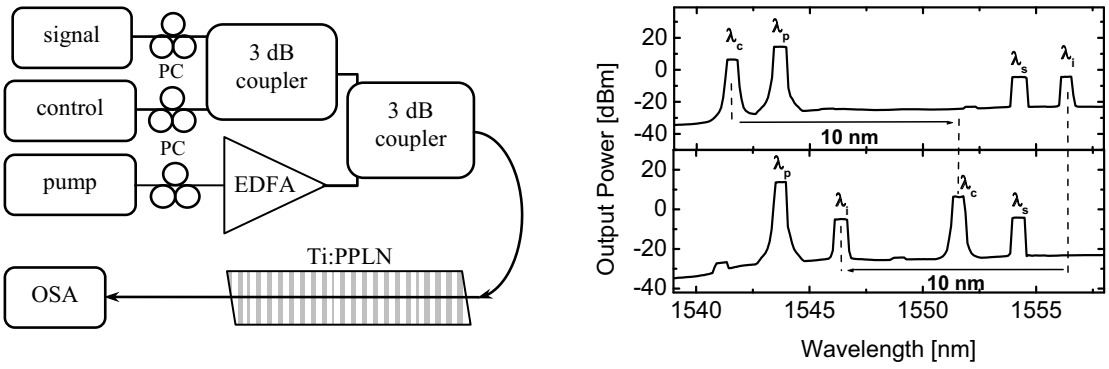

Fig. 6.2: Left: Setup to investigate cSFG/DFG-based tuneable wavelength conversion in a 80 mm long Ti:PPLN-waveguide. Right: Optical spectrum at the output of the packaged and pigtailed, polarization dependent wavelength converter. 10 nm of tuneability is shown as an example.

With coupled pump power of P_p = 80 mW, a 7 dB depletion of the signal wave (P_s ~ 5 mW → P_s ~ 1 mW) due to the generation of the SF wave results. In this way, an external ($P_{s,\,in}$ / $P_{i,\,out}$) conversion efficiency of -7.5 dB has been achieved. Fig. 6.3 on the left presents the calculated evolution of five interacting waves along a 70 mm long Ti:PPLN waveguide. The measured external efficiency is in good agreement with predicted calculation (Fig. 6.3, left; inset).

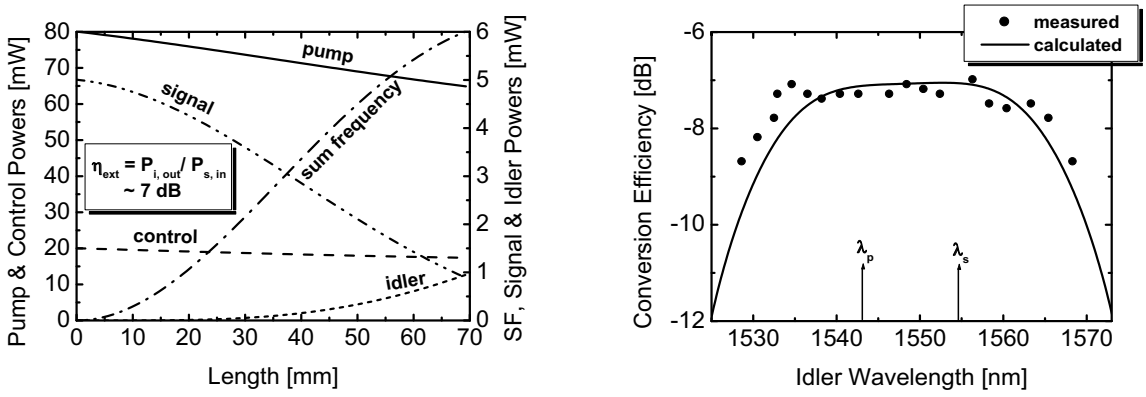

Fig. 6.3: Left: Calculated evolution of pump, SF, signal, control and idler power levels along the waveguide for 80 and 20 mW of coupled pump and control power levels, respectively. Right: Measured and calculated operation bandwidth for fixed signal (λ_s = 1554.2 nm) and pump (λ_p = 1543.2 nm) waves as conversion efficiency versus idler wavelength (λ_i = 1528.7 – 1556.4 nm).

The measured and calculated tuning bandwidth of the idler for a fixed signal wavelength of 1554.2 nm is shown in the Fig. 6.3 on the right. The idler tuning bandwidth with about -7.5 dB of wavelength conversion efficiency covers the whole telecom C-band (1535 nm – 1565 nm).

Polarization-Independent Tuneable Wavelength Converter

A polarisation diversity scheme similar to that of cSHG/DFG presented in chapter 5 is applied to achieve polarisation insensitive cSFG/DFG-based tuneable wavelength conversion.

Fig. 6.4 illustrates the setup used for polarization independent tuneable wavelength conversion. The diversity sheme in a ring configuration similar to that used for the cSHG/DFG-based wavelength converter can be used for the cSFG/DFG as well. In this way, the fibre optic polarization beam splitter (PBS) with polarization maintaining (PM)-pigtails splits pump and control waves into their TM and TE components. Since the TM (e.g. from the left) and the TE (e.g. from the right with 90° rotation as TM wave) components are launched into the converter, by a proper adjustment of the polarization of the pump and control waves, equal conversion efficiencies for both polarization components of the signal wave can be expected. The PBS recombines the polarization components of the transmitted and converted signals and feeds them into an optical spectrum analyzer (OSA).

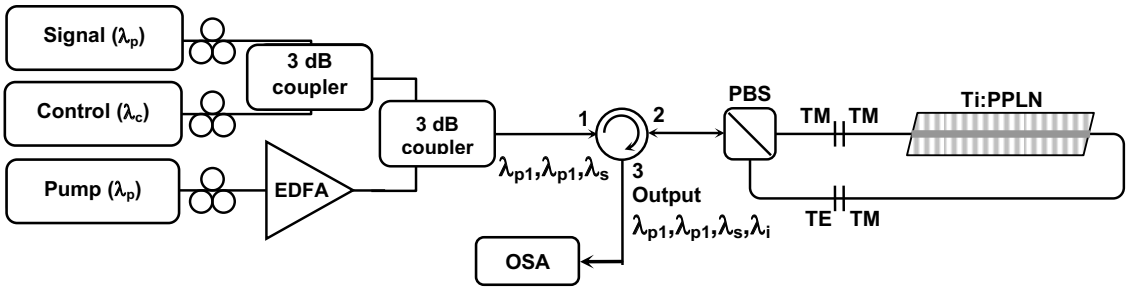

Fig. 6.4: Schematical diagram of the experimental setup for polarization insensitive cSFG/DFG-based tuneable wavelength conversion using a ring configuration to achieve polarization diversity.

Before closing the fibre loop, both single polarization conversion efficiencies (from left-to-right and from right-to-left) have been measured and optimized to achieve identical and maximum conversion for the polarization independent configuration (see Fig. 6.5, left). With coupled P_p = 20 mW and P_c = 5 mW almost identical single polarization conversion efficiencies of ~ -10 dB for both directions have been achieved (Fig. 6.5 left). For polarisation insensitive configuration the wavelength conversion efficiency dropped to -13.2 dB due to the splitting of coupled

pump and control wave powers (Fig. 6.5, right). The experimental results agree well with calculated efficiencies of -8 dB (single-pass) and -11 dB (bidirectional), respectively.

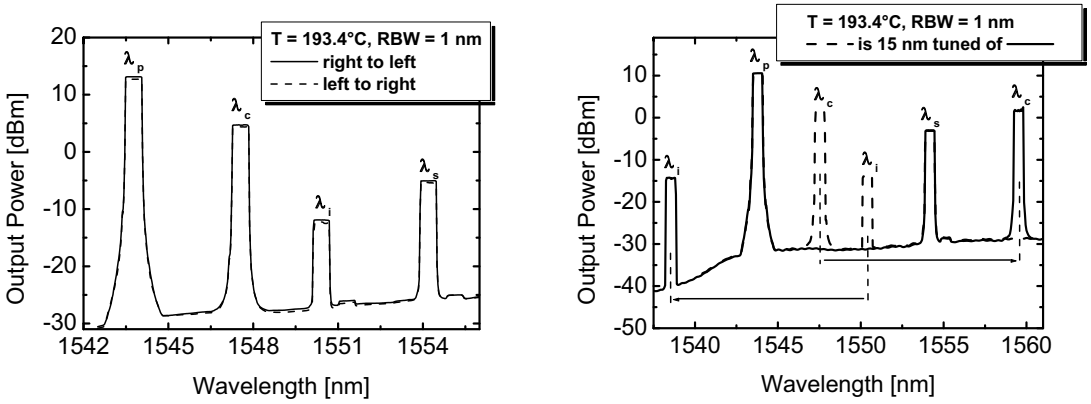

Fig. 6.5: Left: Measured optical output spectra for single polarization operation with propagation from left to right and vice-versa. Right: Polarization-insensitive cSFG/DFG-based tuneable wavelength conversion spectra with abot 15 nm tuned idler (control) in the packaged and fiber pigtailed waveguide sample.

To confirm a polarization insensitive operation the signal polarization was arbitrarily scrambled and the generated idler power was simultaneously recorded versus time for two distinged cases tuned about 15 nm to each other. The resulting variations of the idler power in both cases were about ± 0.5 dB, as shown in Fig. 6.6.

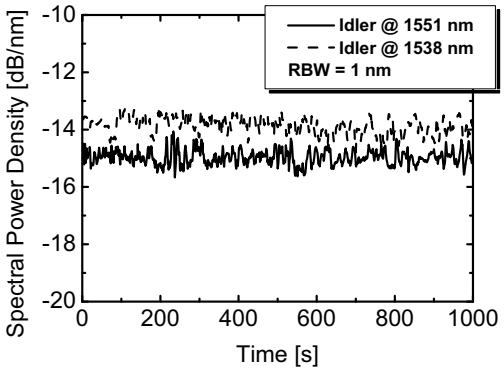

Fig. 6.6: Idler (converted signal) output power versus time (OSA with zero span) for signal polarization scrambled arbitrarily; two distinct situations with ~ 15 nm separation are shown.

6.2 Tuneable cSFG/DFG-Based Wavelength Conversion of Short Optical Pulses

Up to now cSFG/DFG-based tuneable wavelength conversion has been discussed for continuous wave (cw) signals. As real data signals are comprised of short picosecond

(ps)-pulses, additional effects like group velocity mismatch (GVM) and frequency chirping impose a limit on the ultimate data rate due to broadening and distortion of the converted pulses.

In this section simulation results of the pulsed wavelength conversion are discussed. Fig. 6.7 shows the measured cw SFG response of a 70 mm long Ti:PPLN waveguide used in the experiment when the pump wavelength is tuned. The signal wavelength was 1556 nm. The FWHM of 0.4 nm indicates the acceptance bandwidth of the SFG process. Therefore, if the transform limited signal pulse of a Gaussian shape is assumed ($\Delta t\ \Delta \upsilon = 0.442$), then regardless of the walk-off effect, the cSFG/DFG process has no influence on the pulse with a width of $\Delta t > 8.8$ ps.

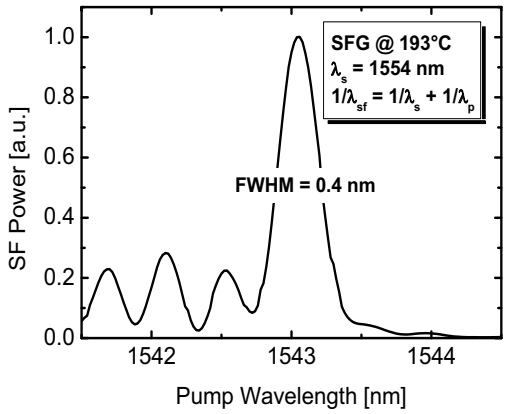

Fig. 6.7: SFG response of a 70 mm long Ti:PPLN waveguide versus pump wavelength for a fixed signal wavelength at $\lambda_s = 1556$ nm. The 0.4 nm FWHM (cSFG/DFG acceptance bandwidth) correspondes to the 8.8 ps of a Gaussian shaped pulse.

To illustrate this, four different input signal pulse-widths of 1.4 ps, 3 ps, 5 ps and 9 ps are assumed for the simulation. Pump and control are considered as continuous waves. The peak power of the signal pulse is assumed to be 100 mW and the power levels of the cw pump and control waves are both 50 mW. The Ti:PPLN waveguide used in the numerical simulation has an interaction length of 70 mm. The central wavelength of the pulsed signal and the pump wavelengths are set at 1543 nm and 1554 nm in order to satisfy the QPM condition for the SFG process. The control wavelength is set at 1565 nm.

The interaction of the signal pulse and the CW pump wave generates a pulsed SF wave via the SFG process. Due to the group velocity dispersion (GVD), there is a strong walk-off between the signal pulse in the 1.5 μm band and the SF pulse in the 0.78 μm band [73], [74], [75]. This gives rise to a broadening of the SF pulse width and a distortion of its shape. Furthermore, the generated SF pulse simultaneously interacts with the control wave to produce an idler pulse via DFG. Thus, GVD lead to a broadening of the converted signal (idler) pulse. The SF to signal walk-off length is defined by [19]:

$$L_{walk-off} = \frac{\Delta t_s}{\frac{1}{\upsilon^g_{sf}} - \frac{1}{\upsilon^g_s}} \tag{6.2}$$

In Eqn 6.2, υ^g_{sf} and υ^g_s are the group velocities of the SF and signal pulses, respectively. $L_{walk-off}$ denotes the propagation length for which the walk-off between the signal pulse of width Δt_s in the 1.5 µm range and SF pulse in the 0.78 µm range amounts due to GVM.

According to Ref. [19], the group velocities of the relevant wavelengths used in our experiment are listed below

$$\begin{aligned} \upsilon^g_{sf} &\sim 0.43730.c_0 \\ \upsilon^g_p &\sim 0.45725.c_0 \\ \upsilon^g_s &\sim 0.45629.c_0 \end{aligned} \tag{6.3}$$

where c_0 is the velocity of light in vacuum. Taking into account the values given in Eqn. 6.3, one obtains:

$$\frac{1}{\upsilon^g_{sf}} - \frac{1}{\upsilon^g_s} \sim 3.2 \frac{ps}{cm} \tag{6.4}$$

Therefore, $L_{walk-off}$ between the signal and SF pulses are about 4.7 mm, 9.4 mm, 15.6 mm and 28mm for 1.4 ps, 3 ps, 5 ps and 9 ps long pulses, respectively. Fig. 6.8 presents the calculated temporal evolution of the idler pulses for input signal pulse widths of 1.4 ps (Fig. 6.8a), 3 ps (Fig. 6.8b), 5 ps (Fig. 6.8c) and 9 ps (Fig. 6.8d) propagating along a 70 mm long Ti:PPLN channel guide for discrete distances in steps of 10 mm in the waveguide.

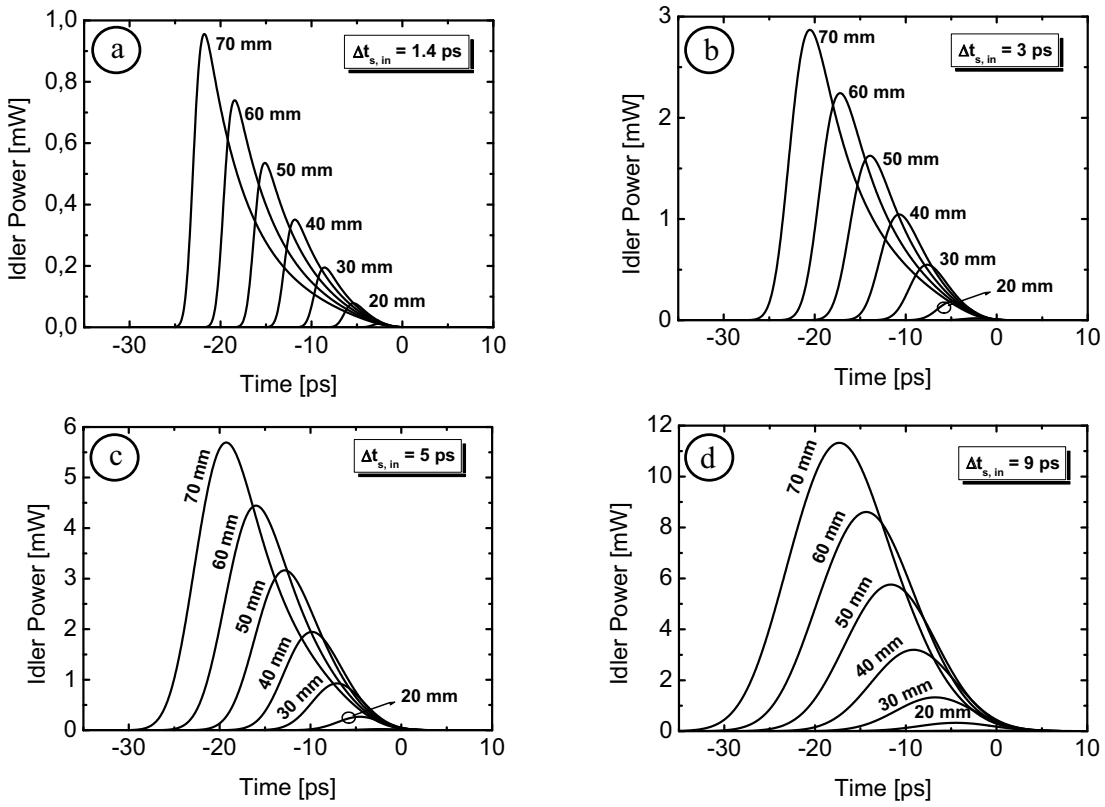

Fig. 6.8: Calculated temporal evolutions of the idler pulse propagating along a 70 mm long Ti:PPLN waveguide for different input signal pulse widths: (a) 1.4 ps, (b) 3 ps, (c) 5 ps, and (d) 9 ps. The signal pulse interacts with the continues pump to generate a pulsed SF. The broadening of the output idler pulses is due to the signal (idler) ↔ SF walk-off effect.

Fig. 6.9 shows the broadening of the output idler pulse for different input signal pulse widths along a 70 mm Ti:PPLN waveguide. Due to the walk-off effect (as the length of the Ti:PPLN waveguide, L = 70 mm, is much larger than the walk-off length, $L > L_{walk\text{-}off}$), the idler pulses are broadened as compared with the input signal pulses. If this broadening does not result in loss of information (caused by any overlapping of a pulse with the neighbouring pulses), tuneable cSFG/DFG-based wavelength conversion from signal wavelength to idler wavelength can be successfully realized for system applications. For instance, if the input pulse is assumed to be 1.4 ps, then even tuneable conversion of 160 Gb/s signal is possible.

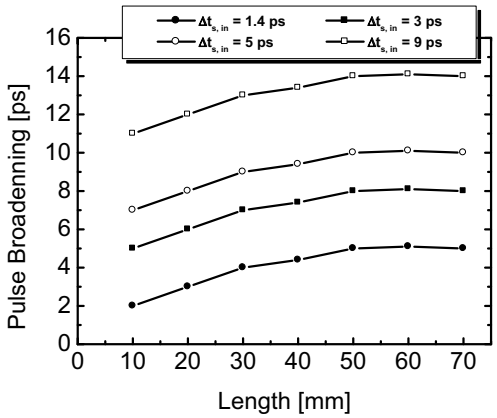

Fig. 6.9: Calculated pulse broadening of the idler wave versus interaction length for different input signal pulse widths.

6.3 Summary

Polarization dependent and polarization independent all-optical tuneable wavelength conversion based on cSFG/DFG in a Ti:PPLN channel guide covering the whole C-band is reported. Calculated evolution of picosecond pulses is presented.

The investigated scheme, with its performance to convert short optical pulses, exhibit a high flexibility for wavelength conversion, which can be potentially exploited in practical optical communication systems.

7. Optical Parametric Amplification

With the development of dense wavelength division multiplexing (DWDM) systems, and their combination with optical time division multiplexing (OTDM) for capacity improvement in a telecommunication networks, broadband and low noise optical amplifiers are required to overcome fiber and interconnection losses. Although, doped fiber amplifiers are useful tools for optical network architectures, they cannot be used in the wide bandwidth required for future optical communication systems. The main reason is their principle of operation: doped fiber amplifiers are based on stimulated emission from the dopants [76]; thus the operation wavelength range is determined by the type of ion used. For example, the erbium doped fiber-amplifier (EDFA) provides only 35 nm bandwidth covering the C-band (1535- 1565 nm). Other kinds of amplifiers such as Raman amplifiers have similar bandwidths. Moreover such amplifiers always induce some amount of their spontaneous emission to the amplified signal resulting to increase the noise in the system [77].

In contrast to (E)DFAs, optical parametric amplifiers (OPAs) rely not on the properties of the doping ions but on the nonlinearity of the medium used [78]. Thus they can in principle be operated in an arbitrary wavelength range where the corresponding phasematching condition is fulfilled. Hence, the OPA bandwidth can be increased to a figure not available with doped fiber-amplifiers or other kinds of amplifiers. For coherent optical encoding schemes in combination with DWDM coherent ultra-low noise amplification will become important. Since, OPA features a phase sensitive amplification, the signal amplification of the coherent (homodyne or heterodyne) systems become possible [79]. In addition OPA does not induce any spontaneous emission to the signal. Its noise determined by spontaneous parametric fluorescence which at a typical pump power level, is extremely weak (quantum-limited). The high gain figures are assessable for OPAs- in excess of 70 dB has already been demonstrated using the $\chi^{(3)}$ process of guided four wave mixing in a highly nonlinear optical fiber [80]. In contrast to doped fiber amplifiers OPA provides unidirectional gain. The OPA can provide additional functionalities, for instance, wavelength conversion, optical reshaping, wavelength exchange, and phase conjugation in future optical networks instead of only amplification.

Although OPA utilizing the $\chi^{(3)}$ nonlinearity in silica fibers has already been demonstrated, guided wave OPA in $LiNbO_3$ would have a number of advantages: first of all and most important, at the required pump power levels $\chi^{(3)}$ related

nonlinear processes like self- and cross-phase modulation or stimulated Brillouin scattering which are detrimental for the OPA-process are negligible in $LiNbO_3$. In contrast to the $\chi^{(3)}$-based OPAs which are limited to the gain saturation, $\chi^{(2)}$-based OPAs have a large dynamic range [81]. Thus, high power amplified signal can be realized [82].

Moreover, $LiNbO_3$ as an outstanding $\chi^{(2)}$ nonlinear medium would allow to achieve significant parametric gain in a few centimeter long waveguide instead of several meters of highly nonlinear fiber leading to rugged and compact devices. Waveguides of excellent properties can be fabricated by Ti-indiffusion or proton exchange. The amplification band and the gain bandwidth of an OPA are determined by phase-matching. The dependence of the sign of the nonlinear coefficient on the orientation of the spontaneous polarization in ferroelectric $LiNbO_3$ opens up new possibilities for quasi-phasematching utilizing artificial domain gratings fabricated by periodic domain inversion. In this way phase matching can be tailored within the whole transparency range of $LiNbO_3$.

In this chapter, a review of the recent work on cSHG/DFG-based OPA using Ti:PPLN waveguides is presented. Results of continuous wave OPA in a Ti:PPLN waveguide are reported in section 8.2. Its low signal gain caused to use a low duty cycle ns pulse laser as pump source to suppress the photorefractive damage. In this way more than 22 dB gain has been achieved with 2.5 W of coupled fundamental peak power (section 8.3). Finally, summary and conclusions are presented.

7.1 Principle of Operation

Due to energy conservation the generation of a converted signal (idler) via difference frequency generation (DFG) is always accompanied by the amplification of the input signal wave. This kind of signal amplification is called “optical parametric amplification” (OPA). OPA is a unidirectional polarization dependent highly coherent process.

cSHG/DFG-based OPA is a two step process:

1. On one hand the pump is internally generated by SHG of an input fundamental wave; by generation of each pump (higher energy) photon, two fundamental (lower energy) photons decay providing energy conservation.

2. On the other hand, simultaneously, OPA is achieved by mixing of an incoming signal with the SH-wave. Here, energy conservation determines the generation of one idler and one additional signal (two lower energy) photons by annihilation of any pump (higher energy) photon. During this interaction an idler wave is

generated at the difference frequency and the signal is amplified; therefore, we call this process cascaded SHG/DFG respectively OPA (cSHG/DFG (OPA)).

Both processes are governed also by (quasi-) momentum conservation also called (quasi-) phase matching. In case of a periodically domain inverted structure quasi-phase matching is mediated by the grating $K = 2\pi/\Lambda_{QPM}$ whit the grating period Λ_{QPM}. As explained in more detail in chapters 2 and 5, in a homogeneous waveguide quasi-phase matching for SHG can be adjusted by choosing the appropriate fundamental wavelength. For DFG/OPA QPM is only approximately achieved away from degeneracy of signal and idler (see Fig. 5.1). A schematic drawing of cSHG/DFG(OPA) together with a calculated evolution of the process in a 90 mm long homogeneous Ti:PPLN waveguide are presented in Fig. 7.1. As the pump power (For DFG/OPA) is generated internally by SHG, the pump power level (dashed graph) starts from zero and saturates in the 2nd half of the waveguide due to depletion of the fundamental power. As a consequence the signal wave is first slightly attenuated due to waveguides losses and then grows beyond its input level due to parametric amplification (as in Fig. 7.1 on the right is ~ 25 dB); simultaneously, the idler is generated.

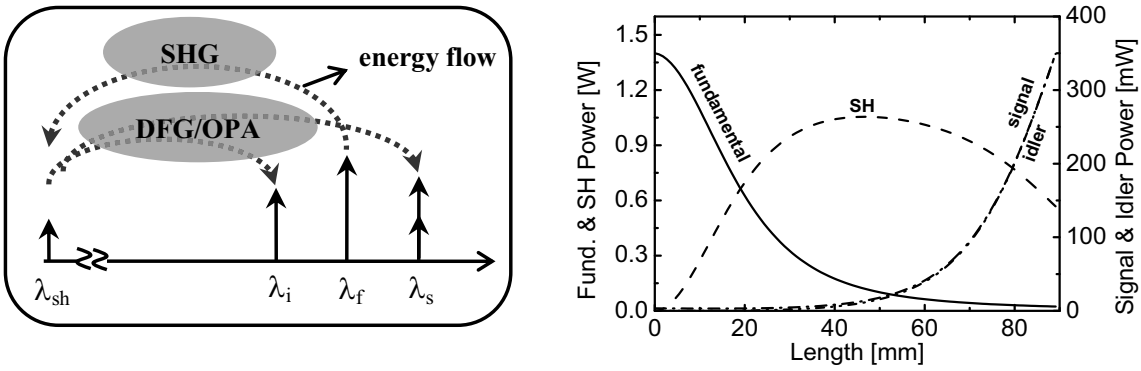

Fig. 7.1: Left: Principle of operation for cSHG/DFG-based OPA: the required pump for DFG/OPA is internally generated by quasi-phasematched SHG and, simultaneously, OPA is achieved by mixing an incoming signal with the SH wave via DFG. The solid arrows indicate the power of the interacting waves whereas the dashed arrows shows the energy flow between them. Right: Numerical calculation of the evolution of fundamental, SH, signal and idler power levels in a 90 mm long Ti:PPLN channel guide as an example.

7.2 Continuous Wave OPA

cSHG/DFG-based OPA was investigated first in cw-operation. Fig. 7.2 shows the experimental set-up. A packaged λ-converter made of an 80 mm long Ti:PPLN channel guide (Pb789z) was used for the experiments. Its SHG efficiency was ~

700 %/W. The micro-domain periodicity of Λ_{QPM} = 16.4 μm allowed to generate a phasematched SH wave at the fundamental wavelength of λ_f = 1543.5 nm at a temperature of 178 °C. A cw signal from an external cavity laser (ECL) was combined with the fundamental wave using a 10/90 coupler and launched into the waveguide. The fundamental wave was amplified using an erbium doped fiber amplifier (EDFA). The output spectrum was observed using an optical spectrum analyser. Polarization of both waves are controlled by a fiber optical polarization controller (PC).

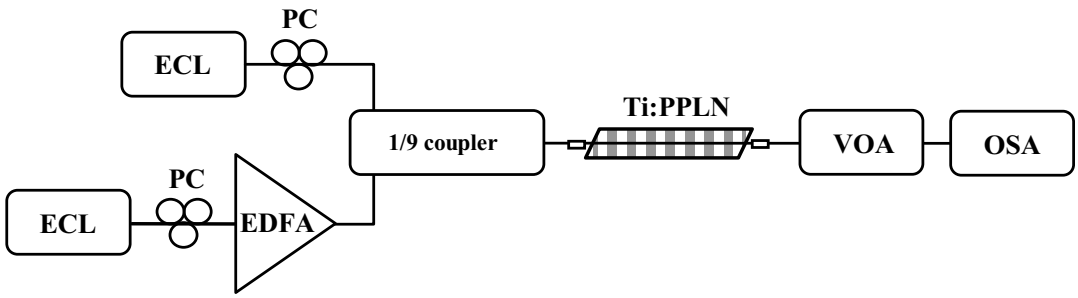

Fig. 7.2: Schematic diagram of experimental set-up for the investigation of cw-operation of a cSHG/DFG-based OPA. ECL- external cavity laser; PC- polarisation controller; EDFA- erbium doped fiber amplifier; VOA- variable optical attenuator; OSA- optical spectrum analyser.

Fig. 7.3 shows the measured and calculated signal gain as function of coupled fundamental power. The gain is defined as follows:

$$G = 10\log\frac{P_{s,out}(\text{fund.on})}{P_{s,out}(\text{fund.off})} \quad [\text{dB}]$$

where P_s(fund. off) is the transmitted signal power without pump and P_s(fund. on) is the output signal signal power with OPA gain.

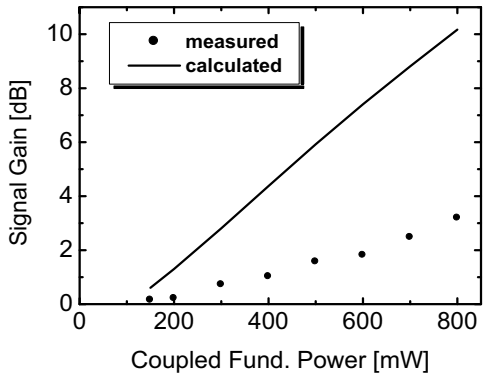

Fig. 7.3: Parametric signal gain vs coupled fundamental power in cw-operation. Main difference between measurement and calculation results from photorefraction effect at high power operation.

As the calculated results show the signal gain should grow gradually as the coupled fundamental power increases. but the highest gain achieved is only ~ 3.2 dB with the coupled fundamental power level of ~ 800 mW. The discrepancy is attributed to increased phase-mismatch due to photorefraction. This limitation motivated the investigation of OPA in a pulsed mode of operation with a low duty cycle of a pulsed laser as fundamental source. In this way, the average pump power could be kept low to reduce photorefraction significantly.

7.3 Pulsed OPA

In this section, pulsed cSHG/DFG-based OPA using a Q-switched diode pumped solid state laser (DPSS) as the fundamental source is reported. The effect of the waveguide inhomogeneity on the transmitted pulses is investigated.

Fig. 7.4 shows the experimental setup. A train of 2.5 ns long pulses of low duty cycle (8.2×10^{-6}) from the passively Q-switched laser was used as fundamental source (λ_f = 1534.5 nm). The continuous wave signal (λ_s = 1552 nm) was combined with the pulsed fundamental radiation using a 3 dB coupler and butt-coupled together into the temperature stabilized waveguide. Both sources are polarization controlled. Two Wollaston prism-based polarizers were used behind the Tango laser (commercialized ns pulsed laser from Cobolt Inc.) in order to change (or attenuate) the input fandamental power in front of the waveguide. At the output a tunable band-pass filter selected the amplified signal (or the transmitted fundamental or the generated idler). The signal (or fundamental or idler) power was monitored by an InGaAs-PIN-photodiode of 15 GHz bandwidth and a digital oscilloscope of 1.5 GHz bandwidth. The generated SH-power could be measured with a Si-photodiode.

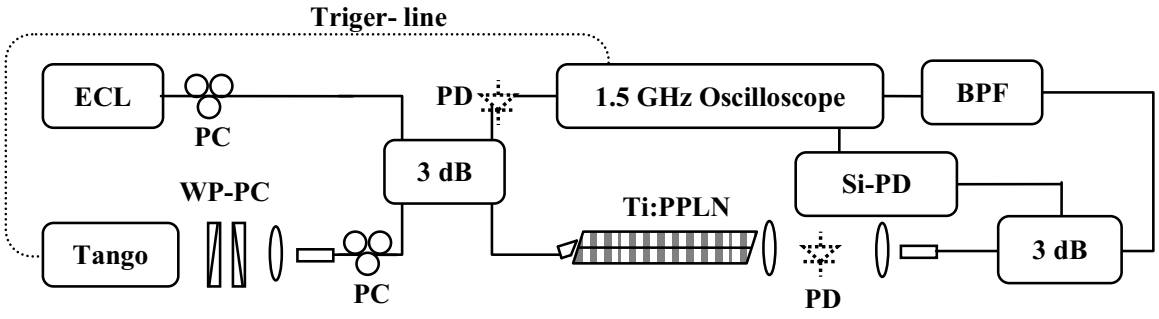

Fig. 7.4: Schematic diagram of experimental set-up for the investigation of pulsed OPA. ECL- external cavity laser; PC- polarisation controller; Tango- Q-switched ns pulsed laser; WP-PC- Wollaston prisms for free space variable optical attenuator; 3 dB- 3dB coupler; PD- InGaAs or Si photo-diode; BPF- band pass filter.

Two different Ti:PPLN waveguide samples were used to investigate pulsed OPA: An 88 mm long (first sample) and a 95 mm long (second sample) waveguides. To avoid Fabry-Perot effects, which might lead to the onset of parametric oscillation, the endfaces of both samples were angle-polished and AR-coated. The 95 mm long waveguide sample has a (theoretically) estimated parabolic inhomogeneity with a maximum amplitude of ~ 60/m. This inhomogeneity is due to imperfection of the sample preparation and/or substrate inhomogeneity. Sinc the waveguide samples had different micro-domain periodicities, the quasi-phasematched SHG for a fixed fundamental wavelength of λ_f = 1534.5 nm, were achieved at two different tempratures (195 °C for the first sample and 165 °C for the second sample). The SHG characteristics of both Ti:PPLN waveguides are shown in Fig. 7.5.

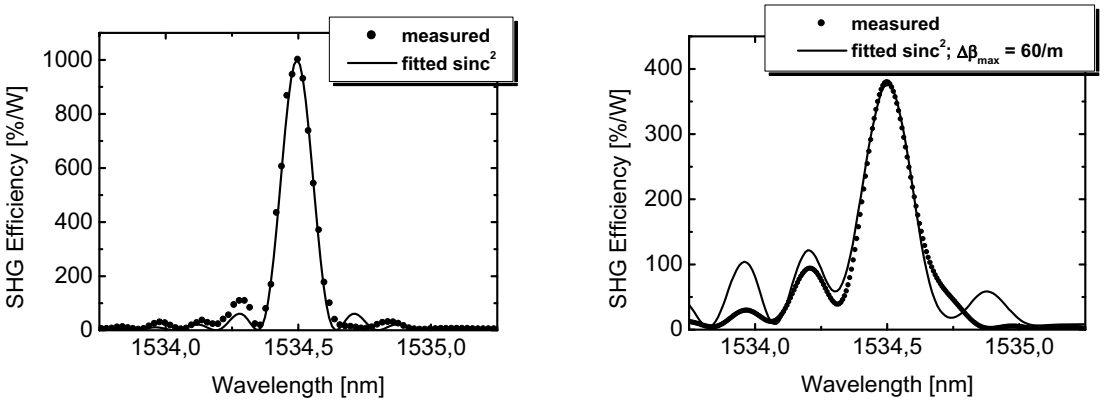

Fig. 7.5: Measured and calculated SHG response of the waveguides used in the OPA experiment. Left: An 88 mm long homogeneous Ti:PPLN waveguide. Right: A 95 mm long inhomogeneous Ti:PPLN waveguide with a (theoretically) estimate parabolic inhomogeneity with maximum amplitude of $\Delta\beta_{max}$ = 60/m. The 0.14 and 0.22 nm FWHM correspond to 77 and 45 mm long effective interaction lengths respectively.

With the homogeneous Ti:PPLN waveguide OPA is demonstrated in the range up to 2.5 W of coupled fundamental peak power. Fig. 7.6 shows the measured and calculated transmitted fundamental, generated SH and amplified signal pulses for 0.6 W (Figs. 7.6a & b) and corresponding calculated evolution of the interacting waves (Fig. 7.6c). At low coupled fundamental peak power the fundamental pulse is continuously depleted leading to a SH pulse with a distinct maximum (Fig. 7.6a). as a consequent the measured (calculated) signal pulse (Fig. 7.6b) shows about 4 dB (~ 10 dB) parametric gain according to the definition:

$$G = 10\log\frac{P_{s,peak}(\text{fund.on})}{P_{s,cw}(\text{fund.off})} \quad [\text{dB}] \tag{7.1}$$

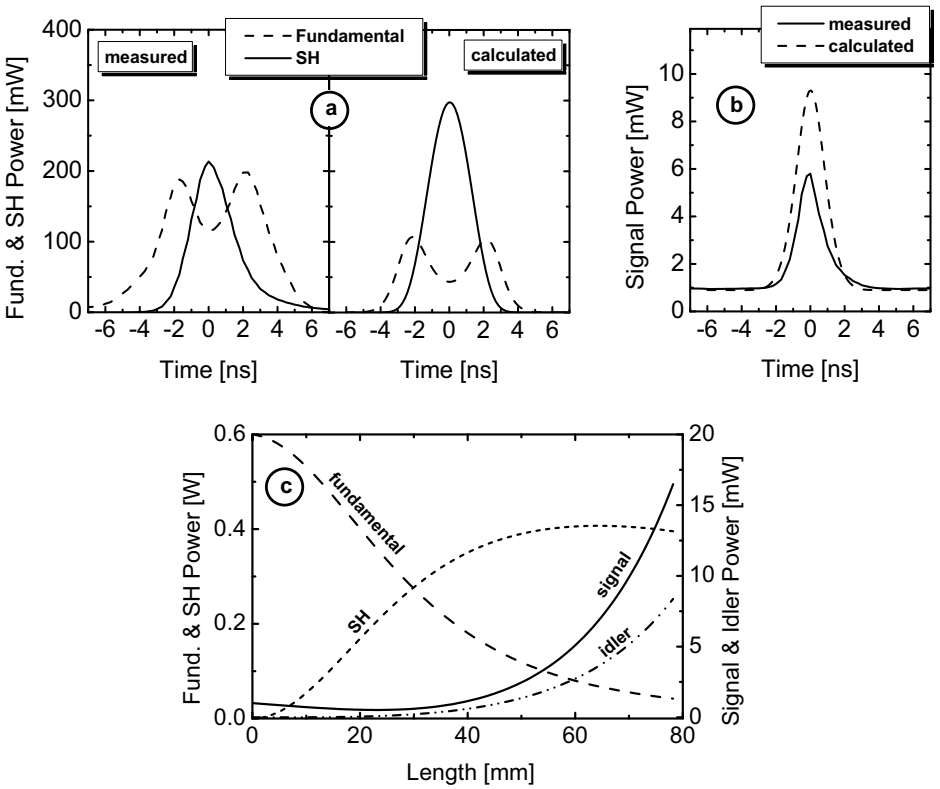

Fig. 7.6: Measured and calculated results of transmitted fundamental (dashed lines) and SH (solid lines) pulses (a) and signal (solid- and dashed lines) pulses (b). The corresponding calculated evolution of the (cw) power level of the interacting waves along a 77 mm homogeneous effective interaction length is shown in (c) for 0.6 W of coupled fundamental peak power. The coupled cw signal power is 1 mW.

Fig. 7.7, as an example of higher power operation, presents the measured and calculated results of transmitted pulses for 1.7 W of coupled fundamental peak power. At higher fundamental power levels, due to higher signal gain (here up to 10 dB measured as shown in Fig. 7.7b), the SH pulse is also continuously depleted (Fig. 7.7a). Measured results agree reasonably well with the theoretically predicted ones. The difference is mainly due to the relatively large discrepancy between measured and calculated device (SHG) efficiency.

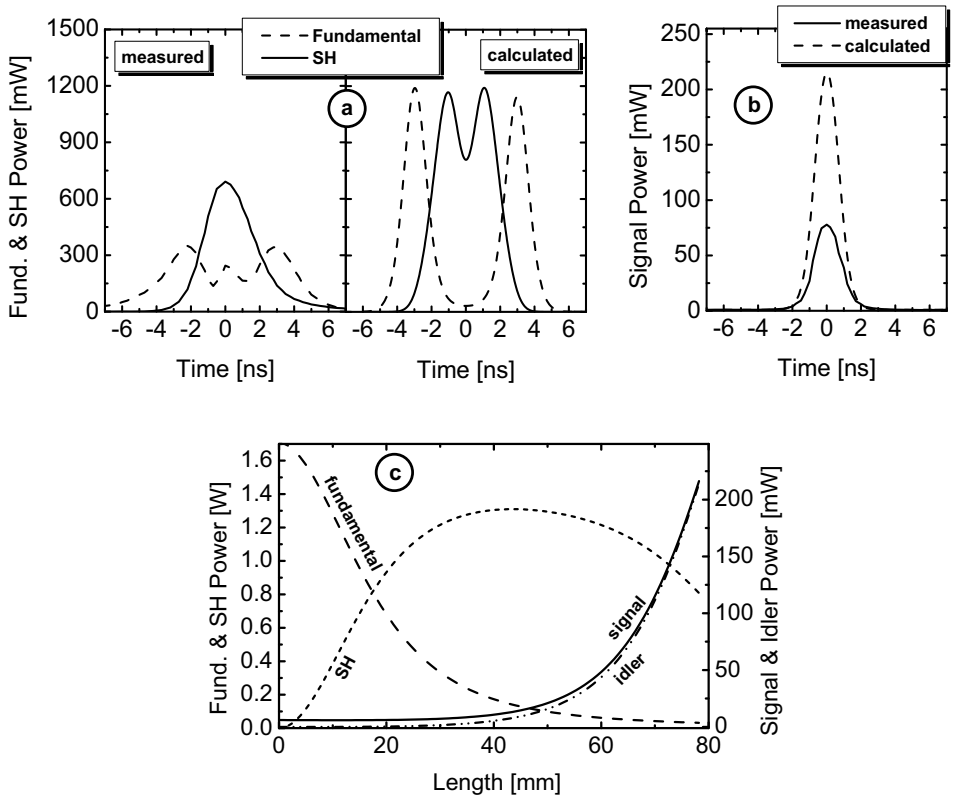

Fig. 7.7: Measured and calculated results of transmitted fundamental (dashed lines) and SH (solid lines) pulses (a) and signal (solid- and dashed lines) pulses (b). The corresponding calculated evolution of the (cw) power level of the interacting waves along a 77 mm homogeneous effective interaction length is shown in (c) for 1.7 W of coupled fundamental peak power. The coupled cw signal power is 1 mW.

For the inhomogeneous waveguide two distinct examples with 0.8 W and 6 W of coupled fundamental peak power are shown in Fig. 7.8. The central portion of the fundamental pulse is depleted due SHG and an amplified signal pulse similar to the SH pulse is generated (Fig. 7.8a). This behavior can be observed up to about 4 W of fundamental peak power. At higher fundamental power levels an inhomogeneous depletion of the fundamental pulse is observed (Fig. 7.8c). The inhomogeneity causes a spatial variation of the propagation constants of the interacting waves. This leads to a disturbed phase relationship between the four interacting waves. Therefore, power level dependent non-monotonic evolutions of the fundamental, SH, signal and idler waves along the channel guide results. As a consequence, the shape of the transmitted pulses can significantly deviate from the initial Gaussian-like pulse of the fundamental at the input.

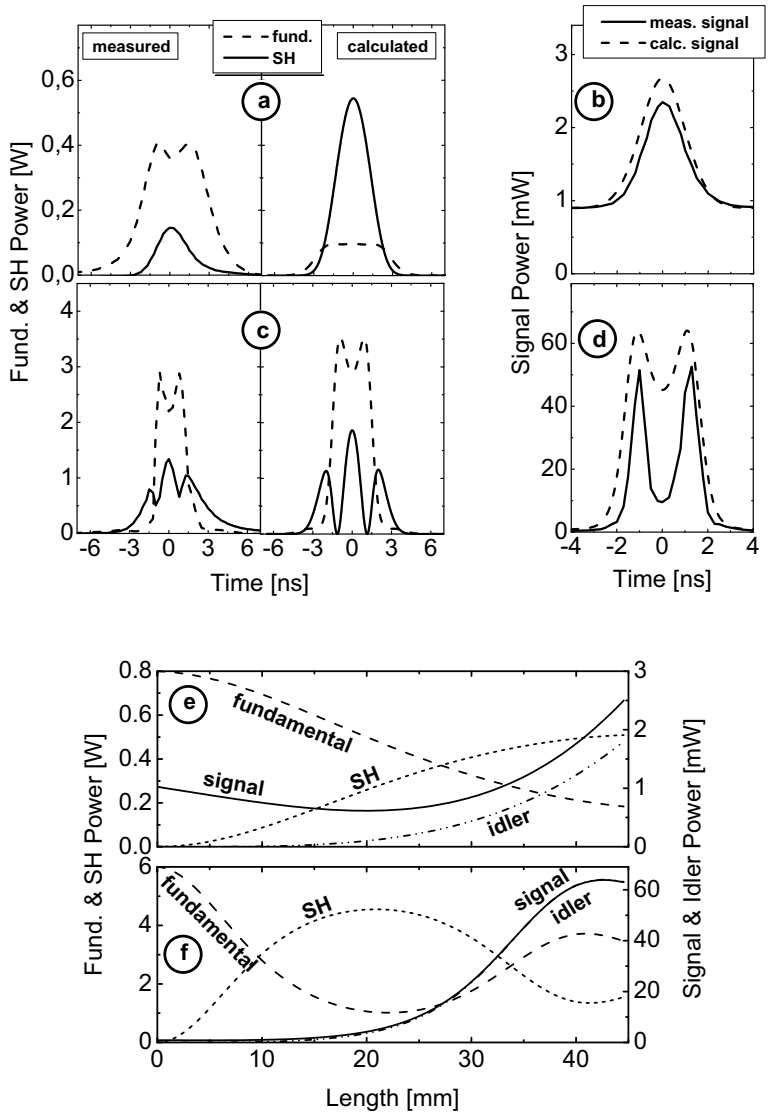

Fig. 7.8: Measured and calculated results of transmitted fundamental (dashed-lines) and SH (solid-lines) pulses (a & c) and signal (solid- and dashed-lines) pulses (b & d). for 0.8 W and 6 W of coupled fundamental peak power respectively in a 95 mm long inhomogeneous ($\Delta\beta_{max}$ = 60/m) Ti:PPLN waveguide. The corresponding calculated evolution of the (cw) power level of the interacting waves are presented in (c). The coupled cw signal power is 1 mW.

In a homogenous waveguide the QMP condition for cSHG/DFG(OPA) is:

$$\Delta\beta_{SHG} = \beta_{sh} - 2\beta_f - \frac{2\pi}{\Lambda_{QPM}} = 0 \approx \beta_{sh} - \beta_s - \beta_i - \frac{2\pi}{\Lambda_{QPM}} = \Delta\beta_{DFG} \qquad (7.2)$$

It can be maintained throughout the whole waveguide by the right choice of the fundamental wavelength. The phase relationship between the SH wave and the driving nonlinear polarization is:

$$\Delta\varphi_{SHG,0} = \varphi_{sh} - 2\varphi_f = \frac{\pi}{2} \text{ and } \Delta\varphi_{DFG,0} = \varphi_{sh} - \varphi_s - \varphi_i = \frac{\pi}{2} \qquad (7.3)$$

It adjusts automatically for an optimum energy transfer from the fundamental wave to the SH wave for SHG process and from the SH to the signal and the idler waves via the DFG process as shown in Figs. 7.6c and 7.7c.

In a inhomogeneous waveguide, the phase relationship can be disturbed by inhomogeneities of the waveguide or even by a small mismatch of the fundamental wavelength. This leads to spatially dependent propagation constants:

$$\beta_j = \frac{2\pi n_{eff,j}}{\lambda_j} \text{ with } j = sh, f, s, \text{and } i$$

Therefore, the ideal phase relation can no longer be maintained throughout the whole waveguide,

$$\Delta\varphi_{SHG} = \int_0^z \Delta\beta_{SHG}(z').dz' + \Delta\varphi_{SHG,0} \approx \Delta\varphi_{DFG} = \int_0^z \Delta\beta_{DFG}(z').dz' + \Delta\varphi_{DFG,0} = f(z) \neq \pi/2$$

As a consequence, for an inhomogeneous waveguide (here parabolic chirp of $\Delta\beta_{SHG \text{ or } DFG,\ max} = 60/m$ as expected from theory) not only a power transfer from the fundamental to the SH but also a back conversion from the SH to the fundamental can be expected (see Fig. 7.8 e & f). This is due to the perturbed phase relationship caused by the inhomogeneity of the waveguide. Therefore, reduced SH, signal and idler power levels result.

In Fig. 7.9 the measured and calculated peak parametric gain is plotted versus the coupled fundamental power for both waveguide samples. The peak parametric gain is defined as Eqn. 7.1. With about 2.5 W more than 22 dB of undistorted parametric gain has been achieved in a homogeneous waveguide. In contrast, to get the same gain in the inhomogeneous waveguide much higher fundamental power had to be used. To get a parametric gain of 20 dB about 6W of coupled fundamental peak power was necessary.

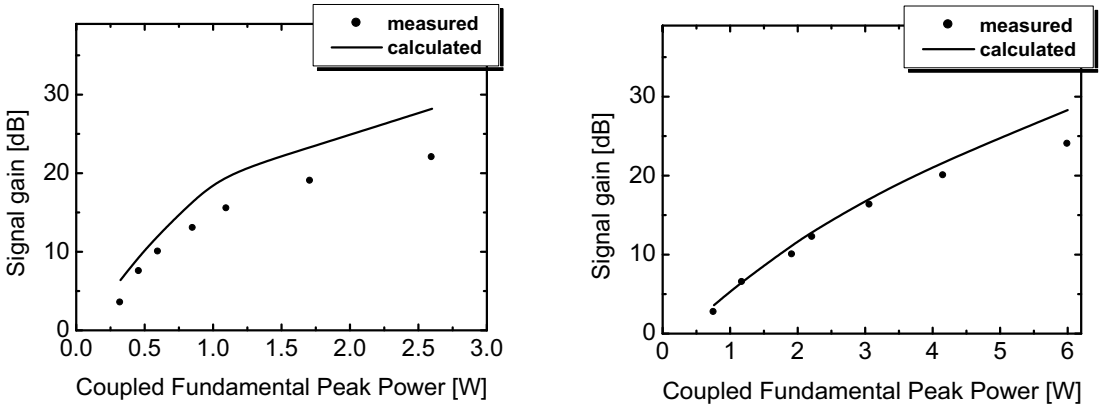

Fig. 7.9: Measured peak signal gain versus coupled fundamental peak power in an 88 mm long homogeneous (left) and in a 95 mm long inhomogeneous (right) Ti:PPLN waveguide.

Fig. 7.10 presents the measured peak signal gain in the homogeneous waveguide as function of the signal wavelength for different fundamental peak power levels. The observed bandwidths for about 4 dB, 10 dB and 20 dB peak signal gain are shown.

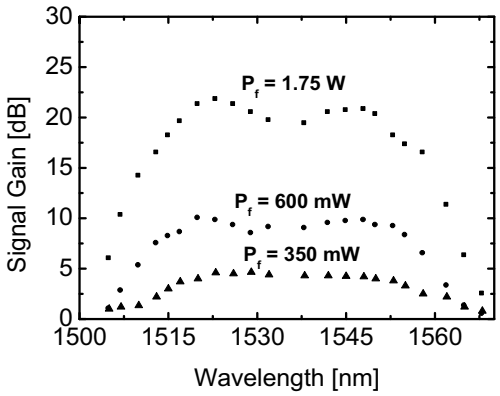

Fig. 7.10: Measured parametric peak signal gain for different coupled fundamental peak power levels versus the signal wavelength.

A 3 dB gain bandwidth of more than 40 nm has been achieved which is wider than the width of the C-band of 35 nm. Compared to the C-band the amplification band is slightly shifted to shorter wavelengths as a result of the chosen fundamental wavelength of 1534.5 nm which was not tuneable for the Q-switched laser. By a proper choice of the micro-domain periodicity and the corresponding fundamental wavelength the gain band can cover any telecommunication window.

7.4 Summary

Recent activities to realize optical parametric amplification in Ti:PPLN waveguides exploiting the $\chi^{(2)}$ nonlinearity via cSHG/DFG(OPA) process are presented in this chapter. In cw operation due to photorefraction effects only up to 3.2 dB of parametric gain could be achieved. To avoid photorefraction at higher power operation a Q-switched DPSS-laser emitting short pulses of low duty cycle has been used. The effect of the waveguide inhomogeneity on the transmitted pulses is discussed and experimentally investigated. With 2.5 W of fundamental peak power more than 22 dB of signal gain within a 40 nm wide operation band has been observed. This result is in reasonably good agreement with numerical simulations.

8. Summary and Conclusions

The essential contributions of this research are the development of techniques to demonstrate efficient all optical wavelength conversion using titanium indiffused periodically poled $LiNbO_3$ (Ti:PPLN) waveguides. They have been successfully demonstrated in system experiments with high bit rate data channels for optical fiber communications [13], [14], [15].

The devices take advantage of the optical nonlinearity of periodically poled lithium niobate (PPLN) waveguides exploiting difference frequency generation (DFG). Although relatively good wavelength conversion efficiency was achieved with only few mW of coupled pump power for a directly pumped DFG-based wavelength conversion, it is difficult to excite a mode-selective pump wave in a waveguide which is multimode in pump wavelength. Therefore, the investigation of the cascaded processes in which the pump wave can be generated internally by second harmonic generation (SHG) or sum frequency generation (SFG) is desirable. These processes are called cascaded SHG and DFG (cSHG/DFG) and cascaded SFG and DFG (cSFG/DFG), respectively. By this way, the phasematched pump mode can be excited selectively. In a 93 mm long straight Ti:PPLN waveguide, the single-pass cSHG/DFG conversion efficiency up to -7 dB of has been achieved with 120 mW of coupled fundamental power.

Efficient generation of the pump (SH or SF) in Ti:PPLN channel guides is investigated using different approaches. The experimental achievements are supported by theoretical modelling [19].

In waveguide resonators, first a resonance of the fundamental wave alone is considered. It is shown that the maximum power enhancement of the fundamental wave, and therefore the maximum SHG efficiency, can be achieved with matched resonators. It can surpass the efficiency of non-resonant guides as great as an order of magnitude, depending mainly on the waveguide losses. Using this scheme SHG efficiency of ~ 10300%/W (10.3 %/mW) has been achieved in a 65 mm long waveguide resonator. The operation of this approach for cSHG/DFG-based wavelength conversion requires narrowband grating mirrors in the waveguide itself which are high reflectors for fundamental and highly transparent to the SH, signal and idler waves. Thus, the SH-wave resonator was investigated as second approach of resonant wavelength conversion.

The waveguide cavities for SH-field enhancement enable the resonant enhancement of the intracavity SH-power. This was expected to significantly reduce the required external fundamental power level. Using this configuration an improvement of ~ 10 dB for cSHG/DFG-based wavelength conversion efficiency (close to the predicted from the theory) has been achieved. However, operation was limited to relatively small pump power levels due to the onset of photorefractive instabilities destroying the cavity stabilization.

In the separated SHG and DFG in a counter-propagation scheme, fundamental and signal waves are launched from opposite sides into the waveguide. A dichroic mirror on the signal launching side is used to superimpose the input signal and the internally generated SH (pump) wave for the DFG process. In contrast to the co-propagating cSHG/DFG where the pump power is maximized at the end of the interaction path, in a counter-propagating scheme (separated SHG and DFG) DFG starts with the maximum pump power leading to an improved conversion efficiency. A 5 dB improvement of the conversion efficiency compared to the co-propagating cSHG/DFG has been achieved.

cSHG/DFG in the long bent Ti:PPLN waveguide with a length of up to 155 mm has been also investigated. A conversion efficiency of -9.6 dB has been achieved with only 95 mW of coupled fundamental power. This, however, is in contradiction to the – 4.3 dB predicted from theory for 81 mm of effective interaction length. Moreover, the inhomogeneity of the waveguide, due to preparation procedure, causes the process to be strong temperature dependence. This phenomenon has to be investigated in more detail in the future.

In a double-pass cSHG/DFG-based wavelength converter all interacting waves were reflected by a broadband dielectric mirror deposited in the one endface of the waveguide. The issue of adjusting the phase difference of the four interacting waves after reflection for an optimum energy transfer to the converted signal was solved using three different approaches. Using this scheme about 5 resp. 9 dB of improvement of the SHG- resp. cSHG/DFG-efficiencies compared to the single-pass have been achieved [83].

The nonlinear parametric processes in PPLN are inherently polarization dependent. Therefore, polarization-independent wavelength conversion requires a diversity scheme in which the two polarization components of the input signal are converted independently. To provide identical quasi-phasematching (QPM) and differential group delay (DGD) for the two components it is ideal to utilize the same waveguide twice. This has been accomplished using a polarization maintaining ring configuration with contra-directional single-pass conversion of the two polarization components in the same waveguide. In this way DGD equalization between the two

converted polarization components is automatically provided. With such polarization diversity scheme an error-free polarization insensitive conversion of 320 Gb/s differential quaternary phase shift keying (DQPSK) data has been achieved (see appendix B).

Theoretical and experimental investigations of the temporal shape and chirp of the converted data pulses in a cSHG/DFG-based wavelength conversion show only very little broadening and chirping indicating the potential for wavelength conversion of even much higher data rates. The pulse broadening of the signal pulses induced by group velocity dispersion can already be compensated to a large degree in the device itself as a consequence of the spectral inversion of the wavelength shifted idler. Therefore, the ultra-fast Ti:PPLN wavelength converters can be designed for bit rates surpassing 3 Tbit/s.

Also wavelength conversion exploiting cSFG/DFG with a tuneable control wave was investigated. This approach results in a tuneable output wavelength of the idler whereas the input signal wavelength can be kept fixed. Corresponding devices have been developed and investigated in a polarization dependent configuration and with a ring type polarization diversity scheme. In a 80 mm long Ti:PPLN channel waveguide a wavelength conversion efficiency of about -7.5 dB has been achieved using 80 mW of coupled pump and 20 mW of coupled wavelength tuneable control power levels. The polarization insensitive conversion with less than ± 0.5 dB of residual polarization dependence has been achieved using a ring type diversity scheme. The tuning range of the idler covers the whole C-band. This result is in good agreement with numerical simulations. However, in contrast to cSHG/DFG-based wavelength conversion pulse broadening of the converted signal will limit the data rate for tuneable wavelength conversion.

For sufficiently high pump power levels wavelength conversion by DFG is accompanied by significant optical parametric amplification (OPA) of the input signal enabling the demonstration of OPA within the C-band in excess of 30 dB. To increase the fundamental power handling flexibility and to avoid photorefractive effect, a Q-switched diode-pumped-solid-state (DPSS) laser has been used as the fundamental source emitting short pulses (2.5 ns) of low duty cycle (~ 8.2×10^{-8}). With 2.5 W of fundamental peak power ~ 22 dB of signal gain has been measured. This result is in reasonably good agreement with numerical simulations. The bandwidth of parametric gain covered a range comparable to the C-band but slightly offset due to the quasi-phase matching conditions for the specific wavelength of the DPSS laser. Further improvements in the power handling capability of the waveguides are required to achieve stable OPA in a cw-mode of operation.

Appendix A: Zinc Indiffused Waveguides

A.1 Zinc Indiffused Waveguides in CLN

The fabrication of Ti:PPLN waveguide involves two steps in a sequence; formation of the channel waveguides followed by the periodically poling of the lithium niobate with certain period of grating that depends on the choice of interaction wavelengths. Although, devices made by Ti:PPLN demonstrate good electro-optic [84] or non-linear optic properties with low propagation losses (< 0.05 dB/cm) and support both TE and TM modes, such a waveguides have high photorefractive effect induced by the incorporation of Ti^{4+} ions, which limits Ti:PPLN-based devices in high power operation [85].

As explained briefly in chapter 4, the current model for the photorefractive effect involves a refractive-index perturbation due to an interaction between the electro-optic effect and the local electric field created by the charge separation under an intense laser illumination. Since the charge generation and trapping centres are strongly related to dopant valence state, the experimental observations proved that dopants with a single valence state ≤ 2**,** such as Mg^{+2} and H^{+}, will have similar effects on reduction of the photorefractive damage [86]. In contrast to that, dopants with multivalent states or a valence state ≥ 3**,** such as Fe^{+3}/Fe^{+2} and Ti^{+4}, increase the photorefractive damage [87]. According to the above arguments Zn^{+2} can also be a dopant increasing photoconductivity of the LN substrate. In this appendix, the fabrication and optical properties of channel guides made by the diffusion of metallic Zn into both congruent and Mg doped $LiNbO_3$ is reported briefly. Waveguides made by Zn indiffusion guide both polarizations and have relatively low propagation losses of about 0.2 dB/cm. They also exhibit very low photorefractive effect as it is reported in more detail in Ref. [89].

The preparation method of Zn:$LiNbO_3$ waveguide is similar to that of Ti:$LiNbO_3$ which is mentioned briefly in section 3.2. In order to fabricate Zn:PPLN waveguides, two fabrication schemes were investigated. The first scheme involves fabricating the Zn:$LiNbO_3$ waveguide before poling the waveguide sample; while the second scheme is poling the sample first and then indiffusing the zinc afterwards. The zinc indiffused area in the sample poled after diffusion is over poled while the other area is completely under poled. It appears that the nucleation of the inverted domains in the waveguide region is affected by the presence of Zn ions. This behaviour for the

sample poled before Zn diffusion was not observed. Different poling behaviour of the waveguide area and substrate can be explained by reduction of the coercive field strength due to Zn diffusion [90]. Thus for poling after Zn diffusion, nucleation starts from waveguide (Zn indiffused) areas where poling needs less electric field to start. Since using this scheme it is difficult to get Zn:PPLN waveguide with uniform gratings, reversed scheme (fabrication of Zn waveguide on existing PPLN), is preferable.

Channel waveguides of widths 5, 6, and 7 µm, were thermally indiffused on the -Z face of the PPLN samples in 900 °C over 2 hours in argon atmosphere. After thermal indiffusion, the residual stresses caused by the formation of PPLN gratings were not clearly visible under a crossed polariser microscope. It was found that the diffusion process had not altered the PPLN structure till 900 °C. The sample diffused in slightly higher temperature (930 °C) doesn't suffer the PPLN domain structure. It is interesting that sample which its domain structure was vanished out during indiffusion can be repaired by reverse poling of the whole waveguide sample.

After waveguide fabrication, the waveguide PPLN samples were cut and the end faces polished to allow optical characterisation. Fig. A.1 on the left shows the results concerning near field pattern and scattering loss measurements. The SHG characteristic of a 40 mm long Zn:PPLN waveguide is shown in Fig. A.1 on the right.

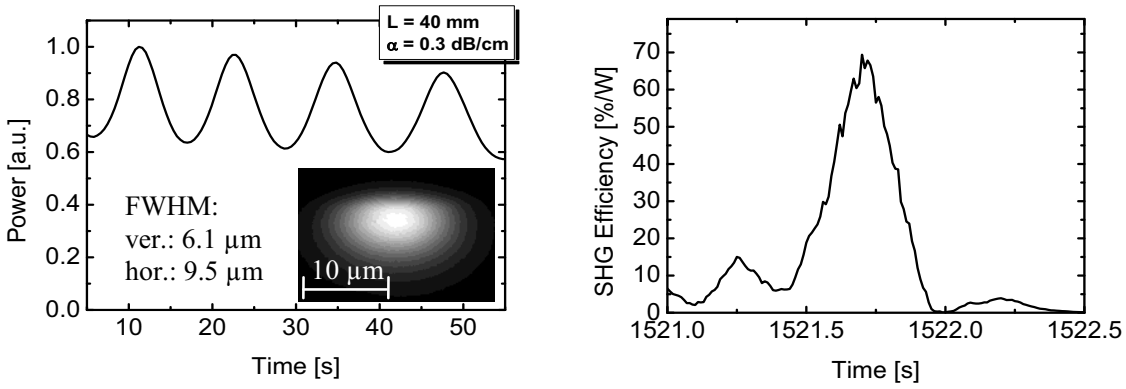

Fig. A.1: Characterization of a Zn:PPLN waveguide around 1550 nm wavelength. Left: Transmitted intensity of the waveguide versus time when its temperature is changing. Measured near field intensity profile of a 7µm wide channel waveguide for TM polarized is shown as inset. Right: SHG response of the Zn:PPLN channel guide as function of fundamental wavelength.

Although the Zn:PPLN waveguide with uniform PPLN gratings and reasonably low losses were fabricated, near field pattern shows the larger mode sizes of this kind of the waveguides. Therefore, less SHG efficiency is expected even though the domain quality is better than of the Ti:PPLN waveguides. The best SHG efficiency

achieved in Zn:PPLN waveguides was 70 %/W in a 40 mm long sample. The micro structure domain periodicity has to be chosen longer in order to operate the device in C-band at temperature below 100 °C. In order to improve the confinement (reasonable mode size) of the waveguide, and keep the damage resistance ability of the Zinc indiffused waveguides, zinc indiffused in Magnazium doped LN waveguides is investigated. This kind of waveguide will describe in next section.

A.2 Zinc Indiffused Waveguides in MgO:CLN

This kind of thermally indiffused waveguide fabrication is based on the result published in Ref [91]. According to this publication the index difference caused by Zn indiffusion in MgOLN is larger than of Zn indiffused in CLN. With such a difference the mode size of the fabricated waveguide should be smaller than what has been shown for Zn:PPLN waveguides. The preparation procedure is similar to the Zn:PPLN waveguides; first the MgOLN substrate is poled and then metallic Zn film is indiffused in 900 °C over 4 hours. Corresponding characterisation results are presented in Fig. A.2. The mode size is reduced as expected and measured loss figure is comparable with Zn:PPLN waveguides. The drawback of this kind of the waveguide is reduced SHG efficiency to only 20 %/W which is too low to operate the device as efficient all optical wavelength converter. The reason of such a huge reduction is not clear to the author.

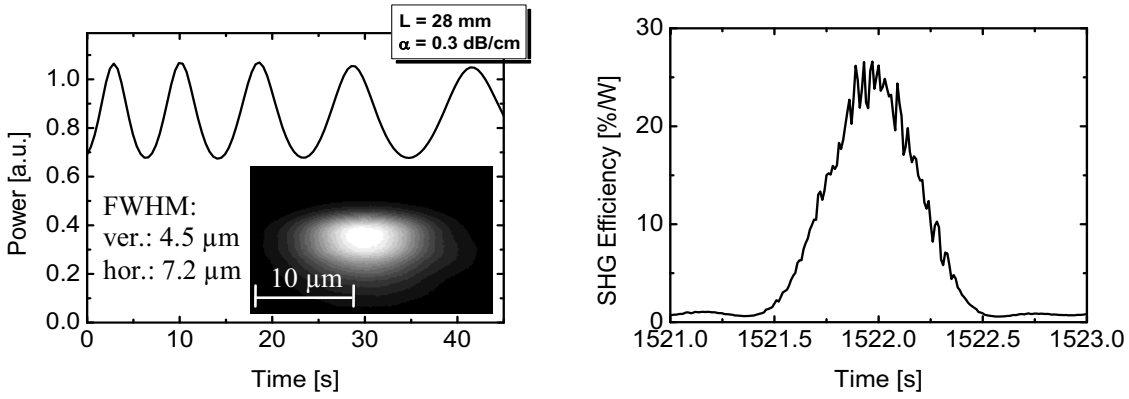

Fig. A.2: Characterization of a Zn:MgOPPLN waveguide around 1550 nm wavelength. Left: Low finesse loss measurement curve. Measured near field intensity profile of a 7µm wide channel waveguide for TM polarized is shown as inset. Right: SHG response of the Zn:MgOPPLN channel guide as function of the fundamental wavelength.

In order to obtain smaller mode sizes, the diffusion conditions can still be improved. In this way, better SHG efficiency is feasible.

Appendix B
Wavelength Conversion of DQPSK Data Signals

The development of high capacity optical networks has accelerated because of the emerging demands for world-wide communications. In order to cope with the continuous increased bandwidth requirement, two main methods have been used. The first one was to increase the channel bit rate using optical time division multiplexing (OTDM) technologies [1], and the second one was to increase the number of wavelengths transmitted over a single fiber from one to several tens or hundreds by dense wavelength division multiplexing (DWDM) technologies [2]. DWDM effectively utilizes fiber bandwidth in the wavelength domain, where multiple independent data channels are transmitted at different carrier wavelengths in order to increase system capacity. In addition, DWDM offers flexible inter-connections based on wavelength routing. However, realization of all-optical transparent DWDM networks requires functions such as switching, wavelength add/drop, wavelength conversion, etc.

However, with the increase of data rates, more advanced ways to encode data on optical wave, i.e., more advanced modulation formats, have been proposed. In recent years differential quaternary phase shift keying (DQPSK) has attracted significant attention and is now considered as one of the most promising candidates for the next generation long-haul transmission systems [92], [93]. DQPSK runs at a reduced symbol rate compared with the binary formats at the same bit rate. It has thus a narrower spectrum and exhibits enhanced tolerance to chromatic dispersion and polarisation mode dispersion (PMD).

In this appendix, the results of the system experiments of a cSHG/DFG-based and tuneable cSFG/DFG-based wavelength conversions which have been performed in the labs of Heinrich Hertz Institute (HHI) in Berlin are presented. The packaged Ti:PPLN waveguide sample used in the all experiments is prepared and characterized in the Applied Physics/ Integrated Optics group of Prof. Sohler in the University of Paderborn. The preparation and its performance for different types of wavelength conversion are described in previous chapters.

B.1 All Optical Wavelength Conversion of 320 Gb/s RZ-DQPSK Signals Using Ti:PPLN Waveguides

The experimental achievements of polarization insensitive cSHG/DFG-based wavelength conversion of a single channel 320 Gb/s RZ-DQPSK are summarized. It preserves the phase information and is transparent to the modulation format [94]. Since a polarization diversity scheme is applied, it can also be used to convert polarization multiplexed signals [95].

The experimental setup for the polarization insensitive all-optical wavelength conversion experiment is shown in Fig. B.1. It included three major parts:

I. The 320 Gb/s RZ-DQPSK transmitter;

II. The all optical wavelength converter;

III. The 320 Gb/s DQPSK receiver.

The RZ-DQPSK transmitter consisted of a pulse source, a 10 GHz-to-40 GHz phase stable pulse multiplier, a DQPSK modulator and a 40 Gbaud to 160 Gbaud optical time division multiplexer (MUX×4). The pulse source was a tunable semiconductor mode locked laser (TMLL), which produced a 1.4 ps, 10 GHz (STM-64) optical pulse train at 1551 nm, multiplied to 40 GHz by a passive phase stable multiplexer (MUX×4). A two stage modulator was used to encode the DQPSK signal. The first stage was a Mach-Zehnder (MZI-mod) $LiNbO_3$ device driven in push-pull mode by a 40 Gb/s PRBS signal (2^7-1) from a pattern generator to encode the π phase shift. The second stage was a $LiNbO_3$ phase modulator to encode the additional $\pi/2$ phase shift, driven by the same electrical signal with a sufficient delay for de-correlation. The modulated 40 Gbaud (80 Gb/s) RZ-DQPSK signal was then multiplexed in time by a passive fiber-delay multiplexer (MUX×4) to generate a 160 Gbaud (320 Gb/s) RZ-DQPSK signal.

In the wavelength converter the generated 320 Gb/s RZ-DQPSK signal was amplified by an erbium doped fiber amplifier (EDFA), then filtered by a 5 nm wide optical band-pass filter (OBF) and finally launched into the polarization insensitive PPLN subsystem through a 3 dB coupler (OC). The average signal power was 15.1 dBm at the input of the polarization insensitive PPLN subsystem. The CW fundamental light at 1546.2 nm was amplified by a high-power EDFA, filtered and launched into the polarization insensitive PPLN subsystem through the second input of the 3 dB coupler. The fundamental power was 24.4 dBm at the input of the polarization insensitive PPLN subsystem. The polarization controller in front of the EDFA was adjusted for maximum polarization insensitive conversion efficiency. At the output of the polarization insensitive PPLN subsystem the signal was launched into a filtering subsystem consisting of two 5 nm wide OBFs, an EDFA in between

and a tunable fiber Bragg grating (FBG). The FBG was used to block the fundamental wave, and the OBFs separated the converted signal at 1541 nm from the fundamental and the original signal waves. The polarization of the data signal was scrambled in front of the converter, to test the polarization insensitivity. In the DQPSK receiver a polarization stabilizer was used to de-scramble the converted data signal in order to mitigate the polarization sensitivity of the receiver.

The 320 Gb/s RZ-DQPSK receiver consisted of an optical pre-amplification stage, an electro-absorption modulator (EAM) as de-multiplexer, a delay line interferometer (DLI), a balanced photo-detector (BPD), directly attached to an electrical 1:4-demultiplexer and an error analyzer. The EAM de-multiplexer was used to select one of the four 80 Gb/s (40 Gbaud) OTDM tributaries. The DLI had a free spectral range of 40 GHz and was used to demodulate the I or Q channel from the de-multiplexed 80 Gb/s DQPSK signal. Since no DQPSK pre-coder was used in the transmitter, the EAM was programmed to the expected bit pattern, which limited the word length in our experiments to 2^7-1. A variable optical attenuation (VOA) was used at the receiver input to vary the received optical signal to noise ratio (OSNR).

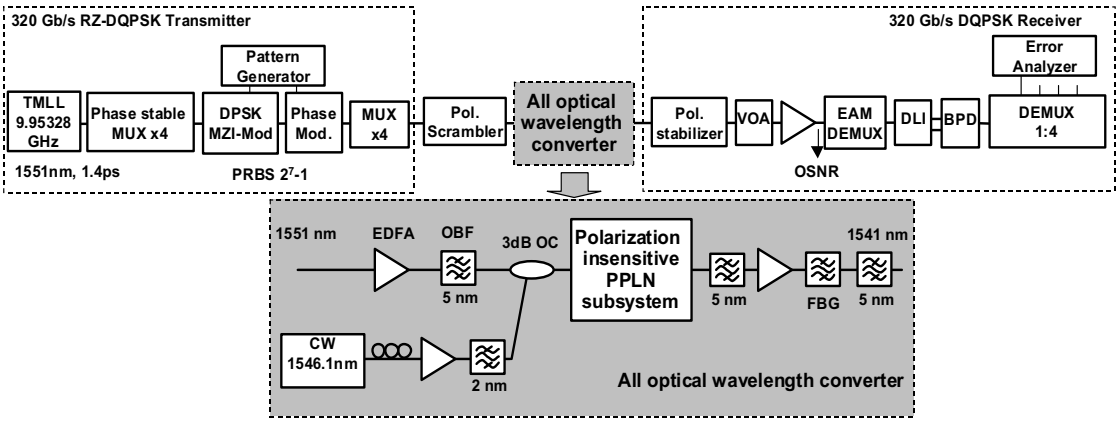

Fig. B.1: Experimental setup for polarization insensitive all-optical wavelength conversion of 320 Gb/s RZ-DQPSK signals: TMLL- tuneable mode-locked laser; MZI- Mach Zender interferometer; MUX- multiplexer; EDFA- erbium doped fiber amplifier; OBF- optical band-pass filter; OC- optical coupler; FBG- fiber Bragg grating; VOA- variable optical attenuator; EAM- electro-absorption modulator; DLI- delay line interferometer; BPD- balanced photo-detector; OSNR- optical signal to noise ratio.

The spectrum at the input and the output of the polarization insensitive PPLN subsystem is shown in Fig. B.3, left. The conversion efficiency for the 320 Gb/s RZ-DQPSK signal with polarization scrambling is –21 dB. It could be improved if the total insertion loss of the PPLN-subsystem including the fiber-optic components would be reduced. Nevertheless, the internal efficiency of about –11 dB is in good agreement with theoretical calculations assuming 17.4 dBm of fundamental power

launched in each direction into the PPLN-waveguide. The spectrum of the wavelength converted signal at 1541 nm after filtering is shown in Fig. B.2, right. The fundamental light is well suppressed by the FBG notch filter. The power of the residual fundamental and the original signal are 28 dB lower than to the wavelength converted signal.

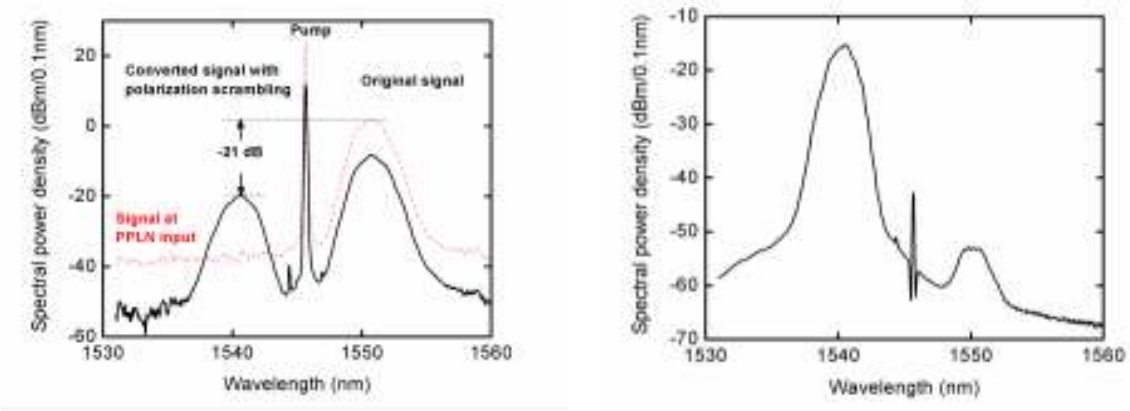

Fig. B.2: Left: Spectrum at the input and the output of the AOWC. Right: The output spectrum of the wavelength converted signal after filtering.

To characterize the residual polarization sensitivity of the PPLN subsystem, the power of the converted signal was measured versus time (50 s) with slow polarization scrambling (using a motorized polarization controller with a scan-rate of 0.08 Hz). The maximum fluctuation was less than 0.5 dB, as shown in Fig. B.3 on the left. The results of the bit-error-rate (BER) measurements are shown in Fig. B.3 on the right as a function of the OSNR at the 320 Gb/s DQPSK receiver. BER curves are plotted for the 320 Gb/s DQPSK signal back-to-back before conversion (wavelength 1551 nm), and for the converted 320 Gb/s DQPSK signal with and without polarization scrambling (wavelength 1546 nm). Polarization insensitive 320 Gb/s RZ-DQPSK wavelength conversion is successfully achieved with an error-free performance (BER 10^{-9}).

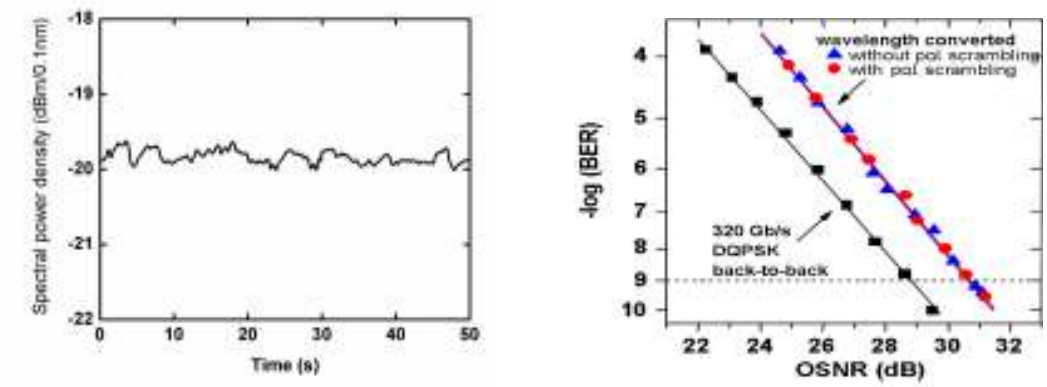

Fig. B.3: Left: Power fluctuation of the converted signal with polarization scrambling. Right: BER measurements for the 320 Gb/s DQPSK signal back-to-back, and for the converted 320 Gb/s DQPSK signal with and without polarization scrambling.

The wavelength conversion causes 2-dB OSNR penalty at the BER of 10^{-9} compared with the back-to-back case (unconverted signal). The penalty is partly due to the different sensitivity of the receiver for the different wavelengths of the unconverted and converted signal. However, the results indicate that the additional penalty caused by the polarization scrambling is negligible.

B.2 320 Gb/s In-Line All-Optical Wavelength Conversion in a 320-km Transmission Span

In this section, polarization insensitive in-line all-optical wavelength conversion of a 320 Gb/s RZ-DQPSK signal in the middle of a 320-km transmission span is demonstrated. The experimental setup for the polarization insensitive in-line all-optical wavelength conversion is the similar to that explained in previous section and sketched in Fig. B.2. The 320 Gb/s RZ-DQPSK signal is first transmitted over 160-km dispersion managed fiber (DMF), then converted to a new wavelength, and finally transmitted over another 160-km DMF.

The 320 Gb/s RZ-DQPSK signal at 1551 nm was first transmitted over a 100% dispersion and dispersion-slope compensated 160-km transmission span, consisting of two 80-km DMF spans (53 km Super Large Area fiber (SLA) with D = 20 ps/nm/km and 27 km Inverse Dispersion Fiber (IDF) with D = -40 ps/nm/km, provided by OFS Denmark). Then, the data signal was wavelength converted to 1541 nm and retransmitted over another 100% dispersion and dispersion-slope compensated 160-km transmission span. The launched power into each 80-km span was 10 dBm and the polarization into the transmission span was chosen arbitrarily.

The spectrum at the input and the output of the polarization insensitive PPLN subsystem is shown in Fig. B.4. The conversion efficiency for the 320 Gb/s RZ-DQPSK signal with polarization scrambling is –21 dB (defined as the ratio of the output power of the wavelength converted signal to the input power of the data signal), which includes the 9 dB passive losses of the PPLN subsystem. About 6 dB of the passive losses are due to waveguide coupling (~ 5 dB) and transmission (~ 1 dB); the rest is due to the fiber-optic PBS and the circulator. A further improvement of the coupling efficiency seems to be feasible.

The pulse broadening after the in-line AOWC was also investigated. The back-to-back pulsewidth was 1.48 ps measured by autocorrelation, as shown in Fig. B.4 on the right (dash-dotted). The pulse width was slightly broadened to 1.65 ps after 320-km transmission without AOWC (Fig. 6.8, right (dashed)) mainly due to the small amount of polarization mode dispersion (PMD) of the fiber. The mean differential group delay (DGD) of the fiber link was 0.7 ps. The pulsewidth after 320-km transmission with in-line AOWC was 1.76 ps (Fig. 6.8, right (solid)). The additional slight pulse broadening caused by the AOWC is mainly due to the three filters in the AOWC; as it is explained in more detail in chapter 5, our calculations and experiments show that the broadening of the wavelength converted signal pulses in the Ti:PPLN waveguide is negligible.

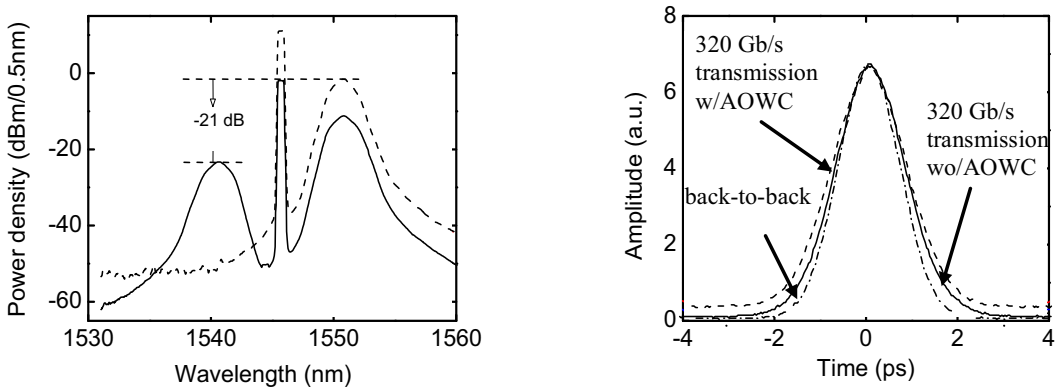

Fig. B.4: Left: Spectrum at the input (dashed line) and the output (black line) of the polarization insensitive PPLN subsystem. Right: Autocorrelation trace of the data pulse back-to-back (dash-dotted) and after 320-km transmission without in-line AOWC (solid) and with in-line AOWC (dashed).

The results of the bit-error ratio (BER) measurements are shown in Fig. B.5 as a function of the received power at the 320 Gb/s DQPSK receiver. BER curves are plotted for the unconverted 320 Gb/s RZ-DQPSK signal back-to-back (1551 nm), the unconverted 320 Gb/s RZ-DQPSK signal after 320-km transmission (1551 nm), and the in-line converted 320 Gb/s RZ-DQPSK signal after 320-km transmission (1541 nm) with and without polarization scrambling.

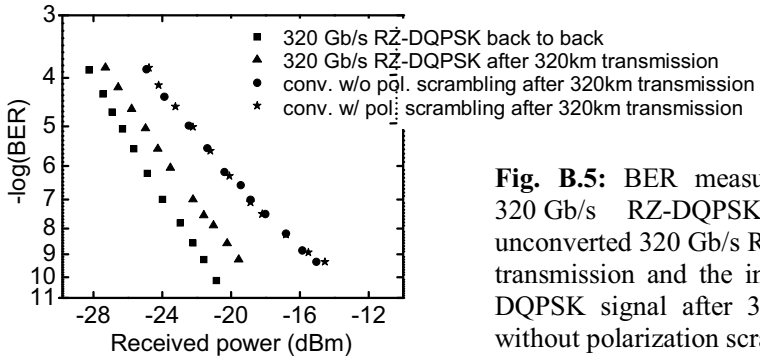

Fig. B.5: BER measurements for the unconverted 320 Gb/s RZ-DQPSK signal back-to-back, the unconverted 320 Gb/s RZ-DQPSK signal after 320-km transmission and the in-line converted 320 Gb/s RZ-DQPSK signal after 320-km transmission with and without polarization scrambling.

Polarization insensitive in-line AOWC for the 320 Gb/s RZ-DQPSK signal after 320-km transmission span was successfully achieved with an error-free performance (BER<10^{-9}). Compared to the back-to-back case, the transmission of the unconverted signal causes about 2 dB power penalty. For the in-line wavelength converted signal the power penalty after transmission is further increased by 4.5 dB. These penalties partly result from the different sensitivities of the receiver for the different wavelengths of the unconverted and converted signal and the slight phase distortion in the converted signal. The upcoming error-floor is due to the OSNR limitation from the AOWC and the transmission span.

However, the results indicate that the additional penalty caused by the polarization scrambling is almost negligible, which demonstrate the polarization insensitivity of the in-line AOWC.

B.3 Mid-Span Polarization Insensitive Spectral Inversion of 160 Gb/s RZ-DQPSK Signals

Optical phase conjugation (OPC), which is approximately (mid-span) spectral inversion, is a useful technique to compensate the dispersion effect of a transmission link [95]. In addition, compared with dispersion compensation fiber (DCF) modules, the OPC technique can not only save the extra insertion loss of the DCF modules but also cancels out nonlinear impairments resulting from the Kerr effect such as self phase modulation (SPM), intra-channel nonlinear effects and nonlinear phase noise [96]. In this section, an experimental demonstration of error-free polarization insensitive 160 Gb/s return-to-zero (RZ)-DQPSK signal transmission over 110 km single-mode fiber (SMF) using optical phase conjugation is reported. The technique is based on cSHG/DFG in a Ti:PPLN waveguide.

The experimental setup for the 160 Gb/s RZ-DQPSK signal transmission over 110 km SMF using cSHG/DFG-based OPC in a Ti:PPLN waveguide is again similar

to Fig. B.2. It included a 160 Gb/s RZ-DQPSK transmitter, two fiber spans consisting of 52.8-km SMF and 57.6-km SMF with the OPC in the middle, and a 160 Gb/s DQPSK receiver. The generated 160 Gb/s RZ-DQPSK signal was filtered by a 1-nm optical band-pass filter (OBF) to have a full width at half maximum (FWHM) of 2.7 ps and then transmitted over 52.8 km SMF (attenuation 0.2 dB/km, dispersion 17 ps/nm/km, PMD < 0.05 ps/km$^{1/2}$). The polarization of the data signal was scrambled in front of the OPC, to test the polarization insensitivity. The phase conjugated (wavelength converted) signal was transmitted over another SMF of 57.6 km behind the TiPPLN subsystem. Since the dispersion of the SMF is lower for the converted signal compared to the unconverted signal, the length of the second span was chosen for minimum accumulated dispersion at the receiver.

The spectrum at the input and the output of the polarization insensitive PPLN subsystem is shown in Fig. B.6, left. The conversion efficiency for the phase conjugated (wavelength converted) 160 Gb/s RZ-DQPSK signal is -22 dB (defined as the ratio of the output power of the phase conjugated signal to the input power of the data signal), which includes the 9-dB passive losses of the polarization insensitive PPLN subsystem. The filtered spectrum of the phase conjugated (wavelength converted) signal is shown in Fig. B.6 on the right.

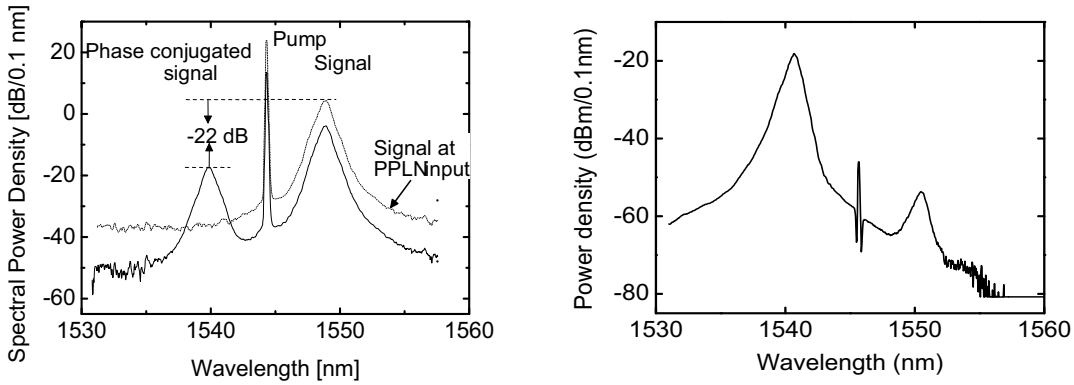

Fig. B.6: The optical spectrum at the input and at the output (left) and the filtered optical spectrum at the output (right) of the polarization insensitive Ti:PPLN subsystem.

The pulse broadening after the optical phase conjugation (OPC) transmission was also investigated. The pulse width was broadened from 2.7 ps FWHM (measured by autocorrelation, assuming sech^2 pulses) to 3.5 ps after the 110 km OPC transmission, as shown in Fig. B.7 on the left. The broadening is mainly due to third-order dispersion which cannot be compensated by the OPC.

The results of the bit-error ratio (BER) measurements as a function of the OSNR at the 160 Gb/s DQPSK receiver are shown in Fig. B.7 on the right. BER curves are

plotted for the 160 Gb/s DQPSK back-to-back signal before the OPC transmission, and for the 160 Gb/s DQPSK signal after the 110-km OPC transmission with and without polarization scrambling. 160 Gb/s RZ-DQPSK phase conjugation transmission is successfully achieved with an error-free performance (BER<10^{-9}). The 160 Gb/s RZ-DQPSK signal after the 110-km OPC transmission without and with polarization scrambling shows negligible OSNR penalty at the BER of 10^{-9} compared with the back-to-back case. The additional penalty caused by the polarization scrambling is also negligible, which demonstrates the polarization insensitivity of the optical phase conjugator.

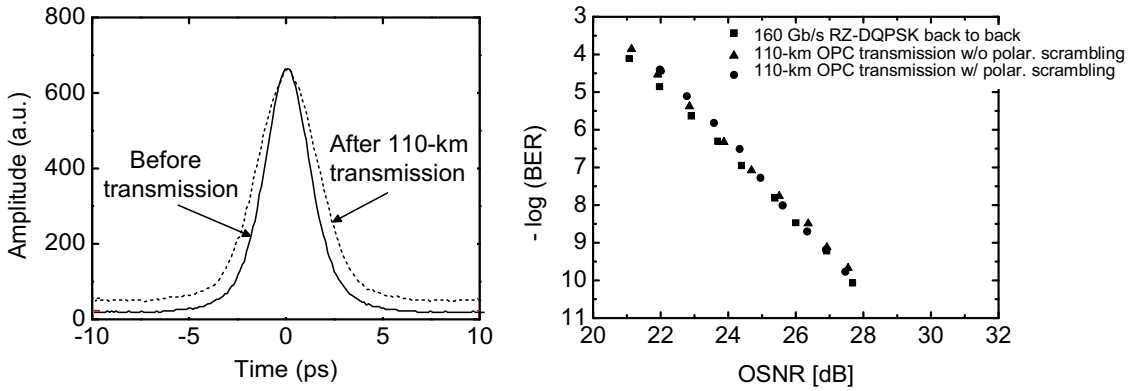

Fig. B.7: Left: Autocorrelation trace of the data pulses before transmission and after 110-km OPC transmission. Right: BER measurements for the160 Gb/s DQPSK back-to-back signal, and for the 160 Gb/s DQPSK signal after the 110-km OPC transmission with and without polarization scrambling.

B.4 Summary

The polarization insensitive 320 Gb/s RZ-DQPSK wavelength conversion using a Ti:PPLN waveguide in a polarization diversity scheme has been demonstrated. Less than 0.5 dB polarization sensitivity was obtained. Error-free operation with 2 dB OSNR penalty for the converted signal was achieved using a polarization scrambled input data signal. In addition, we investigated the characteristics of the polarization insensitive PPLN subsystem. The results show that the conversion efficiency of the AOWC is almost constant over the whole C-band and that the AOWC has a large input signal power dynamic range of more than 17 dB. The conversion efficiency for the 320 Gb/s RZ-DQPSK signal with polarization scrambling is –21 dB, which includes the passive losses of the PPLN subsystem. The BER measurements and eye-diagrams show that the wavelength converted signals with and without polarization scrambling in front of the AOWC have identical performance.

The demonstration of the polarization insensitive in-line AOWC for a 320 Gb/s RZ-DQPSK signal in the middle of a 320-km transmission span using a Ti:PPLN waveguide in a polarization diversity scheme shows error-free performance for the scrambled in-line converted signal after 320-km transmission. The BER measurements show identical performance with and without polarization scrambling, demonstrating the polarization insensitivity of the in-line AOWC.

The mid-span spectral inversion of a 160 Gb/s RZ-DQPSK signal over 110 km SMF in a polarization insensitive PPLN subsystem was reported. Error-free operation with a negligible OSNR penalty for the signal after the 110 km transmission line was achieved. The BER measurements show that the signals after the optical phase conjugation with and without polarization scrambling have identical performance, which demonstrates the polarization insensitivity of the optical phase conjugator.

Appendix C: PULSPROP Software

In this appendix a brief discription of the PULSPROB software used to simulate the parametric processes in this dissertastion is presented. This software has been created during Dr. Werner Grundkötters Ph. D. period. The fast Fourier transform (FFT) split step beam propagation method is used, to evaluate the nonlinear interaction in the time domain and the dispersion effects are treated in the frequency domain [19]. Two models and the corresponding numerical solvers have been developed including a graphical user interface (see Fig. C.1).

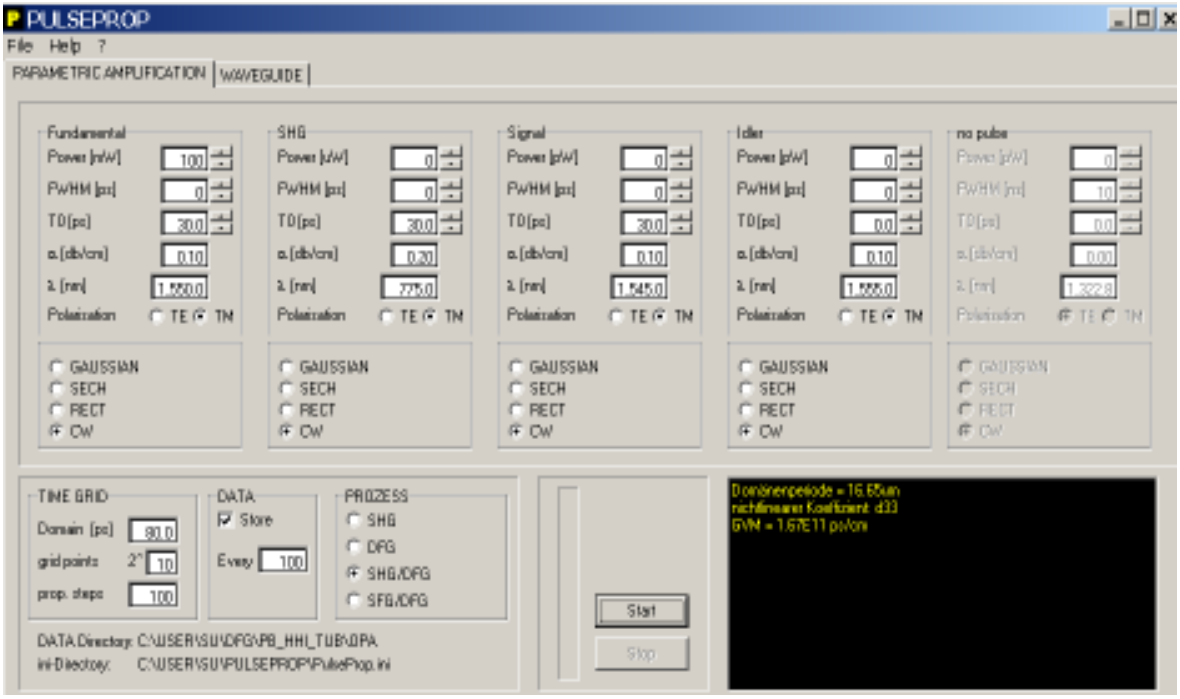

Fig. C.1: Graphical user interface for the calculation of three wave and four wave (cascaded) nonlinear optical interactions in Ti:PPLN waveguides.

The evolution of the interacting waves can be calculated for cw-operation at any point along the interaction distance. For pulsed mode operation the temporal amplitude and envelope phase distribution can be evaluated. The numerical code takes the waveguide chromatic dispersion into account.

In the WAVEGUIDE window all the relevant waveguide parameters like Ti-stripe width and thickness prior to the diffusion, diffusion conditions and a possible chirp (linear or quadratic) of the domain structure are inserted. In the PARAMETRIC AMPLIFICATION window the configuration can be set to second harmonic generation (SHG), to directly pumped difference frequency generation (DFG) resp. optical parametric amplification (OPA) or to the cascaded SHG/DFG process. For each of the waves INPUT POWER/PULSE ENERGY, full width at half maximum (FWHM), time window (T_0) for pulsed operation, waveguide attenuation α, wavelength and polarization have to be specified. In a separate window the program displays the calculated domain period for perfect phase matching and the group velocity dispersion (GVD) between pump- and signal wave for pulsed mode operation.

Bibliography

[1] C. A. Brackett, “Dense wavelength division multiplexing networks: principles and applications”, IEEE J. Select. Areas Commun. 8, 948-964 (1990).

[2] Hans-Georg Weber, and Masataka Nakazawa, “Introduction to ultra-high-speed optical transmission technology”, Optical and Fiber Communications Reports, Springer Verlag, ISBN: 978-3-540-23878-2 (Print) 978-3-540-68005-5 (Online)

[3] M. Möller, “High-Speed Electronic Circuits for 100 Gb/s Transport Networks,” presented at the Proc. Optical Fiber Commun. Conf., 2010, paper OThC6.

[4] Gabriel Charlet, “Progress in Optical Modulation Formats for High-Bit Rate WDM Transmissions”, IEEE Journal of Selected Topics in Quantum Electronics, Vol. 12, No. 4, July/August 2006.

[5] X. Zhou, J. Yu, M-F. Huang, Y. Shao, T. Wang, P. Magill, M. Cvijetic, L. Nelson, M. Birk, G. Zhang, S. Ten, H. B. Matthew, and S. K. Mishra, “Transmission of 32-Tb/s Capacity Over 580 km Using RZ-Shaped PDM-8QAM Modulation Format and Cascaded Multimodulus Blind Equalization Algorithm”, Journal of Lightwave Technology, Vol. 27, No. 3, Feb. 15, 2010.

[6] S. J. B. Yoo, “Wavelength conversion technologies for WDM network applications”, Journal of Lightwave Technology. Vol. 14, pp 955-966 (1996).

[7] R. Salem, M. A. Foster, A. C. Turner, D. F. Geraghty, M. Lipson and A. L. Gaeta, “Signal regeneration using low-power four-wave mixing on silicon chip”, Nature Photonics 2, 35 - 38 (2008).

[8] M. A. Foster, A. C. Turner, M. Lipson, and A. L. Gaeta, “Nonlinear optics in photonic nanowires”, Opt. Express 16, 1300-1320 (2008).

[9] H. Hu, E. Palushani, M. Galili, H. C. Hansen Mulvad, A. Clausen, L. K. Oxenløwe, and P. Jeppesen, "640 Gbit/s and 1.28 Tbit/s polarisation insensitive all optical wavelength conversion," Opt. Express, Vol. 18, pp 9961-9966, 2010.

[10] R. Stolen and J. Bjorkholm, “Parametric amplification and frequency conversion in optical fibers”, IEEE J. Quantum Electron. 18 (7), 1062 (1982)

[11] K. Gallo, G. Assanto, G.I. Stegeman: "Efficient wavelength shifting over the erbium amplifier bandwidth via cascaded second order processes in lithium niobate waveguides", Appl. Phys. Lett., Vol. 71, No. 8, pp 1020-1022(1997).

[12] G. Schreiber, H. Suche, Y.L. Lee, W. Grundkötter, V. Quiring, R. Ricken, and W. Sohler "Efficient cascaded difference frequency conversion in periodically poled Ti:$LiNbO_3$ waveguides using pulsed and cw pumping", Applied Physics B, Special Issue on Integrated Optics, vol. 73, 501-504 (2001).

[13] H. Hu, R. Nouroozi, R. Ludwig, B. Hüttl, C. Schmidt-Langhorst, H. Suche, W. Sohler, C. Schubert, "Polarization insensitive all-optical wavelength conversion of 320 Gb/s RZ-DQPSK signals using a Ti:PPLN waveguide", accepted for publication in Applied Physics B.

[14] B. Hüttl, R. Elschner, H. Suche, A. Gual i Coca, C.-A. Bunge, C. Schmidt-Langhorst, R. Ludwig, R. Nouroozi, H.G. Weber, K. Petermann, W. Sohler, and C. Schubert, "All-Optical Wavelength Converter Concepts for High Data Rate D(Q)PSK Transmission", in Proc. of Asia-Pacific Optical Communications Conference 2007 (APOC), Wuhan (China), paper 6783-77 (2007).

[15] H. Hu, R. Nouroozi, R. Ludwig, C. Schmidt-Langhorst, H. Suche, W. Sohler, and C. Schubert, "110 km transmission of 160 Gb/s RZ-DQPSK signals by mid-span polarization insensitive optical phase conjugation in a Ti:PPLN waveguide", Opt. Lett., in press.

[16] J. A. Armstrong, N. Bloembergen, J. Ducuing, and P. S. Pershan, "Interactions between light waves in a nonlinear dielectric", Phys. Rev. 127(6), 1918–1939 (1962).

[17] K. K. Wong, "Properties of Lithium Niobate", ISBN: 0-85296-799-3 & 978-0-85296-799-7.

[18] S. L. Jansen, D. van den Borne, B. Spinnler, S. Calabro, H. Suche, P.M. Krummrich, W. Sohler, G.-D. Khoe, and H. de Waardt: "Optical phase conjugation for ultra long-haul phase-shift-keyed transmission", J. Lightw. Techn., vol. 24, no. 1, 54-64 (2006).

[19] Werner Grundkötter, "Dynamik nichtlinearer Wechselwirkungen zweiter Ordnung in integriert optischen Wellenleitern", Ph. D. dissertation, Physics Department, Paderborn, 2006.

[20] M. Asobe, O. Tadanaga, H. Miyazawa, Y. Nishida, and H. Suzuki, "Multiple-quasi-phase-matched device using continuous phase modulation of $\chi^{(2)}$ grating and its application to variable wavelength conversion," IEEE J. Quantum Electron. Vol. 41, No. 12, pp 1540–1547, 2005.

[21] A. Yariv, Quantum Electronics (Wiley, New York, 1975).

[22] R. W. Boyd, Nonlinear Optics (Academic, 1992).

[23] Y. R. Shen, The Principle of Nonlinear Optics, Wiley, New York, 1983.

[24] Gerhard Schreiber, "Quasi-phasenangepasste Frequenzkonversion mit periodish gepolten Ti:$LiNbO_3$ Wellenleitern", Ph. D. dessertation, Desember 2001, Physics Department of the University of Paderborn.

[25] M. L. Bortz, S. J. Field, M. M. Fejer, D. Nam, R. Waarts, and D. Welch, "Noncritical Quasi-Phasematched Second Harmonic Generation in an Annealed Proton-Exchanged $LiNbO_3$ Waveguide", IEEE J. Quantum Electron. Vol. 30, pp 2953-2960, Dec. 1994.

[26] M. M. Fejer, G. A. Magel, D. H. Jundt, R. L. Byer, "Quasi-phase-matched second harmonic generation: tuning and tolerances," IEEE J. Quantum Electron. **28**, 2631-2654 (1992).

[27] R. Osellame et al., "Integrated all-optical nonlinear device for reconfigurable add/drop and wavelength shifting of WDM signals", Appl. Phys. B 73, pp. 505-509 (2001)

[28] J.H. Lee, Y.H. Min, W. Grundkötter, V. Quiring, and W. Sohler: "All-optical wavelength selective switching exploiting the nonlinear phase shift induced by cascaded sum and frequency generation (cSFG/DFG) in a Ti:PPLN channel waveguide", Proc. 11th European Conference on Integrated Optics (ECIO '03), Prague, April 2003,Vol. 1, p. 101.

[29] R. V. Schmidt and I. P. Kaminow, "Metal-diffused optical waveguides in LiNbO3", Applied Physics Letters, Vol. 25, No. 8, pp 458– 460, October 1974.

[30] Hubertus Suche, Ph. D. dissertation, 1981, University of Dortmund.

[31] W. Sohler, "optical parametric oscillation in Ti-indiffused $LiNbO_3$ optical waveguide reonators", Proc. Conf. on Integrated Optics and Optical Communications IOOC'81, IEEE Conf. Proc. Vol. 144, p88, San Francisco, USA, 1981.

[32] D. Janner, T. F. Lucchi, P. Vergani, S. Giurgola, V. Pruneri, "Grinding free electric-field poling of Ti indiffused *z*-cut $LiNbO_3$ wafer with submicron resolution", Appl. Phys. A: Materials Science & Processing, Vol. 91, pp 319–321, 2008.

[33] Dirk Hofmann, “Nichtlineare, integriert optische Frequenzkonverter für das mittlere Infrarot mit periodisch gepolten Ti:LiNbO3-Streifenwellenleitern“, Universität Paderborn, Dissertation, 2001.

[34] R. Regener and W. Sohler, "Loss in Low-Finesse Ti:$LiNbO_3$ Optical Waveguide Resonators," Appl.Phys. B 36, 143-147 (1985).

[35] T. Suhara and M. Fujimura, “Waveguide nonlinear-optic devices” ISBN: 3-540-01527-2 Springer Verlag Berlin, 2003

[36] I. Camlibel, “Spontaneous Polarization Measurements in Several Ferro-electric Oxides Using a Pulsed-Field Method”, J. Appl. Phys. Vol. 40, pp 1690-1695, 1969.

[37] S.W. Kwon, Y.S. Song, W.S. Yang, H.M. Lee, W.K. Kim, H.Y. Lee, B.Y. Kim, M.H. Lee and D.Y. Lee, ”Influence of annealing temperature on domain shape of periodically poled $LiNbO_3$ for Ti:LN waveguides”, Thin Solid Films Volume 515, Issue 3, pp 922-926 23, November 2006.

[38] S. Orlov, W. Grundkötter, D. Hofmann, V. Quiring, R. Ricken, H. Suche, and W. Sohler: "Mid infrared integrated optical parametric generators and oscillators with periodically poled Ti:LiNbO 3 waveguides" in "Mid-Infrared Coherent Sources and Applications", M. Ebrahimzadeh and I.T. Sorokina (Eds.), NATO Science Series - B: Physics and Biophysics, Springer, Dordrecht, 2008.

[39] D. Marcuse, Theory of Dielectric Optical Waveguides, Academic Press, Boston, 1991.

[40] Amnon Yariv, “Optical Electronics”, Saunders College Publishing, 1991, ISBN 0–03–04744–2

[41] A. Ashkin, G. D. Boyd, J. M. Dziedzic, R. G. Smith, A. A. Ballman, J. J. Levinstein, and K. Nassau, “Optically-induced refractive index inhomogeneities in $LiNbO_3$ and $LiTaO_3$. Applied Physics Letters, Vol. 9, No. 1, pp 72-75, 1966.

[42] K. Buse, “Light-induced charge transport processes in photorefractive crystals; models and experimental methods”, Applied Physics B - Lasers and Optics, Vol 64, No. 3, pp 273-291, 1997.

[43] F. S. Chen, “Optically induced change of refractive indices in $LiNbO_3$ and $LiTaO_3$”, Journal of Applied Physics, Vol. 40, No. 8, pp 3389- 3396, 1969.

[44] A. M. Glass, D. van der Linde, and T. J. Negran, “High-voltage bulk photovoltaic effect and the photorefractive process in $LiNbO_3$”, Applied Physics Letters, Vol. 25, No. 4, pp 233-235, 1974.

[45] K. Buse, S. Breer, K. Peithmann, S. Kapphan, M. Gao, and E. Krätzig, "Origin of thermal fixing in photorefractive lithium niobate crystals", Phys. Rev. B, Vol. 56, No. 3, pp 1225-1235, 1997.

[46] Y. Furukawa, M. Sato, K. Kitamura, Y. Yajima, and M. Minakata, "Optical damage resistance and crystal quality of $LiNbO_3$ single crystals with various [Li]/[Nb] ratios", Journal of Applied Physics, Vol. 72, No. 8, pp 3250-3254, 1992.

[47] Y. Furukawa, K. Kitamura, S. Takekawa, A. Miyamoto, M. Terao, and N. Suda, "Photorefraction in $LiNbO_3$ as a function of [Li]/[Nb] and MgO concentrations", Applied Physics Letters, Vol. 77, No. 16, pp 2494-2496, 2000.

[48] T. Volk, N. Rubinina, M. Wohlecke, "Optical-damage-resistant impurities in lithium niobate", Journal of Optical Society of America B, Vol. 11, No. 9, pp 1681- 1687, September 1994.

[49] R. Gerson, J. F. Kirchhoff, L. E. Halliburton, and D. A. Bryan, "Photo-conductivity parameters in lithium niobate", Journal of Applied Physics, Vol. 60, pp 3553-3558, 1986.

[50] F. Jermann, M. Simon, and E. Kratzig, "Photorefractive properties of congruent and stoichiometric lithium niobate at high light intensities," Journal of the Optical Society of America, Vol. 12, No. 11, pp 2066–2070, 1995.

[51] K. R. Parameswaran, J. R. Kurz, R. V. Roussev, M. M. Fejer, "Observation of 99% pump depletion in single-pass second-harmonic generation in a periodically poled lithium niobate waveguide", Optics Letters, 27, p. 43-45 (January 2002).

[52] H. Suche, R. Regener and W. Sohler, "CW-Second Harmonic Generation in Optical Waveguide Resonators", ECIO'81, post-deadline paper, IEE conference publication 201, p. 19, London, 1981.

[53] R. Regener and W. Sohler, "Efficient second-harmonic generation in Ti:LiNbO3 channel waveguide resonators", J. Opt. Soc. Am. B, no. 2, p. 267, 1988.

[54] J. Webjorn, F. Laurell, and G. Arvidsson, "Blue Light Generated by Frequency Doubling of Laser Diode Light in a Lithium Niobate Channel Waveguide", IEEE Photon. Technol. Lett., no. 1, p. 316, 1989.

[55] E. J. Lim, M. M. Fejer, R. L. Byer, "Second-harmonic generation of green light in periodically poled planar lithium niobate waveguide", Electron. Lett., no. 25, p. 174, 1989.

[56] C. Q. Xu, K. Shinozaki, H. Okayama, and T. Kamijoh, "Second-harmonic generation using a fiber ring resonator with a $LiNbO_3$ waveguide and a semiconductor optical amplifier", Appl. Phys. Lett. 69, 2154 (1996); doi:10.1063/1.117149

[57] M. Fujimura, M. Sudoh, K. Kintaka,T. Suhara, H. Nishihara, "Resonant Waveguide Quasi-Phase-Matched SHG Devices with Electrooptic Phase-Modulator for Tuning", IEEE Journal of selected topics in quantum electronics, Vol. 2, No. 2, June 1996

[58] D. Hofmann, H. Herrmann, G. Schreiber, W. Grundkötter, R. Ricken, W. Sohler: Continuous-wave mid-infrared doubly resonant optical parametric oscillator withperiodically poled Ti:LiNbO3 waveguide, Proc. Europ. Conf. Integrated Optics (ECIO '99), post deadline paper, p. 21 (1999)

[59] M. H. Chou, J. Hauden, M. A. Arbore, and M. M. Fejer, "1.5-µm-Band Wavelength Conversion Based on Difference-Frequency Generation in $LiNbO_3$ Waveguides with Integrated Coupling Structures", Opt. Lett. Vol. 23, pp 1004-1006, July 1998.

[60] H. Suche, R. Nouroozi and W. Sohler, "Ti:PPLN-waveguide with taper coupler and signal/idler multiplexer", milestone 2, final report of the OBS project submitted to DFG (Deutsche Forschungsgemeinschaft)

[61] M. H. Chou, I. Brener, M. M. Fejer, E. E. Chaban, and S. B. Christman, "1.5-µm-Band Wavelength Conversion Based on Cascaded Second-Order Nonlinearity in $LiNbO_3$ Waveguides", Photonics Technol. Lett. Vol. 11, pp 653-655, June 1999.

[62] G. I. Stegeman, D. J. Hagan, and L. Torner, "$\chi^{(2)}$ cascading phenomena and their applications to all-optical signal processing, mode-locking, pulse compression and solitons", Opt. and Quantum Electron. **28**, 1691-1740 (1996).

[63] M.E. Marhic, Fiber Optical Parametric Amplifiers and Related Devices, Cambridge University Press, Berlin, 2008.

[64] Y. Yamamamoto and K. Inoue, "Noise in amplifiers", J. Lightw. Technol. Vol. 21, No. 11, pp 2895–2915, Nov. 2003.

[65] D. Caccioli, A. Paoletti, A. Schiffini, A. Galtarossa, P. Griggio, G. Lorenzetto, P. Minzioni, S. Cascelli, M. Guglielmucci, L. Lattanzi, F. Matera, G.M. Tosi Beleffi, V. Quiring, W. Sohler, H. Suche, S. Vehovc, M. Vidmar: "Field demonstration of in-line all-optical wavelength conversion in a WDM

dispersion managed 40 Gbit/s link", IEEE J. Selected Topics in Quantum Electronics, vol. 10, no. 2, 356-362 (2004).

[66] G. Imeshev, M. Proctor, and M. M. Fejer "Phase correction in double-pass quasi-phase-matched second-harmonic generation with a wedged crystal," Opt. Lett. 23, 165 (1998).

[67] C.-W. Hsu and C. C. Yang "Using a grating structure for phase compensation in achieving an efficient round-trip optical parametric process in periodically poled lithium niobate with an incomplete quasi-phase-matching period," Opt. Lett. 24, 540 (1999).

[68] Y.-C. Huang, K.-W. Chang, Y.-H. Chen, A.-C. Chiang, T.-C. Lin, and B.-C. Wong "A High-Efficiency Nonlinear Frequency Converter with a Built-in Amplitude Modulator," J. Lightwave Technol. 20, 1165 (2002).

[69] J. Buck and R. Trebino, "Nonlinear Optics", Wiley-VCH, 2006.

[70] R. Nouroozi, Y. H. Min, W. Grundkötter, V. Quiring, R. Ricken and W. Sohler: "Efficient Second Harmonic Generation in Matched Ti:PPLN Waveguide Resonators", in European Conference on Integrated Optics (ECIO), paper WG4, Copenhagen, Denmark, April 2007.

[71] H. Furukawa, A. Nirmalathas, N. Wada, S. Shinada, H. Tsuboya, and T. Miyazaki, "Tunable All-Opti-cal Wavelength Conversion of 160-Gb/s RZ Optical Signals by Cascaded SFG-DFG Generation in PPLN Waveguide", IEEE Photon. Technol. Lett. Vol. 19 (6), pp. 384-386 (2007)

[72] Y. H. Min, J. H. Lee, Y. L. Lee, W. Grundkoetter, V. Quiring, and W. Sohler, "Tunable all-optical wavelength conversion of 5-ps pulses by cascaded sum- and difference frequency generation (cSFG/DFG) in a Ti:PPLN waveguide," OFC'03 Atlanta, GA/USA, March. pp. 767-768 (2003).

[73] J. Wang, J. Q. Sun, X. L. Zhang, X. H. Yuan and D. X. Huang, "Experimental observation of tunable wavelength down- and up-conversions of ultrashort pulses in a periodically poled LiNbO", Opt. Commun., vol. 269, pp. 179 2007.

[74] R. Schiek, R. Iwanow, G. Stegeman, T. Pertsch, F. Lederer, Y.H. Min, W. Sohler: "Low-power, multiport, ultrafast, parametric switching in cascaded waveguide couplers" Appl. Phys. Lett., vol. 87, 011109 (2005)

[75] J. Wang , J. Q. Sun , J. R. Kurz and M. M. Fejer "Tunable wavelength conversion of ps-pulses exploiting cascaded sum- and difference frequency generation in a PPLN-fiber ring laser", IEEE Photon. Technol. Lett., vol. 18, pp. 2093 2006.

[76] C. J. Koester and E. Snitzer, “Amplification in a fiber laser”, Appl. Opt. 3 (10), 1182 (1964).

[77] R. J. Mears, L. Reekie, M. Jauncey, and D. N. Payne, “Low-noise erbium-doped fiber amplifier operating at 1.54 μm”, Electron. Lett. 26, 1026 (1987).

[78] R. A. Baumgartner and R. L. Byer, “Optical parametric amplification”, IEEE J. Quantum Electron. QE-15 (6), 432 (1979).

[79] R. L. Byer and A. Piskarskas, “Feature issue on optical parametric oscillation and amplification”, J. Opt. Soc. Am. B 9, 1656–1791 (1993) and 10, 2148 – 2243 (1993).

[80] T. Torounidis, P. A. Andrekson, and B-E. Olsson, “Fiber-Optical Parametric Amplifier With 70-dB Gain”, IEEE Photonics Technology Letters, Vol. 18, No. 10, May 15, 2006.

[81] G. P. Banfi, P. K. Datta, V. Degiorgio, and D. Fortusini, “Wavelength shifting and amplification of optical pulses through cascaded second-order processes in periodically poled lithium niobate”, Appl. Phys. Lett. **7**,136-138 (1998).

[82] R. Nouroozi, H. Suche, W. Grundkötter, R. Ricken, V. Quiring, and W. Sohler, “Optical parametric amplification in Ti:PPLN channel waveguides”, ECIO 2010, Cambridge, 7 – 9 April 2010, paper FrD1

[83] R. Nouroozi, H. Suche, A. Hellwig, R. Ricken, V. Quiring, and W. Sohler, “Phase control of double-pass cascaded SHG/DFG wavelength conversion in Ti:PPLN channel waveguides“, Optics Express, vol. 18, no. 13, pp. 14225-14231, 2010.

[84] Nasrin Moeini, “Integriert optische Polarisationssteller mit periodisch gepolten Ti:$LiNbO_3$ Streifenwellenleitern“, M. Sc. Thesis, Phys. Dep. Uviversity of Paderborn, Feb. 2010.

[85] K. Sugji, M. Fukuma, H. Iwasaki, “A study on Ti diffusion into $LiNbO_3$ waveguides by electron probe analysis and X-ray diffraction methods”, J. Mater. Sci., Vol.13, pp 523-533, 1978.

[86] A. Winnacker, R. M. Macfarlane, Y. Furukawa, and K. Kitamura, "Two-Color Photorefractive Effect in Mg-Doped Lithium Niobate," Appl. Opt. Vol. 41, pp 4891-4896, 2002.

[87] R. L. Holman, J. Busch, M. Parmenter, P. J. Cressman, “Lithium niobate waveguides and their susceptibility to optical damage”, Ferroelectrics, Vol. 50, No. 1, pp 171- 177, 1983.

[88] G. E. Peterson, A. M. Glass, and T. J., Negran, “Control of the susceptibility of lithium niobate to laser-induced refractive index changes,” Appl. Phys. Lett., vol. 19, pp. 130-132, 1971.

[89] L. Ming, C. Gawith, K. Gallo, M. O'Connor, G. Emmerson, and P. Smith, "High conversion efficiency single-pass second harmonic generation in a zinc-diffused periodically poled lithium niobate waveguide," Opt. Express Vol. 13, pp 4862-4868, 2005.

[90] S. Kumaragurubaran, S. Takekawa, M. Nakamura, S. Ganesamoorthy, K. Terabe and K. Kitamura, “Domain inversion and optical damage in Zn doped near-stoichiometric lithium niobate crystal”, Conference on Lasers & Electro-Optics (CLEO) Baltimor, USA, 2005.

[91] W. M. Young, M. M. Fejer, M. J. F. Digonnet, A. F. Marshall, and R. S. Feigelson, "Fabrication, Characterization, and Index Profile Modelling of High Damage Resistance Zn-diffused Waveguides in Congruent and MgO:Lithium Niobate", J. Lightwave. Technol. Vol. 10, pp 1238-1246, September 1992.

[92] R. A. Griffin and A.C. Carter, “Optical Differential Quadrature Phase-Shif Key (oDQPSK) for High Capacity Optical Transmission”, in Proc. OFC’02, paper FD6.

[93] P. J. Winzer and R.-J. Essiambre, “Advanced optical modulation formats,” Proc. IEEE, vol. 94, no. 5, pp. 952–985, May 2006.

[94] H. Hu, R. Nouroozi, R. Ludwig, B. Hüttl, C. Schmidt-Langhorst, H. Suche, W. Sohler, C. Schubert, “Wavelength Conversion Transparent to Polarization, Data Rate and Modulation Format” submitted to the Jour. of Lithwave Technology.

[95] S. L. Jansen, D. van den Borne, B. Spinnler, S. Calabro, H. Suche, P.M. Krummrich, W. Sohler, G.-D. Khoe, and H. de Waardt, “Optical Phase Conjugation for Ultra Long-Haul Phase-Shift-Keyed Transmission,” J. Lightw. Techn., vol. 24, no. 1, 54-64 (2006)

[96] S. Watanabe and M. Shirasaki, “Exact compensation for both chromatic dispersion and kerr effect in a transmission fiber using optical phase conjugation,” J. Lightw. Technol., Vol. 14, pp 243–248 (1996).

Acknowledgement

I am heartily thankful to my supervisor, Prof. Wolfgang Sohler, whose encouragement, supervision and support from the preliminary to the concluding level enabled me to develop an understanding of the subject.

I also would like to make a special thanks to Dr. Hubertus Suche. If I have had any luck in my research, it has come from working with him in the lab. His valuable training, advice and criticisms helped me to develop my scientific skills to a new level.

I would like to appreciate Mr. Raimund Ricken and Mr. Viktor Quiring from our technology labs. Without their hard work none of the experiments would have been possible.

I sincerely thank Mrs. Irmgard Zimmermann, the secretary of our group, whom I got help every time I needed. I remember her assistance for the official works from very simple to the very sophisticated ones. Her wonderful advices were always useful in any aspects of my stay in Paderborn.

I thank Sergey Orlov, Ansgar Hellwig, Selim Reza, Mathew George, Abu Thomas and Daniel Büchter. They were always very helpful and optimistic. I am so grateful for having worked with them.

In addition, I would like to thank my parents for bringing me up the way I am, for being supportive of my interests.

Finally, I want to thank my family: my wife Nasrin and my daughter Sana for their deep understanding and endless support. Their emotional support over the past six years has significantly contributed to my work at the lab. I dedicate this dissertation to them with love.

Lastly, I offer my regards and blessings to all of those who supported me in any respect during the completion of the project.

Rahman Nouroozi
October 2010